DTIC FILE COPY

④

University of Cincinnati

Cincinnati, Ohio 45221

Dr. Andrew J. Steckl
Ohio Eminent Scholar
Carl Gieringer Professor of
    Solid State Microelectronics

Nanoelectronics Laboratory
Department of Electrical and
    Computer Engineering
899 Rhodes Hall (ML 30)
Cincinnati, OH 45221-0030

Phone: (513) 556-4777
Fax: (513) 556-7326
E-mail: asteckl@ucece1.ecc.uc.edu

AD-A211 711

REACTIVE ION ETCHING OF SPUTTERED SILICON CARBIDE

AND TUNGSTEN THIN FILMS FOR DEVICE APPLICATIONS

by

Wen-Sen Pan[a] and Andrew J. Steckl[b]

Rensselaer Polytechnic Institute

(a)   Current address: Intel Corporation, 2250 Mission College Blvd., MS SC9-24, Santa
        Clara, CA 95052-8121

(b)   Author to whom correspondence should be addressed.
        Current address: University of Cincinnati, 899 Rhodes Hall, ML 30, Cincinnati,
        OH 45221-0030

**DTIC
ELECTE
AUG 0 7 1989
S B D**

89   8 04 075

OFFICE OF NAVAL RESEARCH

Contract N00014-81-K-0605

Task No. NR 056-768

FINAL REPORT

Reactive Ion Etching of Sputtered Silicon Carbide

and Tungsten Thin Films for Device Applications

by

W.-S. Pan and A.J. Steckl

Nanoelectronics Laboratory
University of Cincinnati
Cincinnati, OH 45221-0030

1989

REPORT DOCUMENTATION PAGE

1a. REPORT SECURITY CLASSIFICATION	1b RESTRICTIVE MARKINGS
unclassified	

2a. SECURITY CLASSIFICATION AUTHORITY	3. DISTRIBUTION / AVAILABILITY OF REPORT
2b. DECLASSIFICATION / DOWNGRADING SCHEDULE	Approved for public release; distribution unlimited

4. PERFORMING ORGANIZATION REPORT NUMBER(S)	5. MONITORING ORGANIZATION REPORT NUMBER(S)
UC-Final Report	

6a. NAME OF PERFORMING ORGANIZATION	6b. OFFICE SYMBOL (If applicable)	7a. NAME OF MONITORING ORGANIZATION
Nanoelectronics Laboratory University of Cincinnati		Office of Naval Research

6c. ADDRESS (City, State, and ZIP Code)	7b. ADDRESS (City, State, and ZIP Code)
899 Rhodes Hall, ML 30 Cincinnati, OH 45221-0030	Chemistry Program Arlington, Virginia 22217

8a. NAME OF FUNDING / SPONSORING ORGANIZATION	8b. OFFICE SYMBOL (If applicable)	9. PROCUREMENT INSTRUMENT IDENTIFICATION NUMBER
Office of Naval Research		Contract N 00014-81-K-0605

8c. ADDRESS (City, State, and ZIP Code)	10. SOURCE OF FUNDING NUMBERS			
	PROGRAM ELEMENT NO.	PROJECT NO.	TASK NO.	WORK UNIT ACCESSION NO
Chemistry Program Arlington, Virginia 22217	NR056-768			

11. TITLE (Include Security Classification)

Reactive Ion Etching of Sputtered Silicon Carbide and Tungsten Thin Films for Device Application

12. PERSONAL AUTHOR(S)
W.-S. Pan and A.J. Steckl

13a. TYPE OF REPORT	13b. TIME COVERED	14. DATE OF REPORT (Year, Month, Day)	15. PAGE COUNT
Final Report	FROM _____ TO _____	1989	

16. SUPPLEMENTARY NOTATION

17. COSATI CODES			18. SUBJECT TERMS (Continue on reverse if necessary and identify by block number)
FIELD	GROUP	SUB-GROUP	SiC, W, refractory materials, RIE, RTA, etch rate, selectivity, mechanisms

19. ABSTRACT (Continue on reverse if necessary and identify by block number)

See attached sheet.

20. DISTRIBUTION / AVAILABILITY OF ABSTRACT	21. ABSTRACT SECURITY CLASSIFICATION
☒ UNCLASSIFIED/UNLIMITED ☒ SAME AS RPT. ☐ DTIC USERS	unclassified

22a NAME OF RESPONSIBLE INDIVIDUAL	22b. TELEPHONE (Include Area Code)	22c. OFFICE SYMBOL
Dr. David L. Nelson	(202)696-4410	

DD FORM 1473, 84 MAR 83 APR edition may be used until exhausted. All other editions are obsolete.

For high temperature processing and device applications, refractory materials, such as silicon carbide (SiC) and tungsten (W), are actively considered or evaluated as the basic semiconductor and metallization materials for future generations of integrated circuits.

In order to pattern fine lines in SiC and W thin films, a selective and anisotropic etching technique needs to be developed for future device applications. Therefore, the etching process including basic mechanisms and process requirement have been chosen as the overall research goals of this project.

First, materials properties, such as crystallinity, conductivity, refractive index, optical bandgap, etc., of sputtered silicon carbide (SiC) and tungsten (W) thin films have been investigated in conjunction with rapid thermal annealing (RTA) technique. The RTA temperature dependence of the optical bandgap for SiC thin films has been obtained. High crystallinity W thin of low resistivity films were obtained using the RTA process.

Reactive ion etching (RIE) of SiC thin films in a variety of fluorinated gas plasmas, such as SF_6, $CBrF_3$ and CHF_3 mixed with oxygen has been investigated in depth. The emission spectra and induced DC bias of the RF plasma were monitored to explore the etching mechanisms. The argon actinometry technique has been used to convert the plasma emission intensity to relative concentration of plasma species in order to more accurately quantity the etching process. Plasma conditions, such as composition of gas mixture, pressure, power, etc., were investigated in order to achieve the selective SiC-to-Si (and SiO_2) etching and anisotropic patterning of SiC thin films needed for device fabrication. A SiC:Si etch ratio higher than unity was obtained for the first time by using $CBrF_3/75\%O_2$ and $CHF_3/90\%O_2$ at 200W, 20sccm, 20mTorr plasma conditions. The best anisotropic profile was observed by using CHF_3 gas in the RIE mode. A typical DC bias, -300V, is concluded from etching experiments to determine the dependence of SiC etch rate and physical reaction under RIE mode.

A carbon rich surface on the etched SiC film was found for all gases and the roles of fluorine and oxygen were determined in each case. The etching mechanism of SiC by these gases under RIE mode was determined by loading experiments, surface analysis and etching phenomena. The reaction between fluorine and carbon is not supported by experimental results. A combined chemical and physical etching model has been suggested and supported by experiments. A carbon blocking model was proposed to understand the etching profile in all etching gases.

Reactive ion etching of tungsten (W) thin film has also been investigated by using the different fluorinated gas plasmas, such as CF_4, SF_6, $CBrF_3$ and CHF_3 mixed with oxygen. We have achieved our goal of selective patterning of tungsten films over SiC, Si, SiO_2, which required in order to use W in SiC device applications. A very good W:Si and W:SiO_2 selective ratio, 4:1 and 4.8:1, were observed by using $CHF_3/70\%O_2$ gases and under different plasma conditions. The obtaining of anisotropic etching profile in W etching has been suggested and the mechanisms have also been studied.

CONTENTS

ABSTRACT

For high temperature processing and device applications, refractory materials, such as silicon carbide (SiC) and tungsten (W), are actively considered or evaluated as the basic semiconductor and metallization materials for future generations of integrated circuits.

In order to pattern fine lines in SiC and W thin films, a selective and anisotropic etching technique needs to be developed for future device applications. Therefore, the etching process including basic mechanisms and process requirement have been chosen as the overall research goals of this project.

First, materials properties, such as crystallinity, conductivity, refractive index, optical bandgap, etc., of sputtered silicon carbide (SiC) and tungsten (W) thin films have been investigated in conjunction with rapid thermal annealing (RTA) technique. The RTA temperature dependence of the optical bandgap for SiC thin films has been obtained. High crystallinity W thin of low resistivity films were obtained using the RTA process.

Reactive ion etching (RIE) of SiC thin films in a variety of fluorinated gas plasmas, such as SF_6, $CBrF_3$ and CHF_3 mixed with oxygen has been investigated in depth. The emission spectra and induced DC bias of the RF plasma were monitored to explore the etching mechanisms. The argon actinometry technique has been used to convert the plasma emission intensity to relative concentration of plasma species in order to more accurately quantify the etching process. Plasma conditions, such as composition of gas mixture, pressure, power, etc., were investigated in order to achieve the selective SiC-to-Si (and SiO_2) etching and anisotropic patterning of SiC thin films needed for device fabrication. A SiC:Si etch ratio higher than unity was obtained for the first time by using $CBrF_3/75\%O_2$ and $CHF_3/90\%O_2$ at 200W, 20sccm, 20mTorr plasma conditions. The best anisotropic profile was observed by using CHF_3 gas in the RIE mode. A typical DC bias, -300V, is concluded from etching experiments to determine the dependence of SiC etch rate and physical reaction under RIE mode.

A carbon rich surface on the etched SiC film was found for all gases and the roles of fluorine and oxygen were determined in each case. The etching mechanism of SiC by these gases under RIE mode was determined by loading experiments, surface analysis and etching phenomena. The reaction between fluorine and carbon is not supported by experimental results. A combined chemical and physical etching model has been suggested and supported by experiments. A carbon blocking model was proposed to understand the etching profile in all etching gases.

Reactive ion etching of tungsten (W) thin film has also been investigated by using the different fluorinated gas plasmas, such as CF_4, SF_6, $CBrF_3$ and CHF_3 mixed with oxygen. We have achieved our goal of selective patterning of tungsten films over SiC, Si, SiO_2, which required in order to use W in SiC device applications. A very good W:Si and W:SiO_2 selective ratio, 4:1 and 4.8:1, were observed by using CHF_3/70%O_2 gases and under different plasma conditions. The obtaining of anisotropic etching profile in W etching has been suggested and the mechanisms have also been studied.

LIST OF TABLES

LIST OF FIGURES

CHAPTER 1

INTRODUCTION

Silicon carbide (SiC) has become an attractive semiconductor material in recent years for high speed, high density and high temperature device applications due to its wide band gap[1.1], high thermal conductivity, high temperature stability, high breakdown electric field[1.2] and high electron saturation velocity[1.3, 1.4], etc.

Since the metal contact to SiC is required to be stable for high temperature and high current density device application, tungsten appears to be a very good candidate for both Si and SiC technology. W metallization has been of considerable interest because of its refractory nature and deposition versatility, including sputtering and selective deposition. Since interconnections need to be deposited and patterned over various underlying materials with a minimum disturbance of the existing structure, the sputtering technique has been used for our experiments.

Rapid thermal processing (RTP) has become a very powerful processing technique in today's semiconductor applications, because of its to great control and the "thermal budget" (i.e. time temperature regime) loading versatility, as shown in table 1.1. Therefore, we have investigated the effects on SiC and W thin film quality of using rapid thermal annealing (RTA). To precisely control the heat treatment of various processes has many advantages compared to conventional furnace annealing. The thin film quality, including such properties as crystallinity, resistivity, refractive index, optical bandgap, etc., are important for device applications.

Table 1.1 Applications of Rapid Thermal Processing

IMPLANTATION	GATE DIELECTRICS	METALLIZATION
• Damage removal • Dopant activation • Shallow junction formation • Lower sheet resistance • Process control	• Rapid thermal oxidation and nitridation • Improvement of Chemical, mechanical and electrical properties • Reduction of carrier trapping	• Formation of silicide • Formation of refractory metal nitrides • Ohmic contact anneal • CVD deposition/alloy • Reduction of junction leakage
POLYSILICON	BULK SILICON	FUTURE DIRECTIONS
• Activation of Implanted species • Reduction of sheet resistance • In-situ doping • Reflow (PSG, BPSG, AsG, etc.)	• Thermal donor annihilation • Annealing of RIE-Induced defects • Lattice damage repair • Gettering	• Supperlatice of GaAs, Si SiC • Regrowth of Implanted SDS • Oxide reflow • Growth of superconductor • In-situ process

So, using RTA to prepare the high quality thin films and developing a dry etching techniques for patterning SiC and W fine line are the main target for this research. Therefore, a selective and anisotropic etching technique to pattern SiC has been developed by using fluorinated gases, such as SF_6, $CBrF_3$ and CHF_3 and oxygen mixture under reactive ion etching (RIE) mode, which would specially concern not only etching SiC itself, but also selective etching to Si and SiO_2. The basic plasma parameters, such gas composition, pressure, power, flow rate, substrate temperature, emission spectra, induced DC bias, etc., have been varied and monitored to understand and control the etching processes. The etching profile and the etching surface have been analyzed and the etching mechanisms in both chemical and physical reaction model of each gas have been proposed and confirmed by experiments.

Reactive ion etching of tungsten thin films has been performed by using CF_4, SF_6, $CBrF_3$ and CHF_3 mixture with oxygen to achieve selective etching over Si, SiO_2 and SiC. The pressure and power of the plasma have been varied to optimize the selectivity. The etching mechanism of tungsten in these fluorinated gases has been studied and compared to previous results. The etching conditions, such gas, pressure, power, etc., will be suggested to achieve the anisotropic etching. The in-situ patterning processes of SiC and W are considered by using similar fluorinated gases in device applications.

CHAPTER 2

HISTORICAL REVIEW AND TECHNICAL BACKGROUND

2.1 Potential of Silicon Carbide

Silicon carbide (SiC) enjoys a member of superior properties which can be of great potential benefit when developed in conjunction with advances in submicron semiconductor processing technology. As device fabrication technology reached the high density and submicron region, the requirements for devices working under higher heat dissipation, higher operating temperature and higher electrical field have become more difficult for existing materials, such as Si and GaAs, because of their basic material properties. Currently, the single crystal 3C-SiC has become a more attractive material because its refractory nature is considered with high electron mobility (1000 $cm^2/V*s$)[2.1] and high electron saturation velocity (2.5 X 10^7cm/sec), which are comparable to Si at room temperature . The weaker temperature dependence of carrier mobility in SiC than in Si and wider band gap suggests that SiC is a more suitable material for devices operated at high temperature. The basic material properties of SiC, Si and GaAs are compared in Table 2.1.

Two different figures of merit (FOM), which were proposed by E. O. Johnson and R. W. Keyes, are shown in Table 2.2. The figure of merit proposed by Johnson[2.2] relates breakdown electric field (E_B) and electron saturation velocity (V_{sat}) to the power and frequency limits of transistors. Keyes' FOM[2.3 - 2.5] is a relationship between high frequency limitations, minimum device dimensions, and the semiconductor

4

Table 2.1 Materials Properties of SiC, Si, and GaAs

Properties / Materials	Bandgap (eV)	Thermal Conductivity (W/cm°C)	Saturated Drift Velocity (cm/sec)	Breakdown Electric Field (V/cm)	Dielectric Constant (Relative)	Melting Point (°C)
SiC	2.35	5.0	2.5×10^7	4×10^6	9.7	2830
Si	1.12	1.5	1×10^7	3×10^5	11.8	1415
GaAs	1.43	0.5	2×10^7	4×10^5	12.8	1238

properties σ_T (thermal conductivity), V_{sat} (saturation velocity) and K (relative dielectric constant) were considered. From the Si normalized ratios of both figures of merit, it can be seen 3C-SiC is superior in principle to Si and GaAs no matter which FOM is chosen. It is, therefore, in high operating temperature and high speed device applications.

In order to obtain high quality SiC thin films, a variety of gases and processes, such as chemical vapor deposition (CVD)[2.6-2.9], low-pressure chemical vapor deposition (LPCVD)[2.10-2.13] have been utilized. For epitaxial deposition on Si, a carbonized buffer layer was needed to reduce the 20% mismatch between 3C-SiC and Si (4.36Å and 5.43Å). High growth temperature (>1100°C) was required for growing high quality SiC film except in work of Y. Furumura et al.[2.13] who used Si(111) off-axis substrates and $SiHCl_3$-C_3H_8 gas system (instead of SiH_4-C_3H_8) to obtain 3C-SiC film with no buffer layer and at a lower processing temperature (1000°C). A summary of SiC thin films deposition by CVD and LPCVD is shown in Table 2.3.

A few other growth methods, which have been developed for different types of SiC thin films in various applications are shown in Table 2.4. This includes molecular ion beam epitaxy (MIBE)[2.14], dual-source sputter deposition (DSSD)[2.15], plasma chemical vapor deposition (PCVD)[2.16, 2.17], vapor phase epitaxy (VPE)[2.18], sputtering[2.19]. The single type 3C-SiC, polytype SiC (poly-SiC) and amorphous SiC (a-SiC) were grown on different substrates, such as TiC, amorphous Si (a-Si). Low operating temperature and no buffer layer were the common situations for these processes.

Table 2.2 Figure of Merit (FOM) of SiC, Si, and GaAs

Properties / Materials	$\dfrac{Johnson}{E_B V_{sat}/2\pi}$	FOM Ratio To Si	$\dfrac{Keyes}{\sigma_T (V_{sat}/K)^{1/2}}$	FOM Ratio To Si
SiC	1.6×10^{13}	33.3	8×10^3	5.8
Si	4.8×10^{11}	1	1.4×10^3	1
GaAs	1.3×10^{12}	2.7	6.3×10^2	0.5

Table 2.3   The Growth of SiC Film (I)

Gas	Temperature (°C) (Pressure) (Torr)	Substrate	Film Structure	Deposition Rate (um/min)	Method	Ref.
$SiH_4 - C_3H_8 -H_2$	1330	Buffered SiC Si(100) & (111)	3C-SiC(100) & (111)	0.06	CVD	[2.11]
$SiH_2Cl_2-C_3H_8 -H_2$	1350	Poly SiC Si(111)	3C-SiC	0.3~2.1	CVD	[2.12]
$SiH_4 - C_3H_8 -H_2$	1330	Buffered SiC Si(100)	3C-SiC(100)	0.042	CVD	[2.13]
$SiH_4-C_2H_4 -H_2$	1327	Buffered SiC Si(100) & (111)	3C-SiC	0.04	CVD	[2.14]
$SiH_4 - C_3H_8 -H_2$	1360	Buffered SiC Si(100) & (111)	3C-SiC	0.05	LPCVD	[2.15]
$SiH_4 - C_3H_8 -H_2$	1260 (1.5-100)	Buffered SiC Si(100) & (111)	3C-SiC	0.042	LPCVD	[2.16]
$CH_3SiCl_3-H_2$	1100-1400 (200)	Graphite	Poly type 3C-SiC	0.2-1.5	CVD & LPCVD	[2.17]
$SiHCl_3-C_3H_8$	1000 (150)	Si off-axis (111)	3C-SiC	0.03	LPCVD	[2.18]

Table 2.4   The Growth of SiC (II)

Gas & Source	Temperature (°C) (Pressure) (Torr)	Substrate	Film Structure	Deposition Rate (um/min)	Method	Ref.
Si + C$^+$ (ion)	820-1000 (3.8×10^{-7})	Si(100)	3C-SiC	0.0003	MIBE	[2.19]
Si + C	>700 (10^{-6})	Si(100) & Sapphire	Poly-SiC	0.008	DSSD	[2.20]
SiH$_4$-CH$_4$ -H$_2$	250 (0.6)	Si(100)	a-SiC	0.018	PCVD	[2.21]
Evaporated Si - C$_2$H$_2$	1400	TiC	3C-SiC	——	VPE	[2.23]
SiH$_4$- CH$_4$ C$_7$H$_8$, C$_6$H$_6$'	250-270 (10^{-7})	a-Si/Si	a-SiC	0.009-0.012	PCVD	[2.22]
SiC Target - Ar	RT-400 (0.006)	Si(100)	a-SiC	0.01	Sputter	[2.24]

In general, CVD and LPCVD methods have been widely used in today's technology, but the high growth temperature and carbonized buffer layer, are required in most processes. The different types of SiC microelectronic devices which have been reported include light emitting diodes (LED)[2.20-2.23], solar cells[2.24, 2.25], bipolar transistors[2.26, 2.27], MOSFETs[2.28-2.31], MESFETs [2.32], SiC/Si heterojunction bipolar transistors[2.33-2.36], dielectric isolation[2.37], etc.

The sputtering technique used in this work to prepare SiC thin film has the advantage of being essentially substrate-independent, taking place at close to room temperature and being able to cover large areas fairly easily, particular in the applications of solar cells, light-emitting devices and SiC-Si heterojunction devices.

2.2 Potential of Tungsten

Refractory metal tungsten (W) has been increasingly used in VLSI circuits in past decade due to its low resistivity ($5.3\mu\Omega$-cm), superior electromigration resistance and high melting point (3410°C) [2.38, 1.6, 1.7], which has the advantage of high operating temperature. Among the applications[2.39] for tungsten are as a diffusion barrier between silicon contacts and aluminum metallization[2.39, 2.40], it prevents spiking (silicon dissolution effect), thereby permitting the use of shallow junction contact, as a low-resistance shunt for polycrystalline silicon gates and interconnections (in elemental or silicide form), gate metal [2.41, 2.42], and as an alternative to aluminum-based metallization[2.43, 2.44].

2.3 Rapid Thermal Processing (RTP)

2.3.1 Introduction

For today's integrated circuits (ICs), a minimum feature size is required to obtain higher speed and higher packing density. Therefore, the dimensions of device continue to shrink into the submicron region, which pushes integrated circuits from very-large-scale (VLSI) into ultra-large-scale integration (ULSI). The control of impurity profile and material properties becomes ever more critical. A key characteristic of these new processes must be a method of minimizing total thermal exposure to obtain smaller geometry devices, shallower junctions and thin high quality materials.

The inadequacy of conventional furnace annealing has led researchers to investigate alternates to furnace annealing based on lasers, electron beams, lamps, resistance heaters, and ion-beam annealing technology[2.45-2.49]. Since 1977, the first attempt to anneal ion implanted GaAs wafer was made by Surrid t al.[2.50]. In 1980, Nishiyama, Arai, and Watanabe[2.51] were the first to use halogen lamps as a continuous source of radiation to anneal boron-implanted silicon for a very short time (6sec). After that, a very wide applications of rapid thermal processing has been studied in different directions such as ion implant activation[2.52, 2.53], growth of thin film material[2.54, 2.55], silicide formation [2.56], junction formation[2.57, 2.58], annealing growth materials, (dielectric material[2.59, 2.60], silicide[2.61, 2.62]), removing defects from reactive ion etching surface[2.63, 2.64], rapid thermal oxidation process (RTO)[2.65-2.67] and nitridation [2.68-2.70], etc. A

summary of different applications of RTP in semiconductor processes is shown in Table 1.1.

High throughput, low equipment cost, energy saving, control contamination, ease of handling, and lack of a thermal gradient are some of key feature of rapid thermal processing.

2.3.2 Operating principles

Basically, all of the thermal processes can be divided into three groups according to the time of process with reference to the thermal response time[2.71] : (1). adiabatic processing, (2). thermal flux processing, and (3). isothermal processing[2.72]. There are shown in Figure 2.1, where the appropriate temperature distribution is also displayed. Typically, a high power laser beam is used for a time less than about 10^{-6}s in the adiabatic processing case, which is less than the thermal response time of silicon (msec). The dopant redistribution and the formation of ripples occur locally due to the melting surface and the electron beam processing introduces neutral traps in the oxide layer preventing its use in metal-oxide-semiconductor (MOS) device[2.73]. The main disadvantage of thermal flux processing, wherein the processing time (10^{-4}s) is comparable to the thermal response time, is that although defects are removed from the center of scanning spot, thermal stresses are introduced at the boundary of scanning line causing new defects. On the other hand, in rapid isothermal processing, the wafer is heated for about 1-100 sec using incoherent light sources such as tungsten halogen lamps, arc-lamps, or graphite heaters. The unfocused light is allowed to heat the whole

wafer uniformly. No interference effects between the dielectric overlayer and semiconductor are present. The main advantage of rapid isothermal processing over conventional furnace annealing, which takes times in the order of minutes, is that little diffusion of implanted atoms and previously incorporated dopant atoms takes place while dopants are activated completely.

For most metals, dielectrics, and insulators, the response time is less than 1sec. Therefore, during isothermal processing, there are no temperature gradients into the bulk are present. A heating and cooling rates in the temperature range of 30-500°C/sec have been generally used and a typical temperature profile versus processing time is shown in Figure 2.2(a). The pre-heat cycle is occasionally used for high temperature procedures (>900°C), as shown in Figure 2.2(b).

An alternative to in situ doping, diffusion and ion implantation provide means of controllably introducing impurities into semiconductor materials. In SiC, diffusion processes require both temperatures greater than 1800°C and relatively long time[2.74] to accomplish the mass transport required for device fabrication. So, ion implantation is more attractive process to dope SiC and the RTP will be more controllable method for impurity activation and junction depth. The use of ion implantation to form p-n junctions has been successfully reported by several investigators[2.75-2.77] in 6H-SiC. In recent year, the RTP technique has been introduced to activate ion implanted impurities in 3C-SiC by Edmond et al.[2.78] and Ryu et al.[2.79].

The rapid thermal annealing (RTA) process has been introduced in this work to improve the quality of SiC and W thin films prepared for
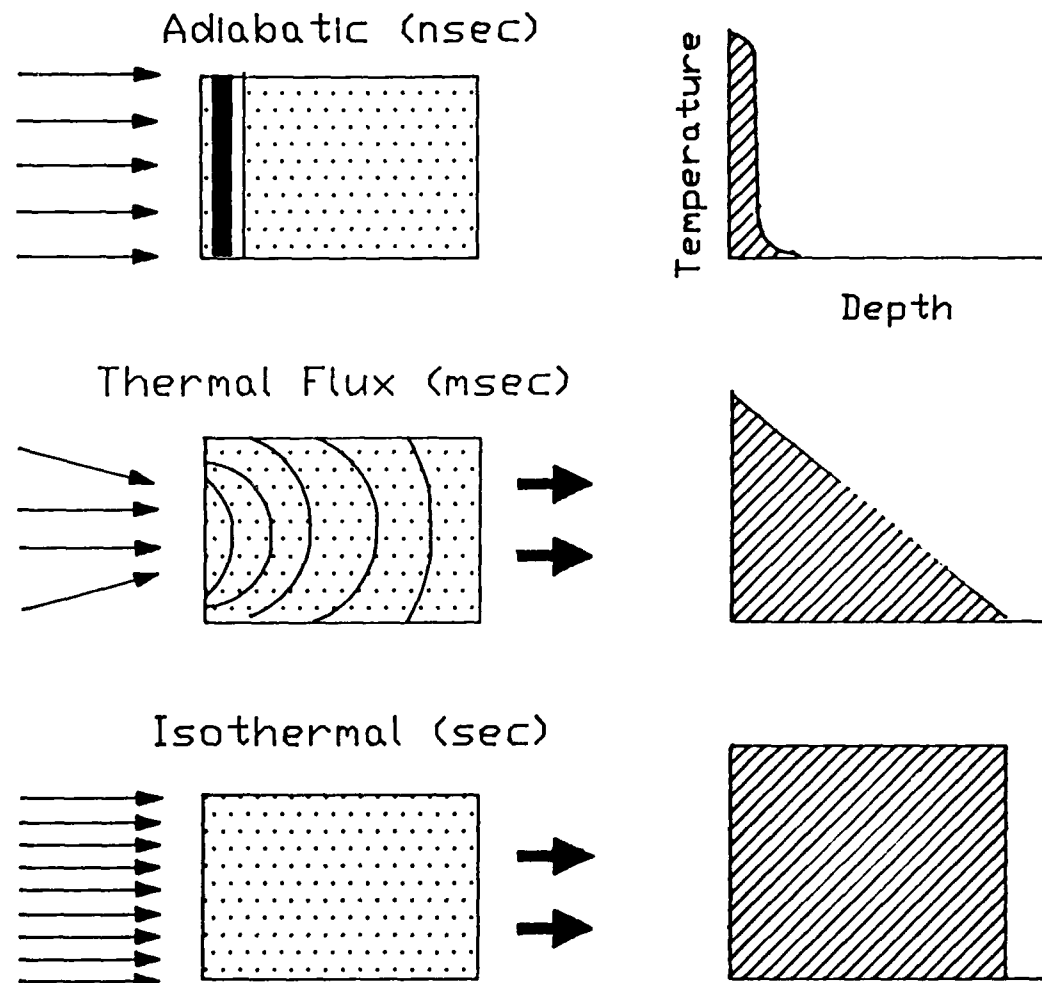
Figure 2.1. Schematic showing the definition of three heating processes (a). adiabatic, (b). Thermal flux, (c). isothermal, and their temperature profile (Ref. [2.81]).
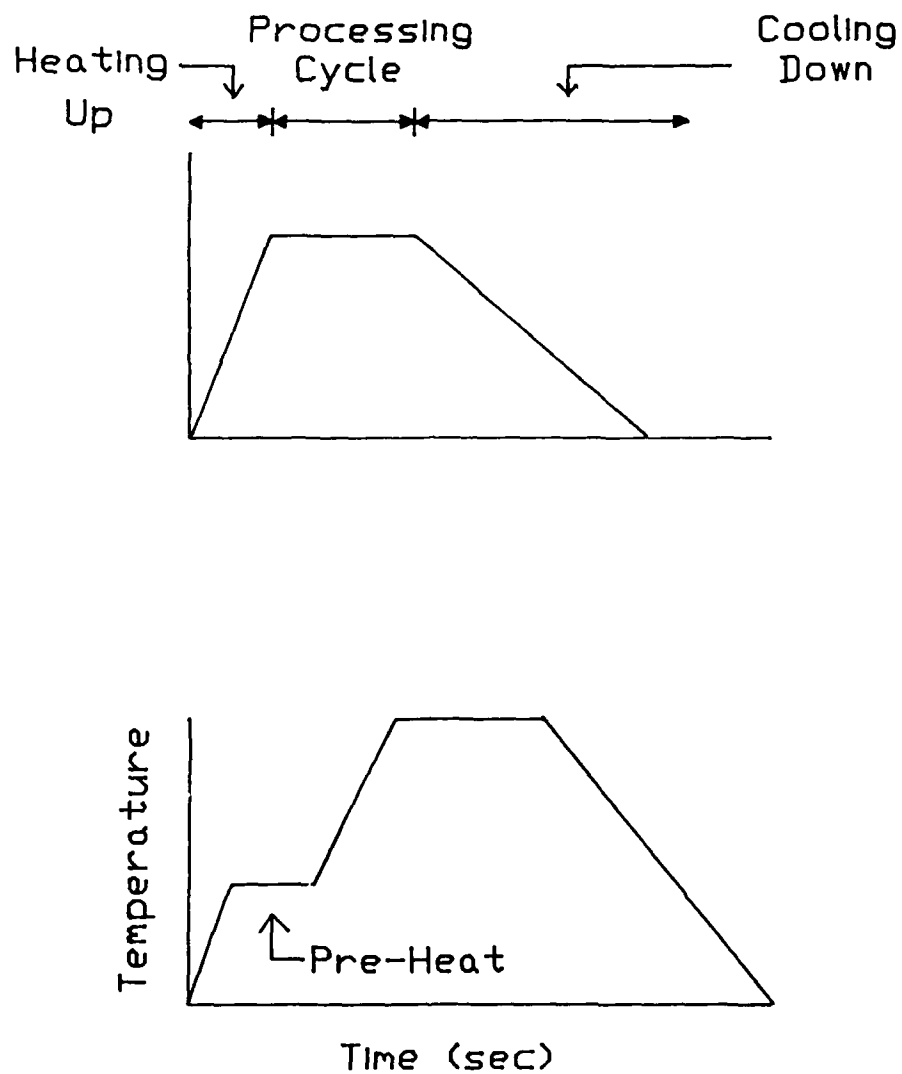
Figure 2.2.   Typical temperature profile of rapid isothermal processing for (a). low temperature (< 700°C), (b). high temperature (> 900°C) range.

our etching studies.

2.4 Reactive Ion Etching

2.4.1 Introduction

Dry etching techniques (plasma etching) have been developed and applied to silicon ICs and dating back to the late 1960s [2.80, 2.81]. As device geometries decrease, spacing between stripes of resist mask also decrease. With micron and submicron patterns, the surface tension of etching solutions can cause the liquid to bridge the space between two resist stripes and etching of the underlying film is thereby precluded. The isotropic nature of the wet etching process limits to the device dimensions. Because the film thickness and the etching rate are often non-uniform, a certain degree of overetching is required. However, when the film thickness is comparable to the lateral film dimension, undercutting can be intolerable. The different types of etching profile are shown in Figure 2.3[2.82]. In general, the isotropic etching profile is caused by a nondirectional chemical reactions. For this reason, plasma etching techniques, which provide more control and the anisotropy, have been developed. Furthermore, plasma etching is a dry process, which is clean and safe.
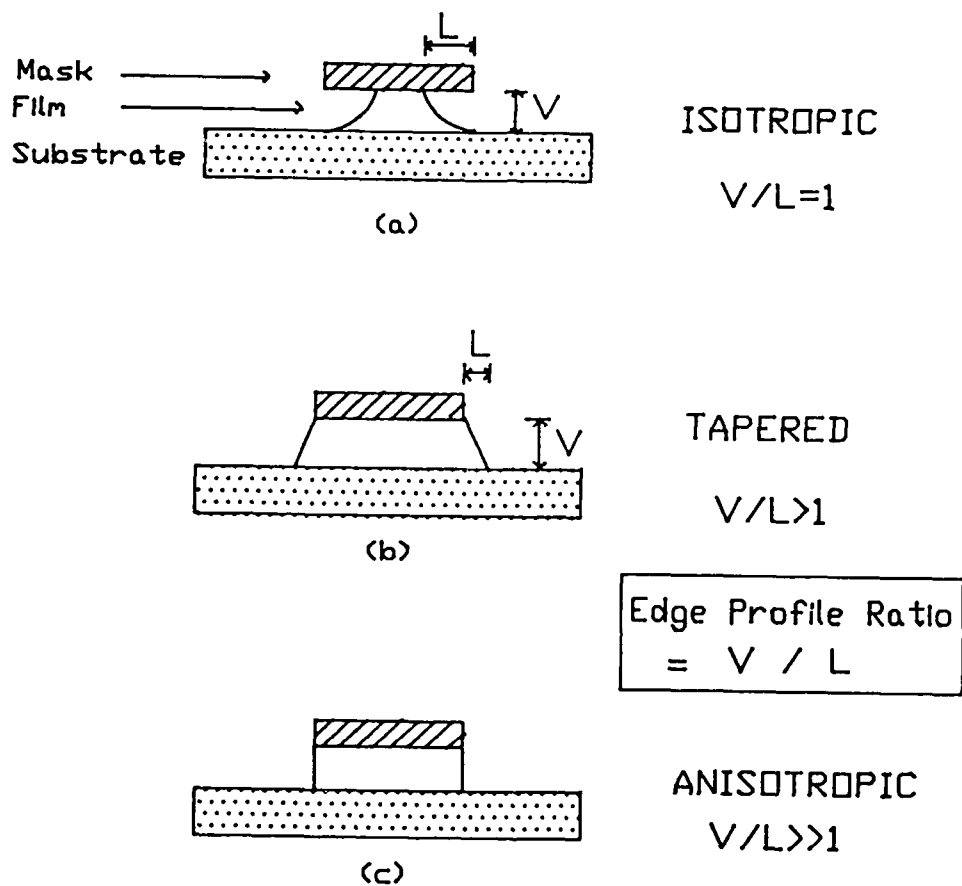
Figure 2.3. The cross section of (a). Isotropic, (b). Tapered and (c). Anisotropic profile of films etched with wet or plasma etchant (Ref. [2.82]).

2.4.2 Basic Operation

A plasma is a partially ionized gas composed of electrons, ions, and a variety of neutral species. It is generally formed by applying a large electric or magnetic field to a volume of gas at different pressures. The electric field could be generated in DC or AC-type glow discharges. Typically, a DC glow discharge operates at pressures exceeding 30mTorr and applied voltages exceeding a few hundred volts. The discharge is visibly nonuniform between electrodes, and is composed of a series of luminous light and dark zones. In AC or RF discharges, a few hundred volt plasma potential ($-V_p$) with respect to ground can be produced in the powered electrode, as shown in Figure 2.4. This self-induces bias is due to the difference in electron and ion mobility, in electrons been readily collected. The strong negative bias will accelerate ions to directionally bombard the powered electrode. This can produce higher a directional etching profile compared to loading the sample on ground electrode. The advantages of RF discharges are : (a). higher efficiency to generate plasma, (b). allowing operation at pressures as low as 1mTorr, (c). electrode material independent, electrode could be covered by insulator.

The large number of parameters that affect the process is one of the most challenging aspects to routine use of plasma etching. Figure 2.5 illustrates some of parameters that impact the gas-phase[2.83] interaction, as well as surface-plasma interactions. Although many macroscopic parameters can be controlled, such as the type of feed gases, power, flow rate, and pressure, the precise effect of making any changes in these parameters is usually not well known and a change in a single
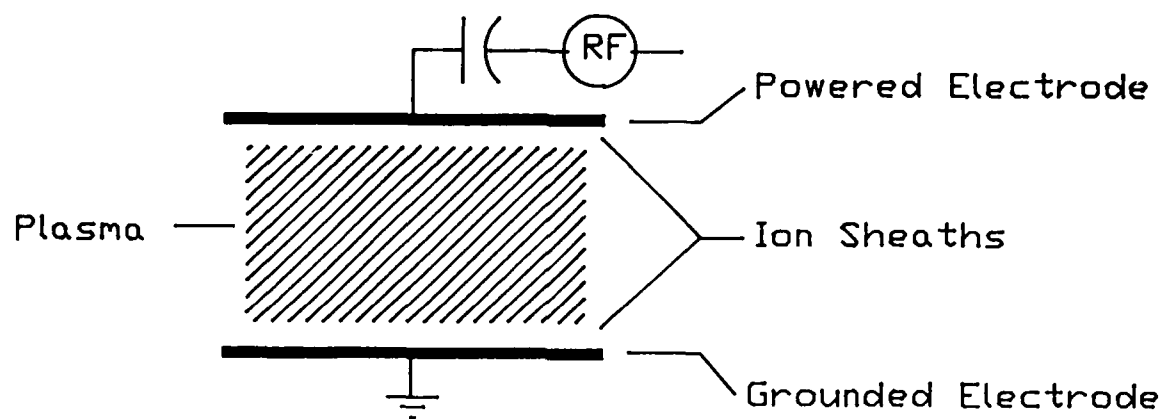
(a)
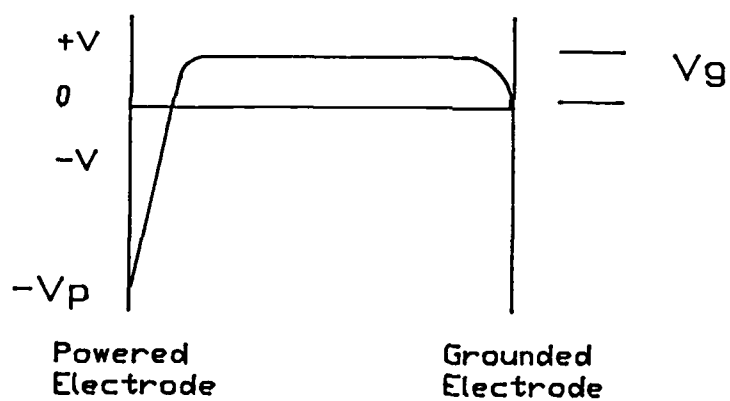
(b)

Figure 2.4.   (a). Schematic view of rf discharge, (b). Induced potential of rf discharge as a function of position.

macroscopic parameter typically alters two or more basic plasma parameters. Plasma-assisted etching can take several different forms for various applications, such as sputtering etching, ion milling, plasma etching, reactive ion etching, reactive ion beam etching, etc. Basically, in reactive ion etching, a physical and chemical reactions are involved simultaneously, which makes the etching mechanisms more complicated. In our work, a low pressure of 1mTorr to 100mTorr has been used to obtain higher induced potential. The processed sample is always loaded on power electrode to gain more directional etching by ion bombardment.
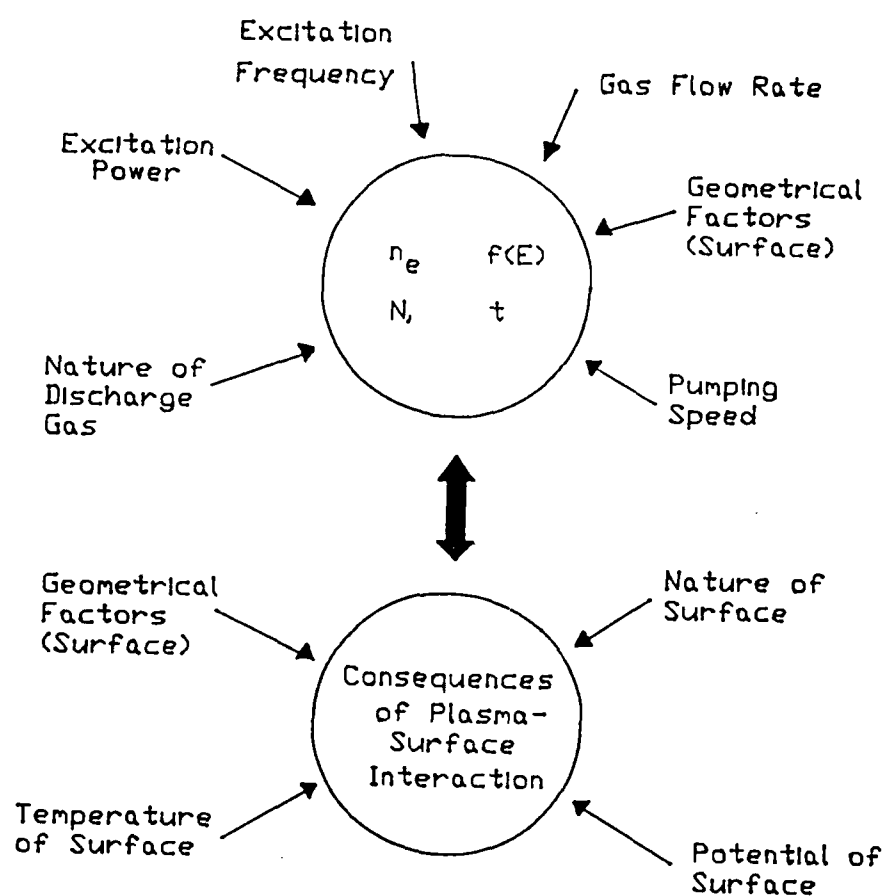
Figure 2.5. Representation of the parameter problem in plasma process (n_e: electron density, f(E): electron energy distribution function, N: gas density, t: resident time) Ref. [2.83].

2.4.3 Plasma Etching of Silicon Carbide

SiC is inert to nearly all commonly used laboratory chemicals. Most of the effective etching methods historically reported for SiC, such as molten salts[2.84-2.90] and gas phase etching[2.84, 2.86, 2.91-2.94], are carried out at temperatures in excess of 500°C, and some even more than 1000°C. This has limited application to semiconductor device fabrication technology and the conventional SiC etching is summarized in Table 2.5 and Table 2.6[2.95].

Plasma etching technique had been introduced at RPI in 1985 to etch SiC by CF_4/O_2, SF_6/He and Ar plasma[2.96]. The use of CF_4[2.97, 2.98], CF_4/O_2[2.96, 2.97, 2.99], NF_3[2.100], SF_6[2.101] plasmas to pattern SiC previously in RPI and summarized in Table 2.7. These results concentrated on etching SiC and no selectivity to Si and SiO_2, etching profile and etching mechanisms still needed to be explored.

In order to incorporate SiC films into Si VLSI technology, a selective and frequently anisotropic etching process with respect to Si and SiO_2 is required[2.102]. To fully utilize plasma-assisted etching for SiC technology, one needs to explore and understand the effect of various plasma parameters including pressure, power, etching species, dilutants, etc. For example, for the SiC homo-device (MOSFET), a selectivity of SiO_2 to SiC higher than unity is required for gate area patterning and an anisotropic isolation etching process is needed for high density device applications, as shown in Figure 2.6(a). For the SiC/Si heterojunction device, fabrication considerations of SiC etching selectivity and anisotropy to define the active area well are required, as shown in Figure 2.6(b).

Table 2.5 Molten Salt Etching for SiC

Etchant	Temperature (°C)	Etch Rate (um/sec)	Ref.
KOH	600-800	1-7	[2.84]
NaOH	900	1.5	[2.85]
$NaF:Na_2SO_2$	950	5	[2.86]
$NaOH:Na_2O_2$ (3:1)	700	7	[2.86, 2.87]
Na_2CO_3	900	0.3	[2.88, 2.89]
$Na_2B_4O_7$	1000	0.3	[2.84, 2.88]
Na_2O_2	700	7	[2.84, 2.90]

Table 2.6 Gas Phase Etching for SiC

Gases	Temperature ($^\circ$C)	Comment	Ref.
F_2	300	Cubic SiC etches faster than hexagonal	[2.91, 2.92]
Cl_2	1000	Rate 0.5um/min. Layer of Carbon left on Surface	[2.84, 2.93]
Cl_2, O_2 (2 : 1)	1000	Rate 1um/min. Etch Rate much faster on (0001) plane	[2.96]
ClF_3	200–400	Etch pits on (0001) plane	[2.86]
H_2	1600–1750	Non preferential. Rate 3um/min at 1700°C	[2.94]

Table 2.7   Summary of SiC Dry Etching Processes

Gases	Mode (RIE/PE)	RF power (W/cm^2)	Presure (mTorr)	Etch rate (Å/min)	Selective Ratio (SiC:Si)	Ref.
SF$_6$ + 50%He	RIE	0.42	20	560	1:6	[2.96]
SF$_6$	PE	0.18	200	240	—	[2.97]
CF$_4$	PE	700V (DC)	2	735	—	[2.97]
	RIE	0.55	40	233	—	[2.98]
CF$_4$ + 4%O$_2$	RIE	0.42	20	375	1:3.3	[2.96]
CF$_4$ + %O$_2$	RIE	0.55	20	150 (50%O$_2$)	—	[2.98]
	PE	0.5	600	170 (67%O$_2$)	—	[2.99]
NF$_3$	RIE	0.44	40	2110	—	[2.100]
Ar	RIE	0.42	20	270	1:1.26	[2.96]

Therefore, various fluorinated gas mixtures, such as SF_6/O_2, $CBrF_3/O_2$ and CHF_3/O_2, have been investigated in this work, in order to fulfill these requirements. Furthermore, the etching mechanisms of using these gases, including high fluorine-containing gas (SF_6) and low fluorine-containing gas ($CBrF_3$ and CHF_3) in RIE has been explored.

2.4.4 Tungsten

The previously reported dry etching of tungsten using fluorine-containing gases, such as CF_4 [2.103, 2.104], SF_6/O_2 [2.105-2.107], CF_4/O_2 [2.106], CF_4/N_2 [2.104], and $CBrF_3/O_2$ [2.108], and XeF_2/Ar [2.109, 2.110], is summarized in Table 2.8. In these previously works, W etching either has not been investigated in the low-pressure RIE mode necessary for fine-line patterning or has not exhibited the necessary selectivity. The main product of using a fluorinated gases to etch tungsten and silicon is WF_6[2.107, 2.110] and SF_4. In Table 2.9, the melting point of different tungsten and Si fluoride, bromide, chloride and oxide compounds[2.111] are displayed. It reveals the advantage to use fluorinated gases to etch W and Si due to their lower melting and boiling point. SiF_4 has a much higher vapor pressure than WF_6 at room temperature. It is, therefore, very difficult to obtain a selectivity ratio of W over Si higher than 1. Patterning a tungsten films over SiC, Si and SiO_2 which is necessary for device applications and has been investigated and not sufficient. Indeed, even CVD and LPCVD techniques which enable selective deposition of W, in multilevel metal structures, where the different depths of contact vias will still require an

S G D

Metallization

Gate Area

n+ p-SiC n+

[Isolation Etching]

n-Si

(a)

C B E B C

Metallization

n-SiC

[Emitter region Patterning]

n+ p+ p-Si p+ n+

n-Si

(b)
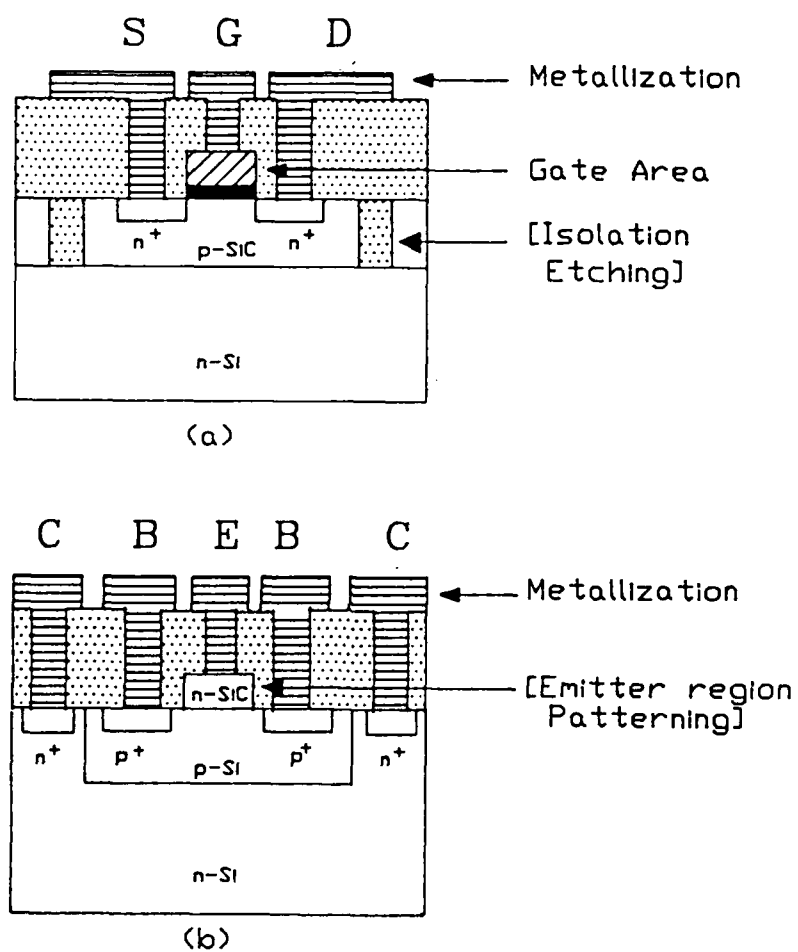
Figure 2.6. Processing requirements for (a). Homo-device structure of SiC MOSFET, (b). Device structure for SiC/Si heterojunction transistor.

etch-back process to obtain planarization[2.112].

We have, therefore, investigated the use of fluorocarbon gases, such as CF_4, SF_6, $CBrF_3$, and CHF_3, mixed with different concentration of oxygen under RIE mode to study the etching behavior of W thin films.

Table 2.8   The Etching of Tungsten by Fluorinated Gases

Gases	W Film	Etching Mode	RF Power (W/cm^2)	Pressure (mTorr)	Etch Rate (um/min)	Ref.
CF_4	RF Sputter	RIE	0.081	76	0.01	[2.103]
CF_4/N_2	RF Sputter	RIE	0.081	76	0.02	[2.104]
CF_4/O_2	PCVD	PE	0.2	200	0.04 (20%)	[2.106]
	Sputter	RIE	300V (Induced)	10	0.135	[2.105]
SF_6/O_2	PCVD	PE	0.2	200	0.08 (30%)	[2.106]
	Foil	PE/RIE	0.7	200	1.4 (70%)	[2.107]
$CBrF_3/O_2$	CVD	RIE	600V (DC)	10	0.023 (13%)	[2.108]
XeF_2/Ar	W(111)	IBAE*	2000 (eV)	0.016	—**	[2.109]

* : Ion Beam Assisted-Etching (IBAE)   ** : Only relative value

Table 2.9   The Melting and Boiling Point of W and Si Compounds

	Name	Formula	Melting Point°C	Boiling Point°C	Name	Formula	Melting Point°C	Boiling Point°C
Tungsten (W)	Fluoride	WF_6	2.5	17.5	Oxytetra-Fluoride	WOF_4	110	187.5
	Bromide	WBr_2	400	—				
		WBr_5	276	333	OxyBromide	$WOBr_4$	277	327
		WBr_6	232	—	Oxychloride	WO_2Cl_2	266	—
	Chloride	WCl_5	248	275.6		$WOCl_4$	211	227.5
		WCl_6	275	346.7				
Silicon (Si)	Fluoride	SiF_4	-90.2	-86				
	Bromide	$SiBr_4$	5.4	154				
		Si_2Br_6	95	240				
	Chloride	$SiCl_4$	-70	57.6				

CHAPTER 3
THIN FILM PREPARATION

3.1 Deposition Technique

3.1.1 Silicon Carbide

SiC thin films were deposited by RF (13.56MHz) sputtering at room temperature onto thermally oxidized or virgin (100) silicon substrates, which had been cleaned by a standard cleaning procedure. The deposition system used was a planar electrode system from Veeco Co.. Before sputtering, the system was pumped down to 2×10^{-6} Torr base pressure. A 5" hot-pressed stoichiometric SiC composite target (99.7% purity) was used as cathode, and cooling water was used to cool down the target during deposition. The distance between the SiC target and the substrate was about 6 cm. The film was deposited in Ar gas plasma of 6 mTorr at an RF power of 200W(1.58W/cm^2). A constant sputtering rate of 11nm/min was used to prepare samples with film thickness from 50nm to 1μm.

3.1.2 Metals Deposition

3.1.2.1 Tungsten

Tungsten films were deposited at room temperature by DC magnetron sputtering from a 2" (99.97% purity) W target in Ar

plasma at 6mTorr pressure and -350V voltage conditions. The base pressure was $7x10^{-7}$Torr. A W sputtering rate of 10nm/min was generally used. A good metal-shining and smooth film was obtained by sputtering W onto Si or SiO_2 substrate. No adhesion problems were observed.

3.1.2.2 Aluminum

The 200nm to 300nm aluminum films, used as a mask for both tungsten and silicon carbide etching experiments, were deposited by a resistive evaporation system (Veeco) at 100nm/min evaporation rate. The Al film was patterned by standard IC photolithography processes, which included positive photoresist (SHIPLEY 1470), visible light wavelength aligner (Perkin-Elmer 140) and 40°C wet etching by solution of 16 H_3PO_4 : 1 HNO_3 : 1 CH_3COOH : 2 H_2O.

3.2 Rapid Thermal Annealing (RTA)

3.2.1 Experimental Procedure

Rapid thermal annealing of silicon carbide and tungsten thin films has been performed by using a Heatpulse 210/T rapid-wafer-annealing system (AG Associates). The system basically consists of an annealing chamber and a microcontroller. The annealing chamber contains upper and lower banks of high-intensity, tungsten-halogen lamps and

water-cooled reflective walls. A quartz diffusion tube is positioned between the lamps banks, as shown in Figure 3.1(a). The banks together contain thirteen 1.5kW lamps and has an 18kW lamps total output limit. A small Si chip with a thermocouple glued to it is located in the annealing chamber and functions as a temperature sensor, as shown in Figure 3.1(b). Both temperature and intensity control mode are available, but only the temperature control mode has been used in this research. A typical temperature profile for 500°C to 1100°C peak heating for a 10sec cycle in the temperature control mode is shown in Figure 3.2. A ramp-up rate of 100°C/min was used. A 400°C, 10sec pre-heat cycle was designed for warming up the lamp system and reducing the thermal stress for the high temperature process. The limitations of the system are a maximum of 300 sec for annealing time and a temperature range of 300°C to 1250°C.

3.2.2 Refractive Index of SiC

After deposition, the SiC thin films are treated by rapid thermal annealing (RTA), basic optical properties have been obtained directly by measuring the refractive index and the optical energy bandgap. An automated ellipsometer (Rudolph Research model) was used to determine the refractive index at a wavelength of 632.8nm. The silicon substrate is assumed to have a refractive index of 3.858 and an absorption index of 0.018[3.1]. Figure 3.3 illustrates the dependence of the refractive index of SiC films on annealing time from 0 to 90sec at different annealing temperatures from 1000°C to 1200°C, in nitrogen ambient. After
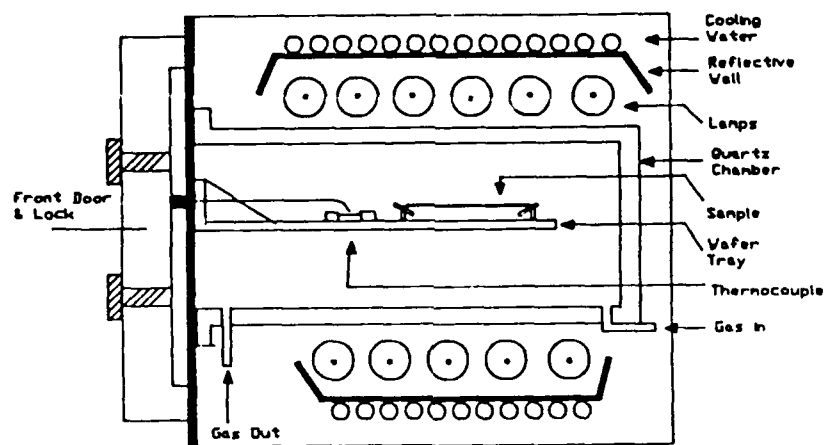
(a)
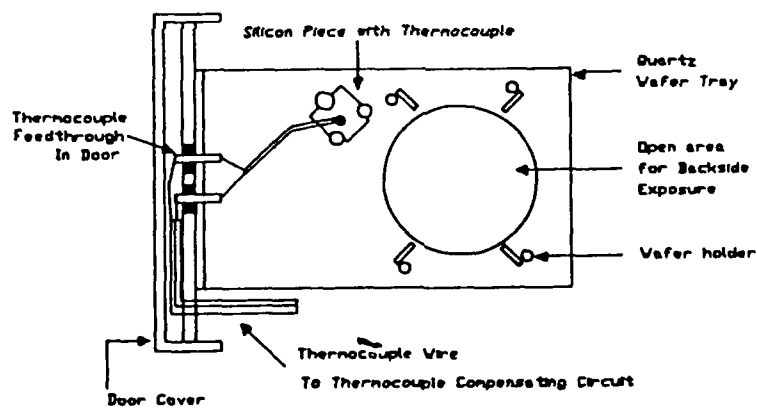
(b)

Figure 3.1.   (a). Rapid thermal annealing system, (b) Relative position of wafer position and thermocouple.
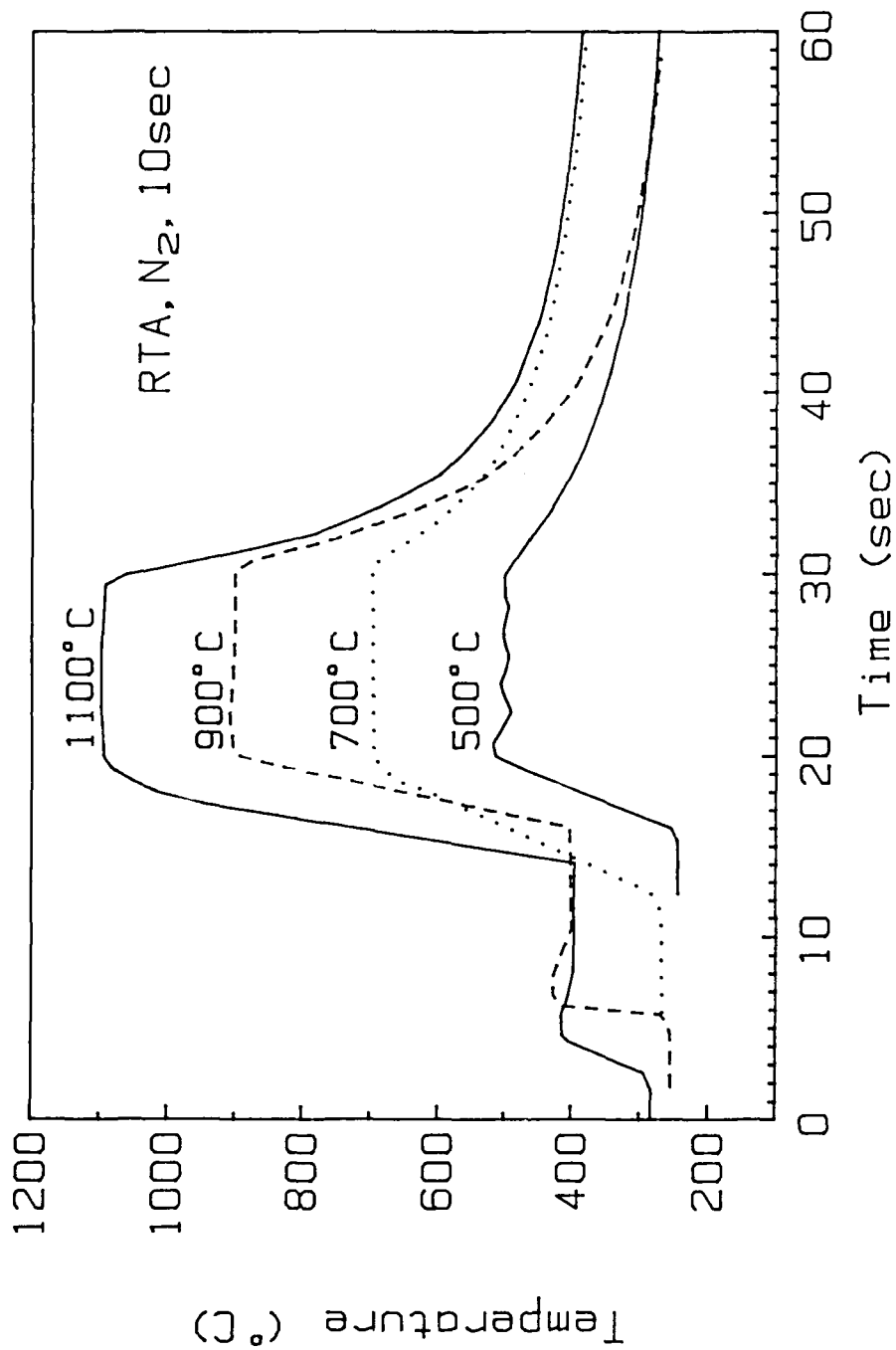
Figure 3.2. Temperature profile of RTA system for 10 sec annealing cycle.

annealing, SiC samples were etched by diluted HF solution (HF:H_2O = 1:50) 1min to remove possible oxide layers, which may disturb the index measurement. When the temperature was lower than 1000°C, no significant change of refractive index was observed during the same annealing period, which is similar to results using conventional furnace annealing[3.2]. The different ambients, Ar, Ar+3%H_2, and N_2 used for index measurements resulted in quite similar values.

The refractive index of as-sputtered SiC films is between 3.0 to 3.6. As shown in Figure 3.3(a) and (b), at annealing temperature of 1000°C and 1050°C, the index does not approach the SiC bulk value of 2.65[3.3], even for annealing times as long as 90sec. However, for annealing temperatures of 1100°C and 1200°C, as shown in Figure 3.3(c) and (d), in only 20sec annealing time the index reaches an average value close to SiC bulk value. The summary of results of index measurements by using the RTA technique for 30sec at different temperatures is shown in Figure 3.4(a). These results are comparable to the conventional furnace annealing process[3.2], shown in Figure 3.4(b). However, the RTA processing time is at least 60 times faster than the furnace operation. This "time" savings is an important factor for not only increasing the throughput but also fabricating advanced design in SiC device applications.

The variation across the wafer of film thickness and refractive index for a 600nm SiC thin film deposited on 3" Si(100) substrate and annealed by RTA at 1100°C, 30sec, in N_2 ambient, is shown in Figure 3.5. A bell-shaped thickness profiles of sputter-deposited material are expected, due to the angular distribution of the sputtering system.
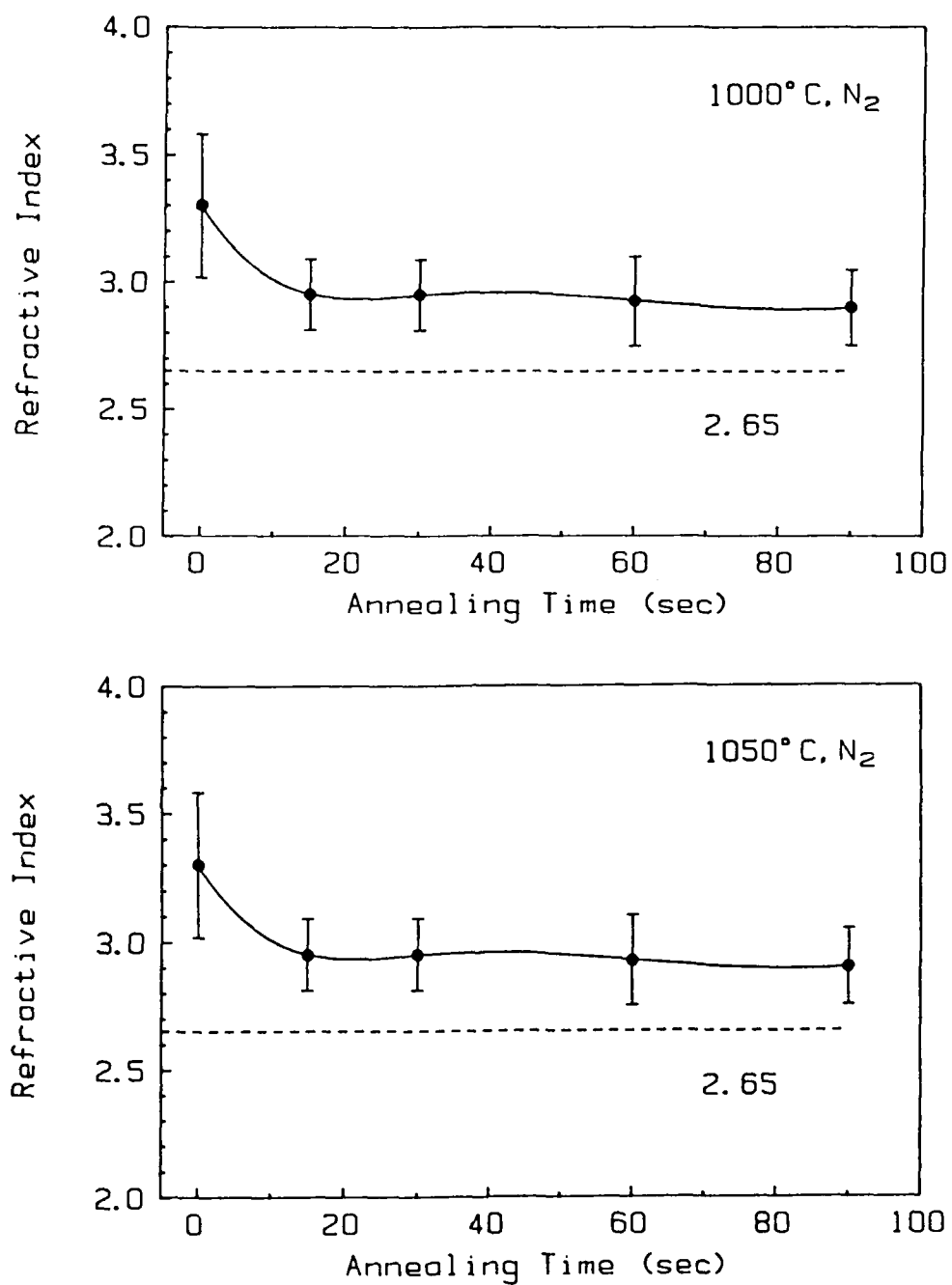
Figure 3.3.   Refractive index of SiC as a function of annealing time at (a). 1000°C, (b). 1050°C.
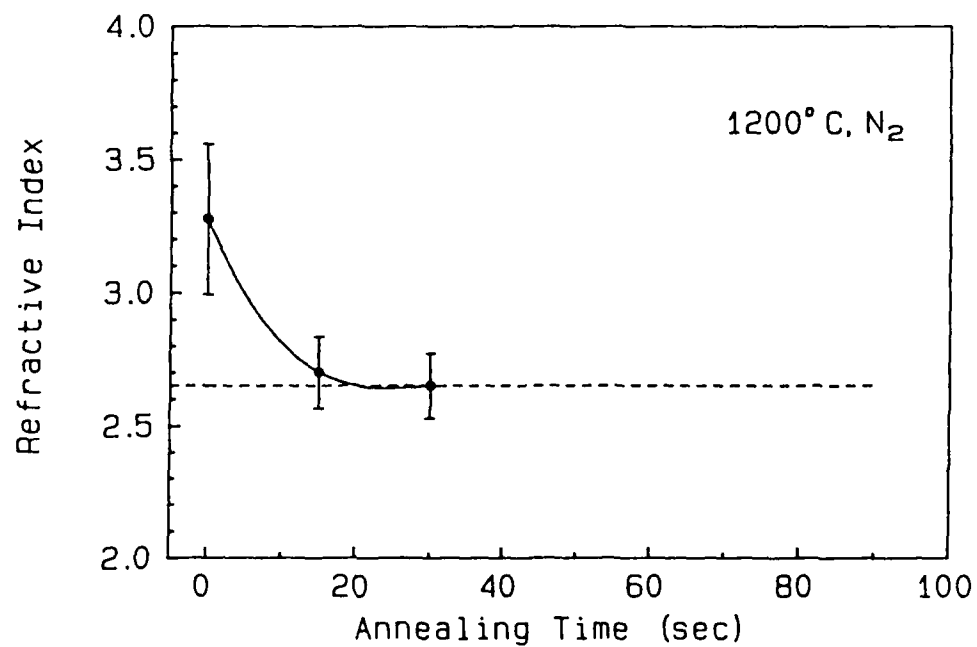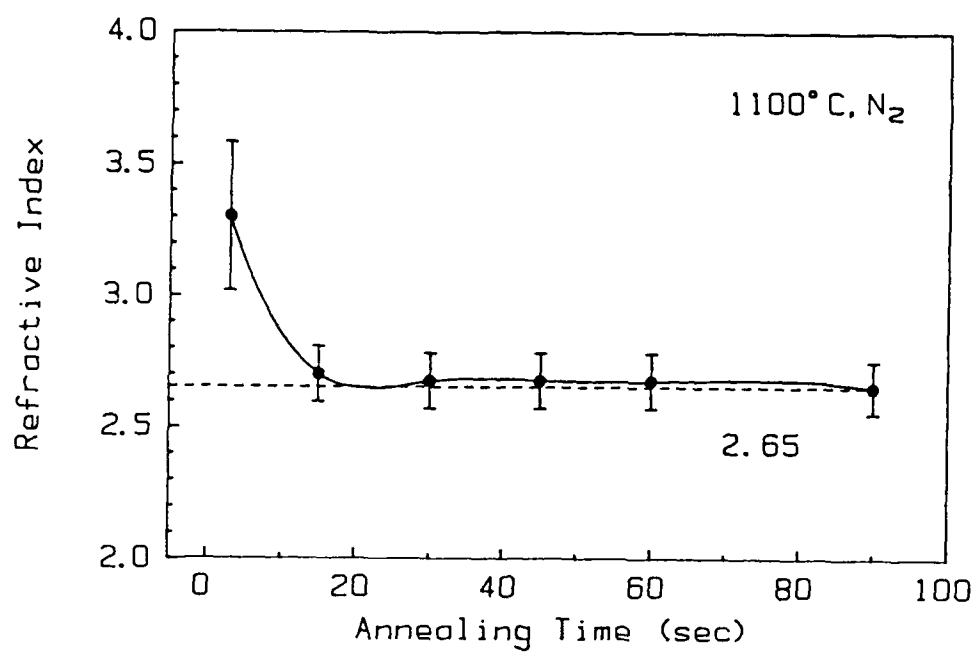
Figure 3.3. Refractive index of SiC as a function of annealing time at (c). 1100°C, (d). 1200°C.
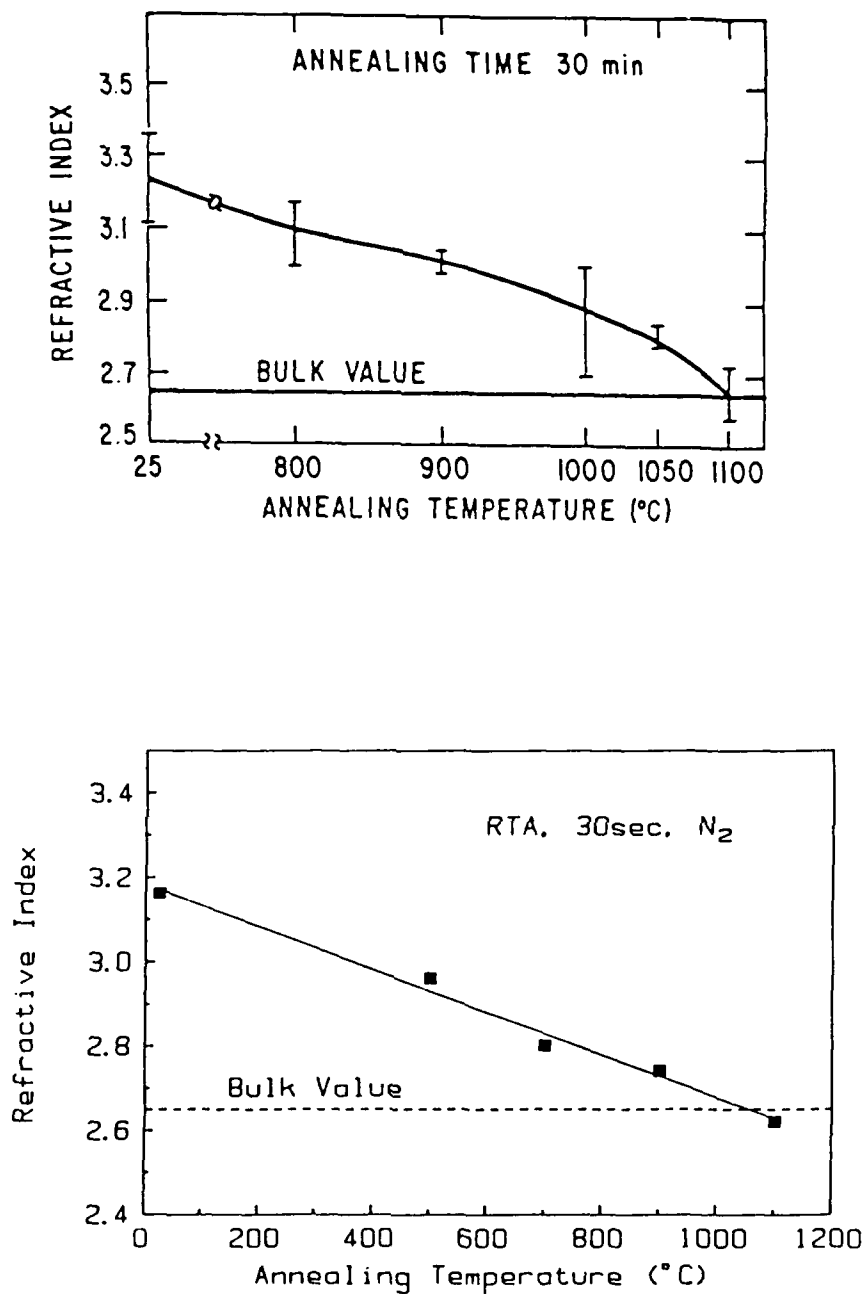
Figure 3.4.   The summary of refractive index as a function of annealing temperature by (a). furnace (30min) (Ref. [3.2]), (b). RTA (30sec).

However, using a large size of target (5") would improve the thickness distribution for large area substrates. The 11% variation of index was caused by nonuniform thermal heating. The edge has a higher heat dissipation rate than the center area, causing the temperature of the edge of wafer to be lower than the center area. The SiC films generally used in this research have a thickness of 600nm and are annealed at 1100°C by either using RTA, 30sec or by furnace annealing, 30min. The center part (close to 2" dia. area) of each 3" wafer is actually used for experiments.

The crystallinity of SiC films after annealing treatment for 1100°C, 30sec furnace is obtained by X-ray diffraction spectroscopy situations was shown in Figure 3.6[3.2]. Only one peak was detected at 35° (corresponding 2.51Å). Therefore, the phase of SiC could not be determined. The Si peak at 70°(1.36Å) corresponds to the (400) plane. For anneals at temperature lower than 900°C, SiC films exhibit an amorphous structure. The crystal structure obtained by RTA is believed to be the same as for the furnace procedure.

3.2.3 Optical Bandgap Measurement of SiC

3.2.3.1 Introduction

The calculation of the band structure was first reported in about 1960[3.4, 3.5] for simple SiC structures, such as cubic SiC. However, the large size of the unit cells of the more common
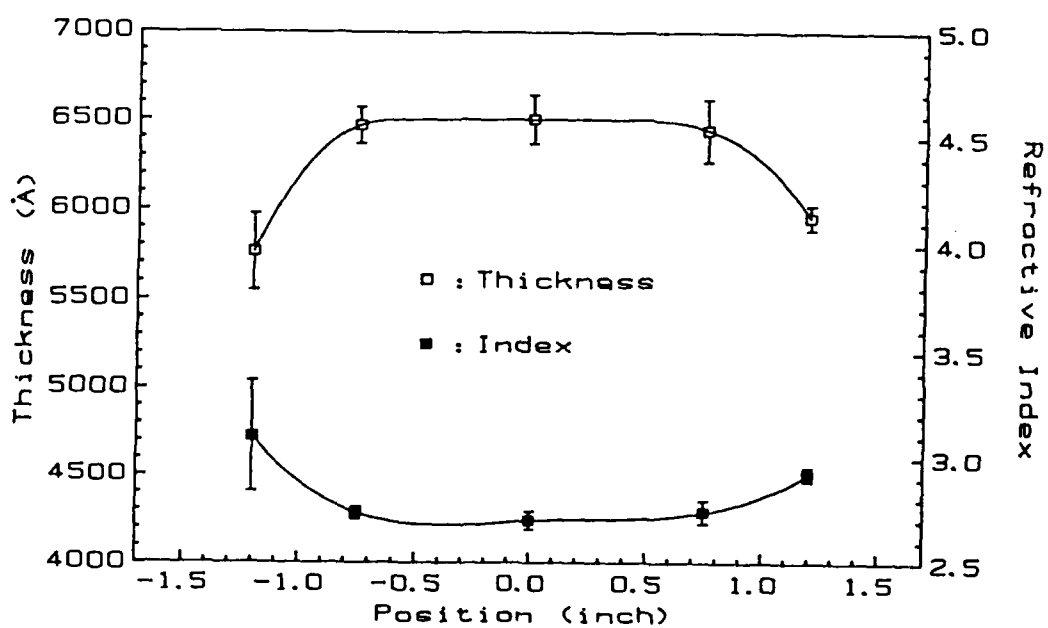
Figure 3.5.   The uniformity of thickness and refractive index of sputtered SiC film as a function of position of a 3" wafer.
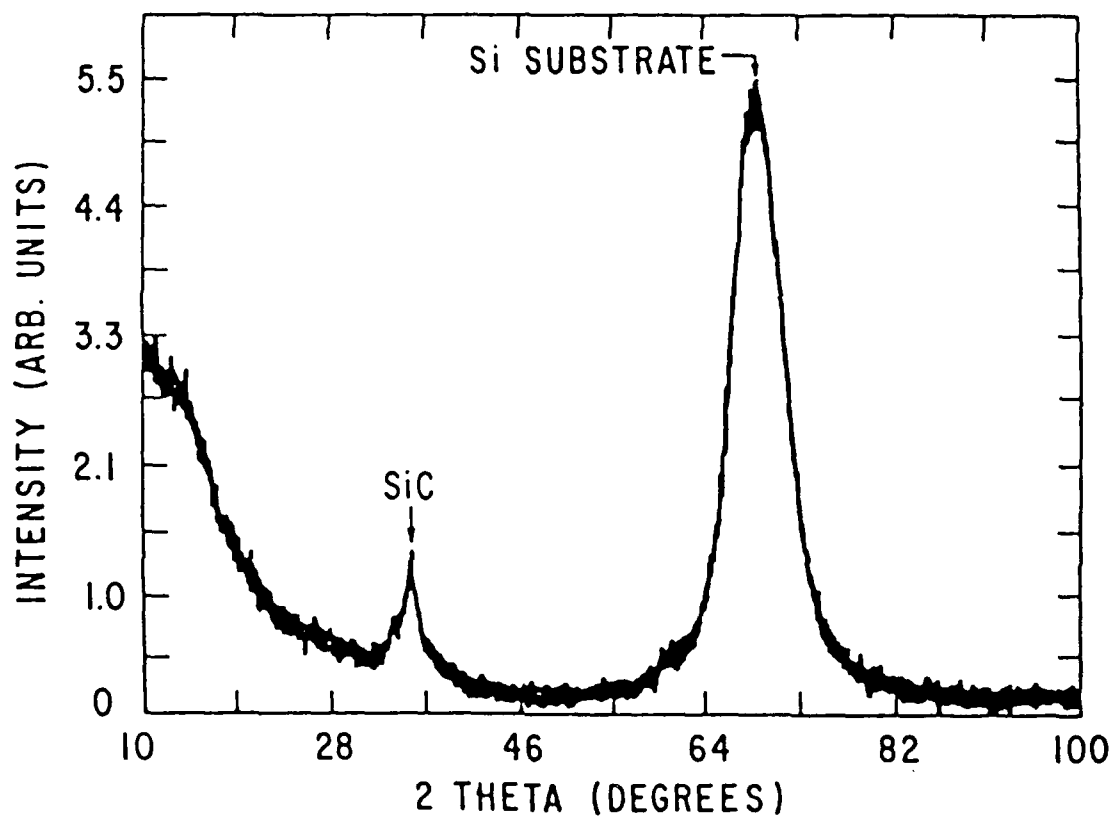
Figure 3.6.   X-ray diffraction spectrum for SiC film (Ref. [3.2]).

polytypes had not been calculated until the greater knowledge of SiC polytypes and better computer facilities were available.

The bandstructure of 2H, 4H and 6H has been studied by Hermal et al.[3.6] and Junginger and Van Haeringer[3.7]. The results suggest that the direct energy gap of all polytypes is nearly the same and the large difference of the optical (indirect) gaps are due to a delicate balance which cause the conduction bands to move up and down.

Herman et al.[3.8] have speculated that the strikingly linear relation between band gap and hexagonality may have a deeper reason. They notice that the lowest conduction band minima of 2H lie at different position in the reduced zone than minima of the other polytypes. For 2H, the conduction band minima are at point K. For the other polytypes they lie along a line joining points L and M. Thus Herman suggests the K-gap and the L-M gap are linearly related to the hexagonality, the former one decreasing and the latter one increasing with increasing hexagonality. Such a correction between hexagonality and bandgap is plausible since the hexagonality is reflected in the axial ratio c/a which in turn is a measure of the lattice distortion. This model is illustrated in Figure 3.7 and the known gap of SiC polytypes are marked.

Optical absorption in solids results from any of the following five principal processes : (1) excitation of crystal vibrations, (2) formation of excitons, (3) excitation of free electron and holes within allowed bands, (4) excitation of free electrons and holes from one band to another of the same type, (5) excitation of electrons across
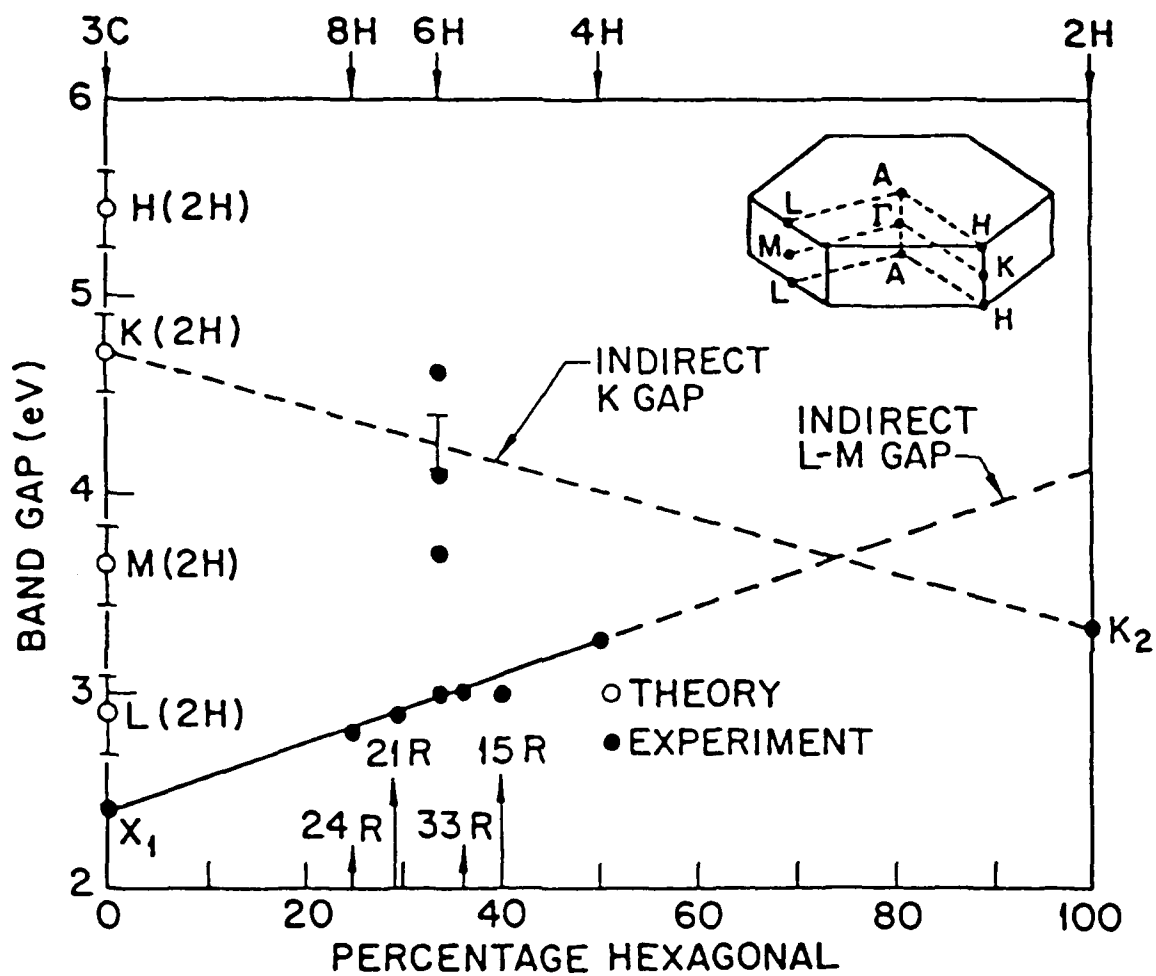
Figure 3.7. Relation between indirect energy gap and hexagonality in SiC polytypes.

the gap from valance band to the conduction band[3.9, 3.10]. Only case (5), involving excitation of electrons across the forbidden gap, gives rise directly to photoconductivity. The abrupt increase of the absorption coefficient a (cm^{-1}) at a certain wavelength indicates that the photon energy matches bandgap energy.

The definition of the direct and indirect transition are shown in Figure 3.8(a). Phonons are involved in the indirect transition for conservation of energy and momentum, as shown in Figure 3.8(b). Theoretical expressions have been derived[3.9-3.11] which permit a discrimination between direct and indirect transitions, not only on the basis of the magnitude of the absorption coefficient involved, but also on the basis of the dependence of absorption coefficient on photon energy. For direct and indirect transitions, the following dependencies are to be expected,

$$a \quad \propto \quad (E_v - E_i)^{1/2} \qquad \text{for direct transition} \qquad (3.1)$$

$$a \quad \propto \quad (E_{pt} - E_G)^2 \qquad \text{for indirect transition} \qquad (3.2)$$

where E_v is the energy of the top of the valence band and E_i is the energy of the initial state from which the transition is made. E_{pt} is the phonon energy and E_G is the difference between E_i and E_v. In actual practice, for allowed transitions for example, a^2 is plotted against photon energy to give a straight line for the direct

transition, and $a^{1/2}$ is plotted against photon energy to give a straight line for the indirect transition. The intercepts of these straight lines on the energy axis give the value of band gap. For indirect bandgap materials, such Si, Ge[3.12, 3.13], two different slopes of absorption coefficient are expected for indirect and direct bandgap energy. Indirect transitions were observed in SiC by Choyke and Patrick[3.14], which could be adequately described by a single phonon energy of 0.09eV over a wide temperature range.

3.2.3.2 Experiments and Results

High quality quartz substrates were used for the SiC optical bandgap measurement, with no absorption of at wavelengths from 200nm to 900nm. The optical absorption measurement was carried out with a Perkin-Elmer 7500 UV system over the wavelength range from 190nm to 900nm.

First, SiC films of different thickness were deposited and measured in the unannealed condition. As shown in Figure 3.9, all data points for unannealed samples fall basically on the same curve. Two different variations of absorption coefficient are apparent for the indirect and direct transition region of the SiC thin film. The 150nm SiC films were then annealed by furnace for 30min or RTA for 30sec at temperatures from 500 to 1100°C in N_2 ambient. The indirect transition was observed in all annealing cases and is shown in Figure 3.10. The data points for the indirect transition region (dash line and lower absorption coefficient) have been replotted

according to Eq. 3.1 and shown in Figure 3.11 for each RTA annealing temperature. The intercept of the x-axis gives the value of the optical bandgap. Similar results were obtained by furnace annealing (FA). The relation of bandgap and annealing temperature has been summarized in Figure 3.12. At first, the band gap shift is rather small, going from 0.95eV in the unannealed situation to 1eV after 500°C RTA. For higher temperature anneals, a linearly increasing bandgap was observed from 1eV to 1.7eV by increasing the annealing temperature from 500°C to 1100°C. For FA, the gap shows little deviation for low temperature anneals (500 to 700°C) and almost same result was obtained for the high temperature region (900 to 1100°C).

Different results has been obtained for various growth procedures of amorphous SiC thin films. A 1.6eV (unannealed) and 2.1eV (600°C 1hr. in vacuum annealing) optical band gap was measured by Fagen[3.15]. From Rahman and Furukawa[2.16], a bandgap of 1.8eV resulted from using plasma chemical vapor deposition (PCVD) to grow SiC thin films at 250°C. The reason for these variations is not clear yet.

3.2.4 Sheet Resistance of W

0.6μm W films have been prepared on oxidized Si(100) substrates and annealed by RTA in Ar gas ambient. The variation of annealing temperature was from 500°C to 1100°C and 0sec to 90sec for annealing time. The sheet resistance of W film was measured by 4-point probe (FPP-100, Veeco system) and a typical result of sheet resistance versus
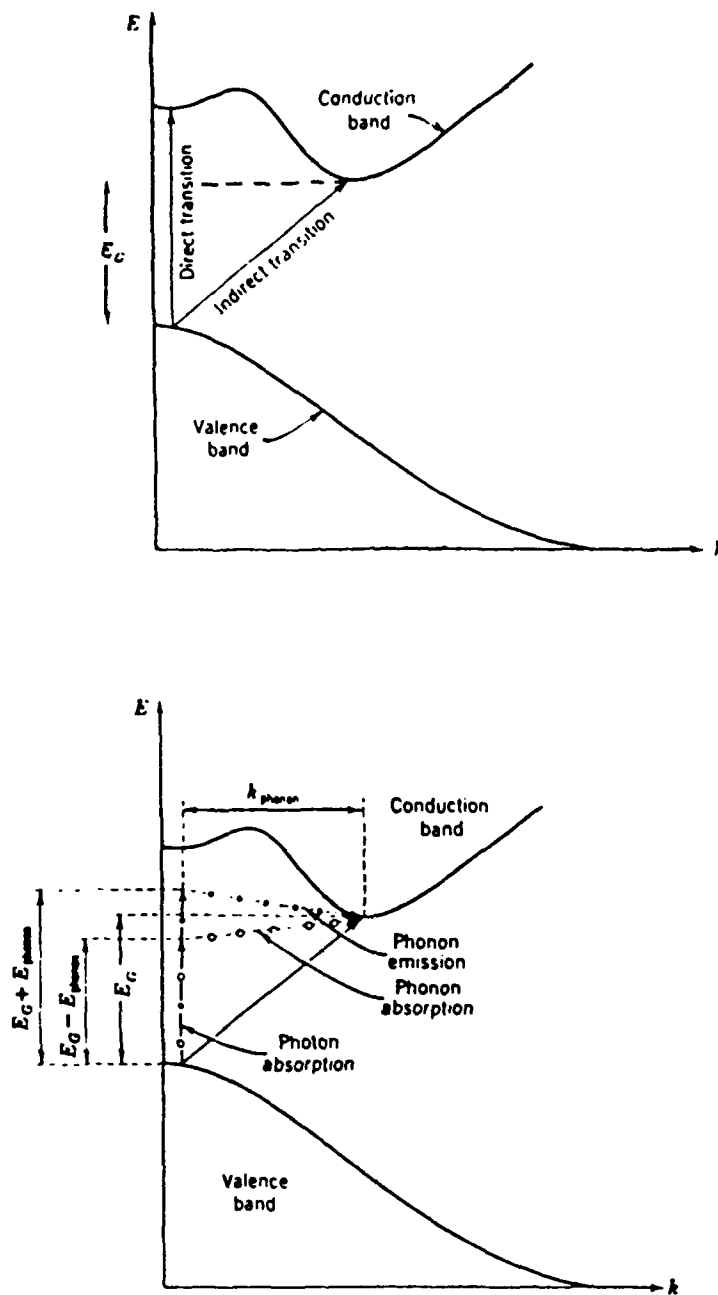
Figure 3.8. (a). Direct and indirect transition between valance and conduction bands, (b). Indirect transitions : absorption and emission phonon.
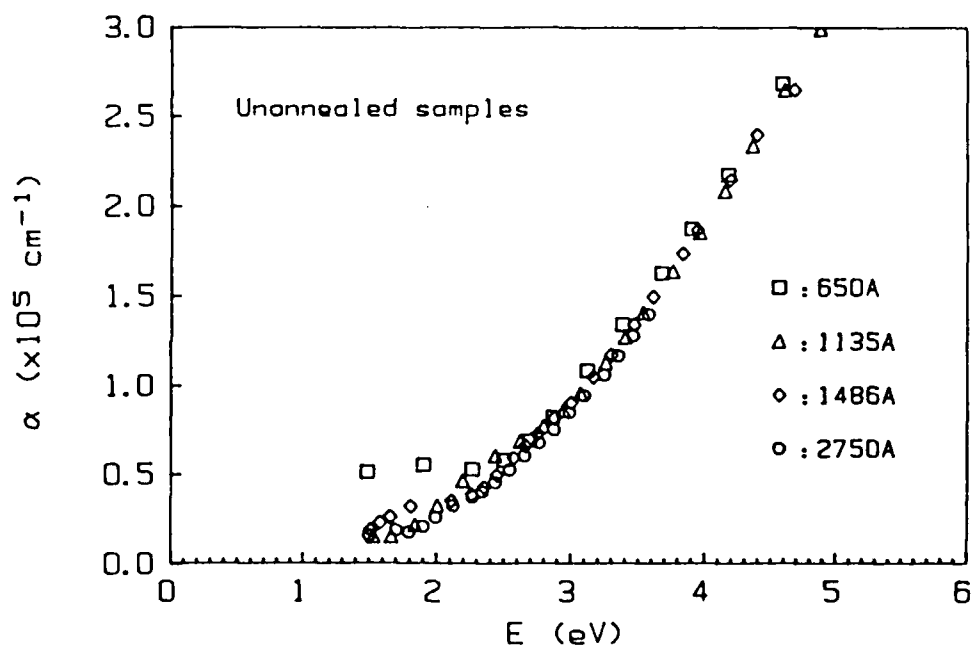
Figure 3.9.   The optical bandgap measurement for unannealed sample at different film thickness.
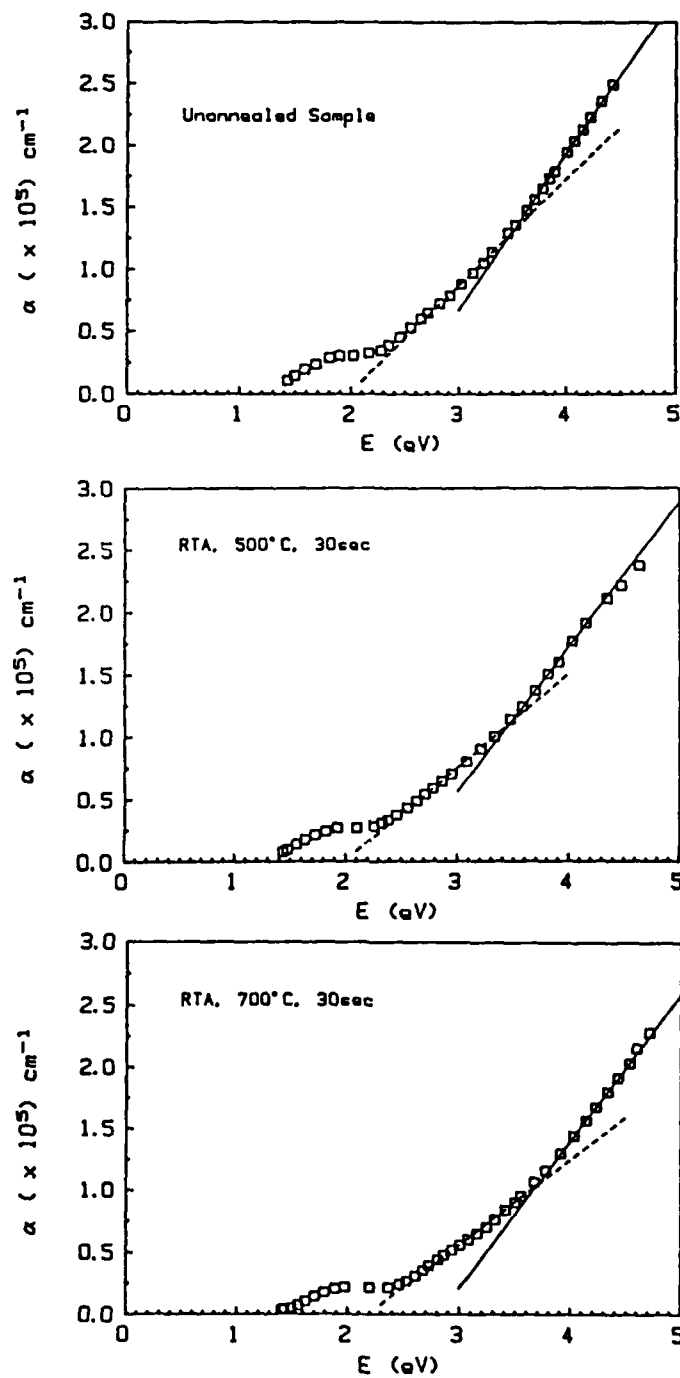
Figure 3.10.   The optical band gap measurement by using RTA in N_2. ambient, 30sec and (a). unannealed, (b). 500°C, (c). 700°C
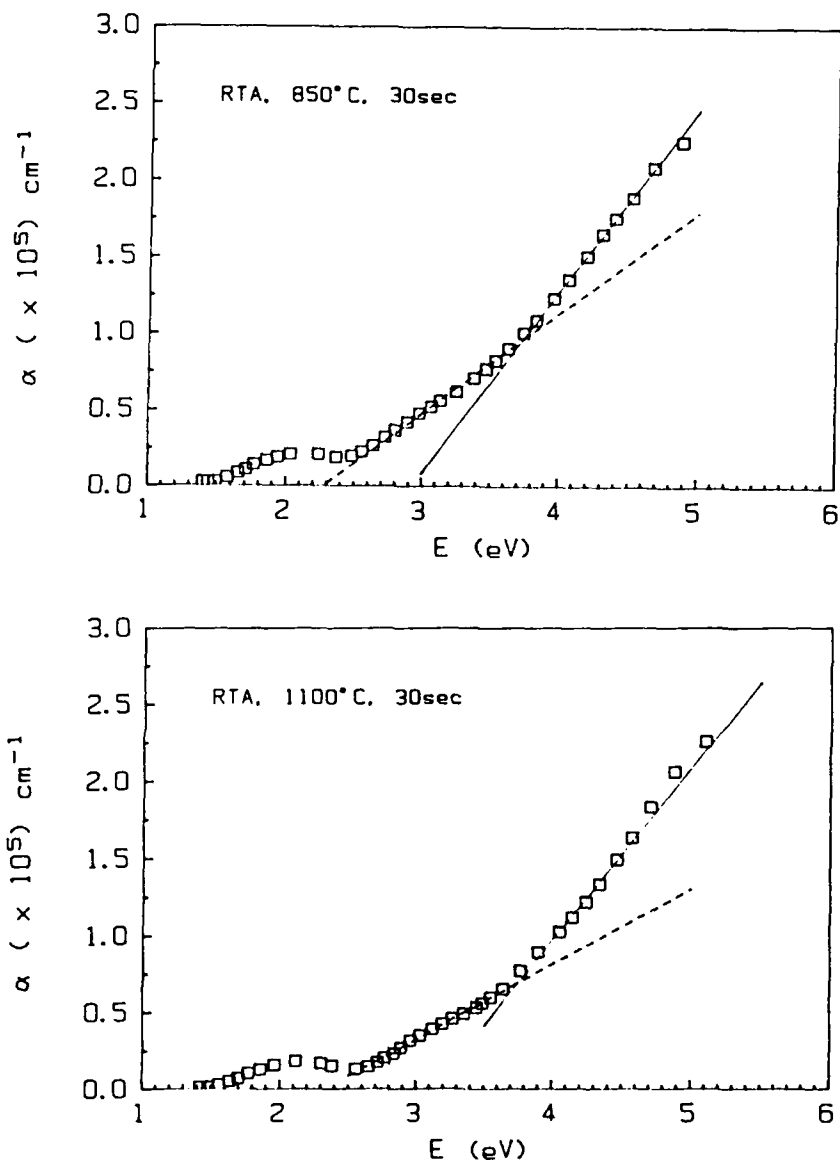
Figure 3.10.   The optical band gap measurement by using RTA in N_2 ambient, 30sec and (d). 850°C, (e). 1100°C
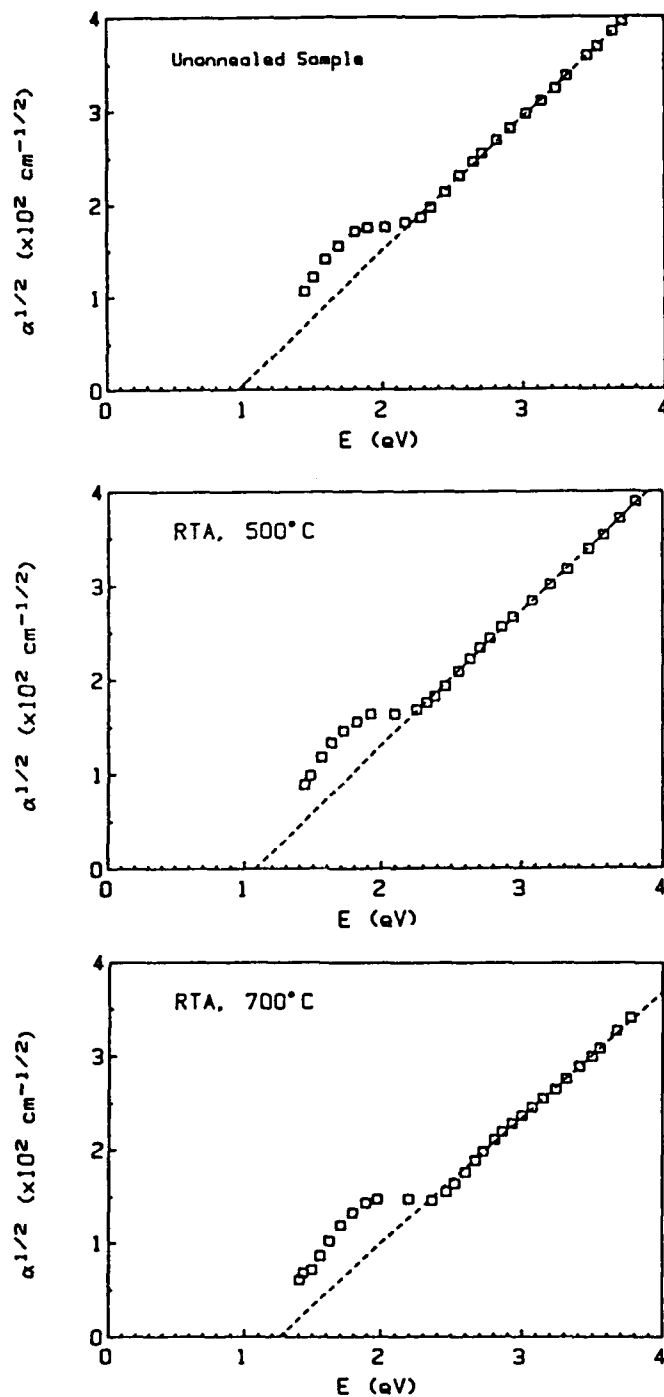
Figure 3.11.   Analysis of absorption spectra by indirect transition of SiC film in (a). unannealed, (b). 500°C, (c). 700°C
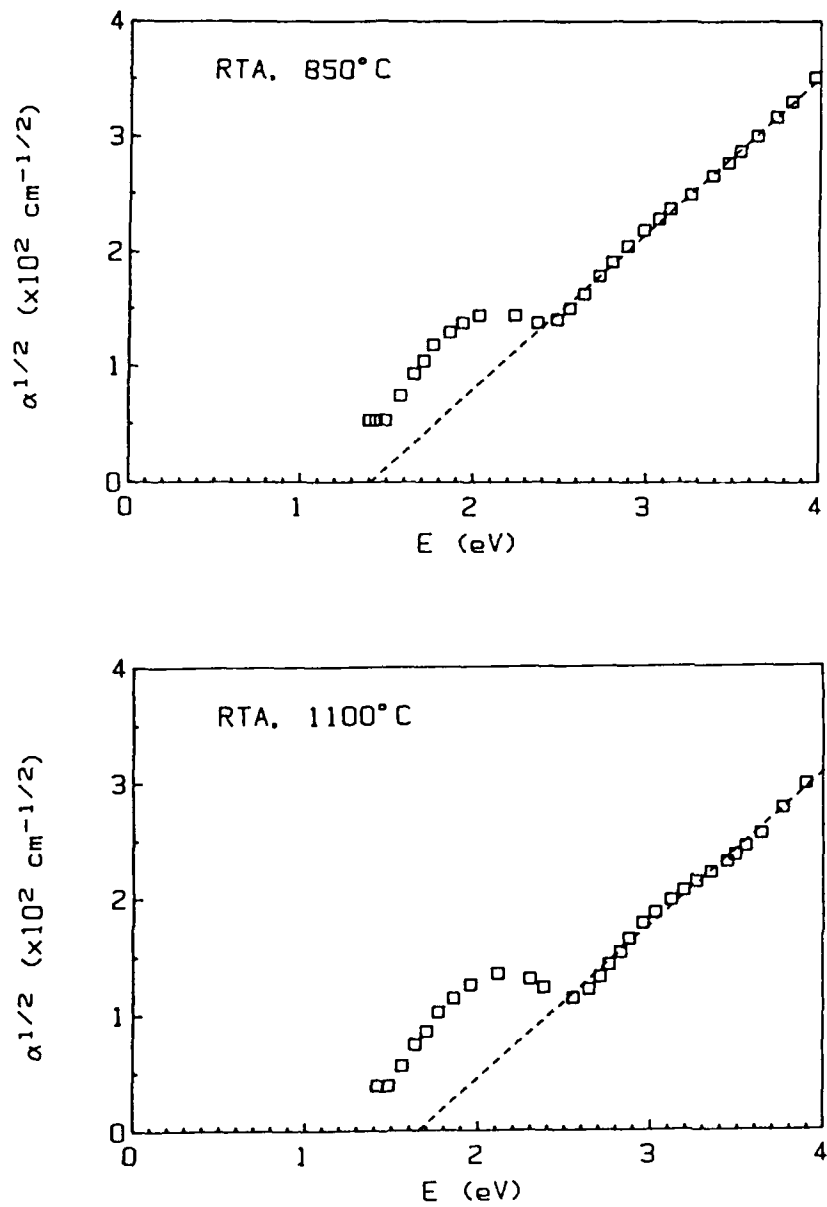
Figure 3.11.   Analysis of absorption spectra by indirect transition of SiC film in (d). 850°C, (e). 1100°C
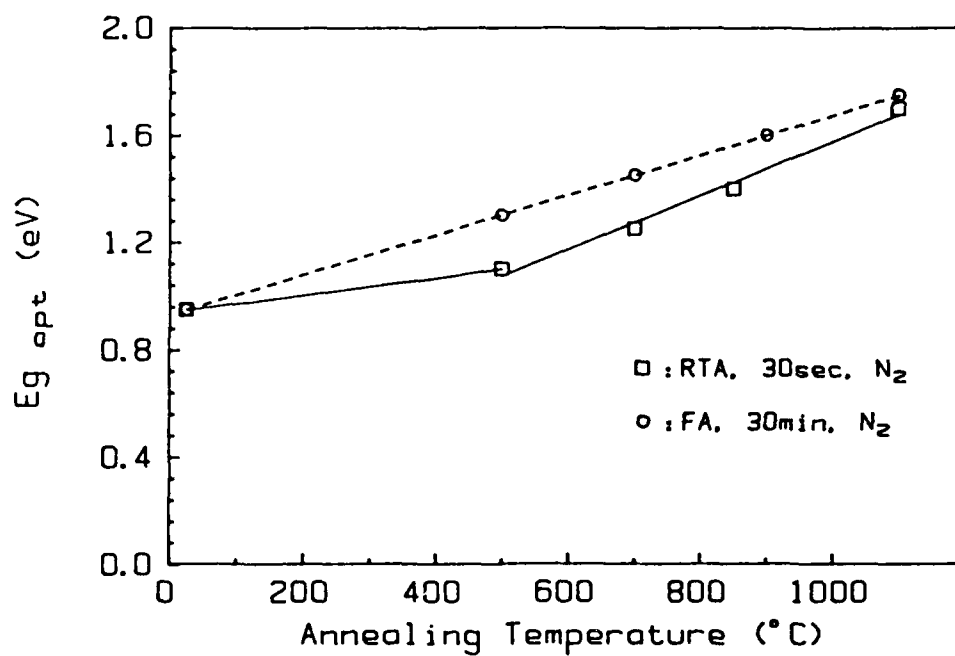
Figure 3.12.   The optical bandgap energy as a function of annealing temperature for furnace, 30min, and RTA, 30sec, in N_2 ambient.

annealing time at 1100°C is shown in Figure 3.13(a). The sheet resistance of W films dropped about a factor of 3 compared to the unannealed condition and only a small variation after 30sec annealing is observed. The behavior at different annealing temperatures, from 500 to 1100°C, is similar except for the final value of the sheet resistance achieved. The summary of temperature effect on W film resistivity at 60sec RTA is shown in Figure 3.13(b) (converted from sheet resistance measurement). Basically, the final resistivity decreased as the anneal temperature increased. A value of 13μohm-cm was obtained by annealing at 1100°C, which is considerably better than that reported for films obtained by the same or similar sputtering techniques but annealed by conventional furnace treatment[3.16, 3.17]. All W films prepared for subsequent etching experiments were deposited on Si or SiO_2 substrate, then annealed by RTA at 1100°C, 60sec in Ar ambient.

3.2.5 Crystallinity of W

X-ray diffraction spectra of W thin films were measured for each annealing temperature at 60sec. It is found that with increasing temperature the W films became more crystalline. The polycrystallinity of W films was confirmed by observing two peaks at 40.3° (corresponding to (110) orientation) and 73.2° (corresponding to (211) orientation). The peak intensity of (110), shown in Figure 3.14, was much stronger than (211). The higher intensity and sharper diffractive peak indicates a higher degree of film crystallinity, as the annealing temperature is increased.
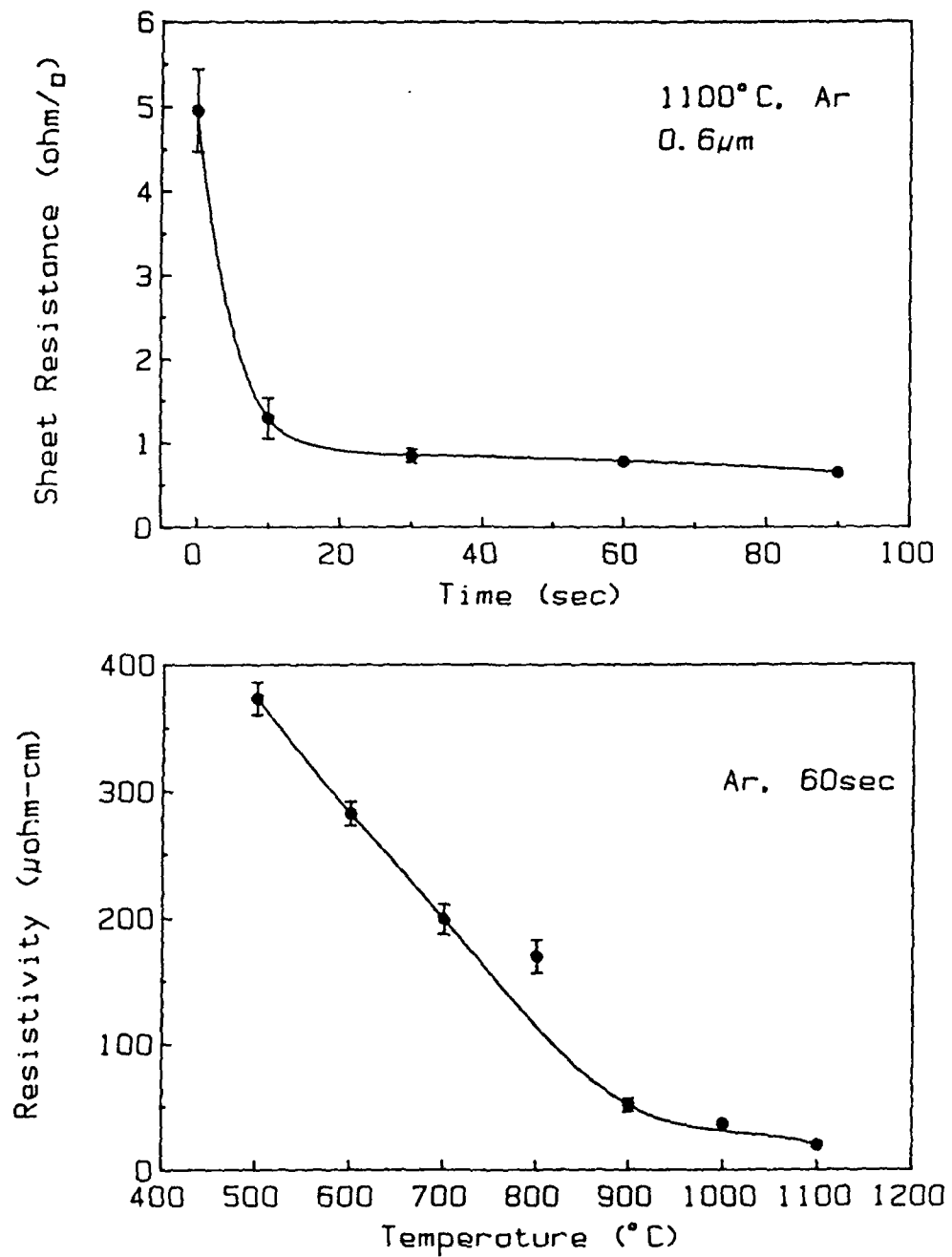
Figure 3.13.   (a). Sheet resistance of W film as function of annealing time, (b). Summary of W film resistivity at 60sec, by RTA.

The oxidation of W film was observed easily by using furnace annealing at temperature higher than 500°C under 1 atm. The WO_c was the major oxide product and can be detected by X-ray diffraction spectra at 25.8° and 30.3°. However, using RTA technique, the oxidation effect of W at high temperature annealing under 1 atm was not found as no oxide peak appeared in the X-ray diffraction spectra in all cases. The W film was still metal-shiny with good adhesion to Si or SiO_2 as deposited.
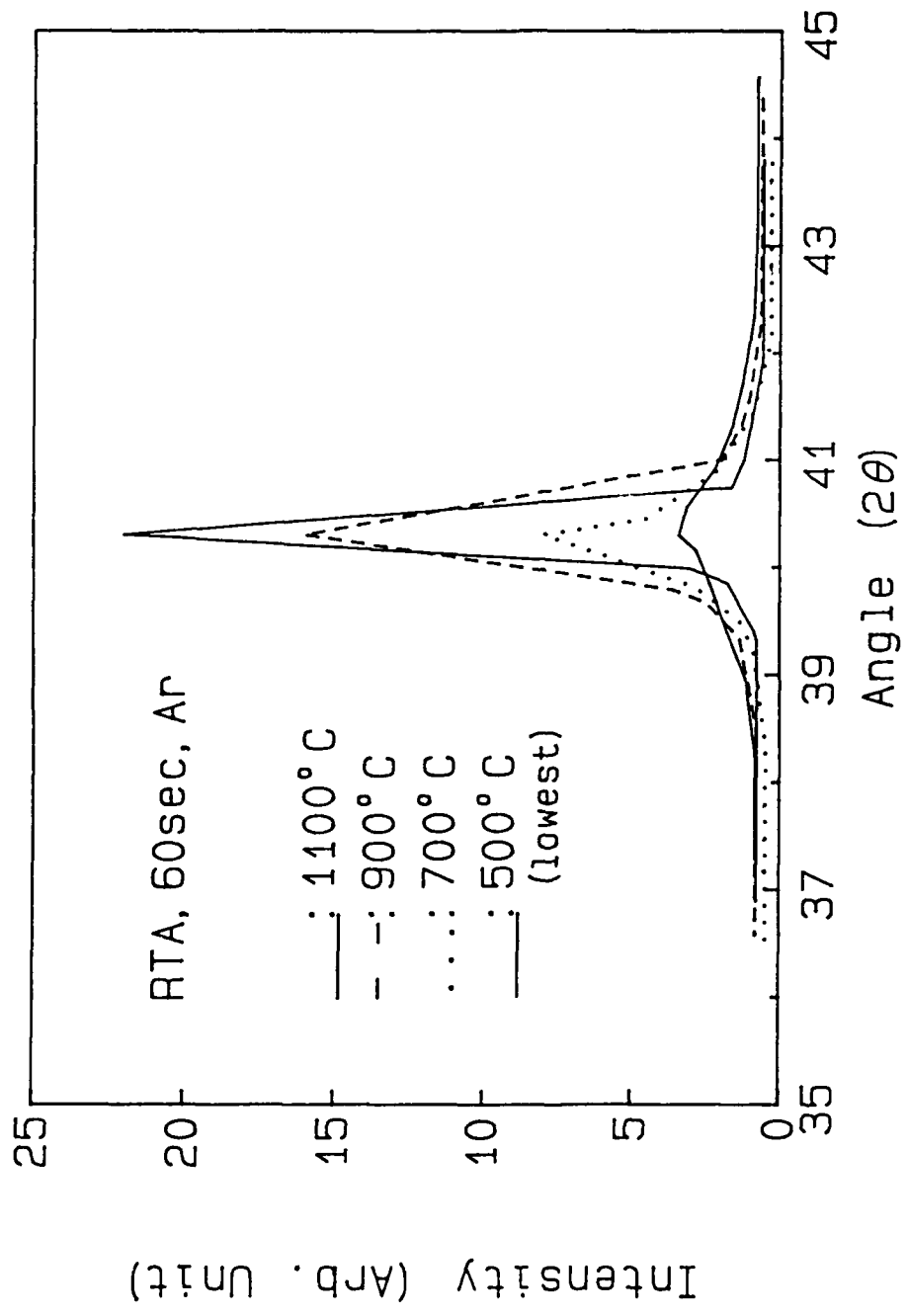
Figure 3.14. X-ray diffraction spectrum of W (110) orientation by RTA in Ar ambient at different temperature and 60sec.

CHAPTER 4

REACTIVE ION ETCHING : SILICON CARBIDE

4.1 Experimental Procedure

4.1.1 Equipment Setup

The etching experiments were carried out in a parallel plate reactor (Plasma Therm PK1241 PE/RIE Dual System) with a diffusion pump system, as shown in Figure 4.1(a). The base pressure of the system was less than 2×10^{-5} Torr. A cross sectional view of the reactor chamber and the computer-controlled grating monochromator are shown in Figure 4.1(b). The figure indicates the ground electrode, power electrode, gas flow direction, sample loading position, and exhausting pump. A 3" electrode space was used. The monochromator was placed on the sidewall of chamber to monitor the optical emission spectra in the wavelength range between 200 and 800nm within the plasma. The corresponding wavelength of each species were determined by experience, experiment and Ref. [4.1]. The DC self-bias of the RF electrode was also monitored. The fluorinated gases used in this investigation were CF_4(99.9% purity), SF_6(99.997%), $CBrF_3$(> 99%) and CHF_3 (> 98%) mixed with O_2 (99.99%) and had these calibration factors : 0.42, 0.26, 0.37, 0.5, 1.0 for the mass flow controllers.

The samples prepared for experiments were of small size such that the area ratio of sample to power electrode was less than 1%. Therefore, the samples will not disturb the plasma conditions during processing. To
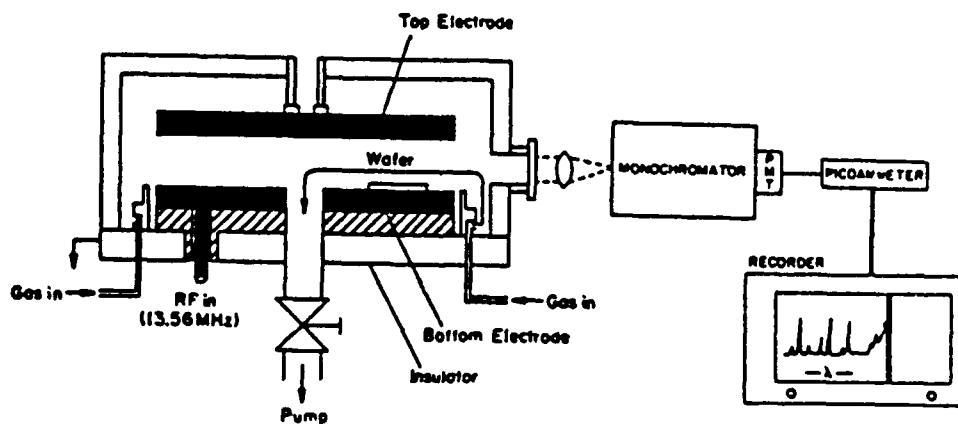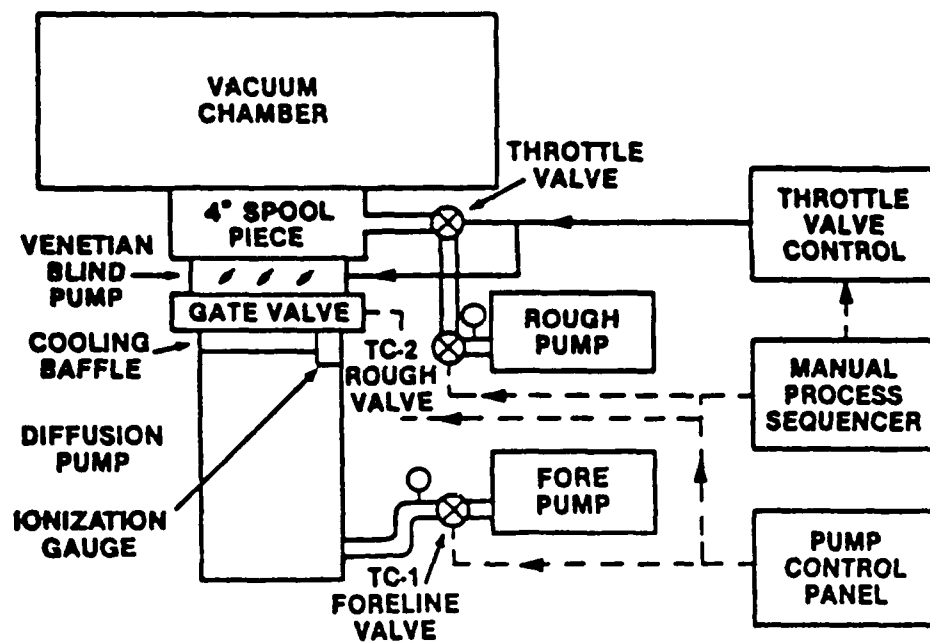
Figure 4.1. (a). The reactive ion etching system, (b). The scheme of chamber and monochromator.

provide a suitable basis of comparison, initially, the RF power, pressure and gas flow rate were generally kept constant at 200W(0.42W/cm^2), 20mTorr and 20sccm for all gases. Then, under a certain composition of gas mixture, which exhibited the best SiC-to-Si or W-to-Si etch rate ratio or the highest SiC and W etch rate, the power and pressure were changed independently to optimize the selectivity and etch rate.

To determine the etch rate in various ambients, Al was used as a thin film mask since it is suitable for both low and high percentage of oxygen. The Al mask was subsequently removed by wet etching for step height determination by profilometer (Dektak). Samples with deeply etched patterns were used to observe the anisotropic etching phenomena by scanning electron microscopy (SEM : Nanometrics Cwickscan II). The composition versus depth profiles of both pre- and post- plasma etched SiC samples were obtained by Auger electron spectroscopy (AES) (Perkin-Elmer : Scanning Auger Microprobe 545C) with 5keV Ar ion beam : Si (92eV), C(272eV), O(503eV), F(647eV), Al(1396eV). The system sensitivity factor for each element (0.3, 0.15, 0.42, 0.48, 0.07), was applied to normalize the peak intensity.

4.1.2 Actinometry Techniques

The concentrations of plasma species which are the reactants during etching are not necessarily linearly proportional to their emission intensities. Noble gas (Ar or N_2) actinometry [4.2, 4.3] has been used of the plasma to promote species from the ground state to the excited state responsible of the optical emission. Thus one can obtain the relation

between measured emission intensity and actual concentration in the plasma. In this work, the Ar actinometry technique was used and the relative concentrations of plasma species, such as F, O, H, and Br were deduced from their emission intensities in different fluorinated gas mixtures[4.4, 4.5]. During experiments, a small amount of Ar gas, 0.6sccm (3%), was added to the constant total flow rate of 20sccm. A linearly increasing Ar(750nm) emission intensity with increasing Ar flow rate was observed, in agreement with previous results. The addition of the Ar gas to the feed dose not alter the emission intensity of the other species present in plasma under different etching gases and conditions. Therefore, all data presented in this work have been calibrated to their relative concentrations simply by dividing their emission intensity by Ar emission intensity. The examples of normalized Ar intensity in CF_4, SF_6, $CBrF_3$ and CHF_3 with different percentage of oxygen plasma at 200W, 20mTorr and 20sccm conditions, shown in Figure 4.2, were used to calculate relative species concentration in each gas.
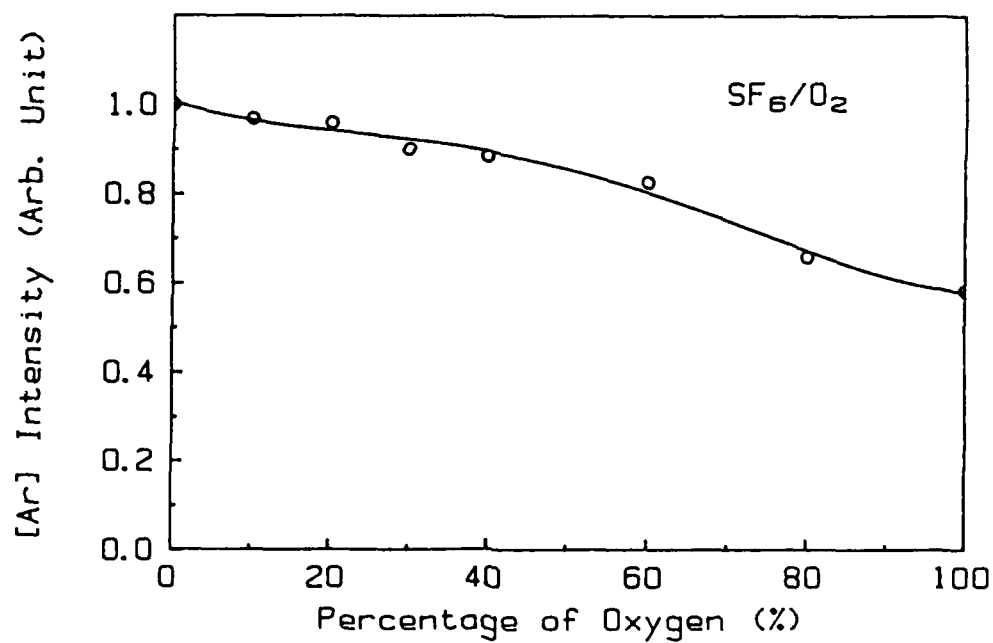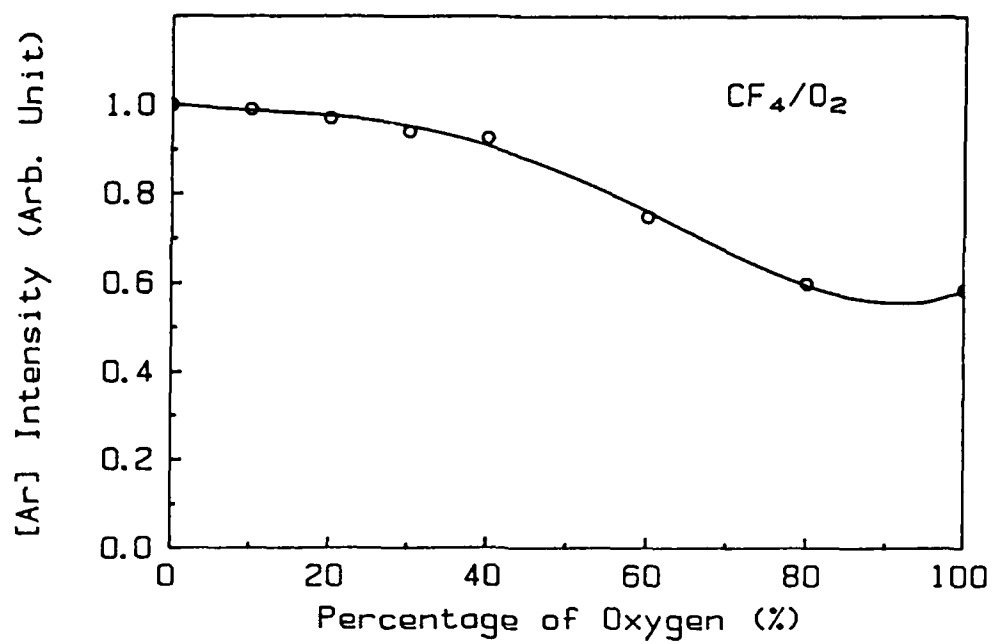
Figure 4.2.   Normalized Ar emission intensity as a function of percentage of oxygen in (a). CF_4, (b). SF_6 plasma.
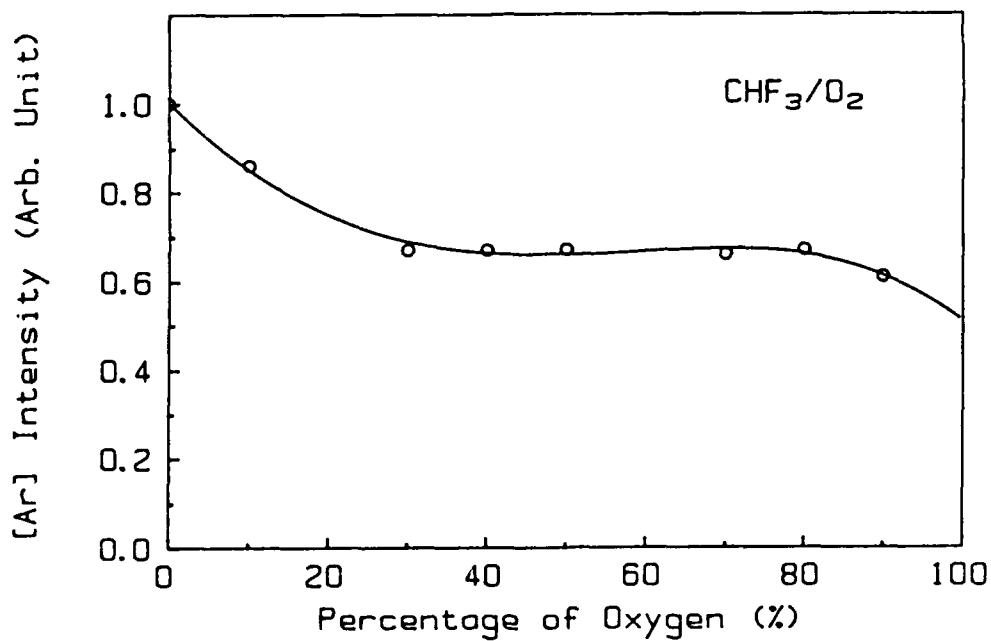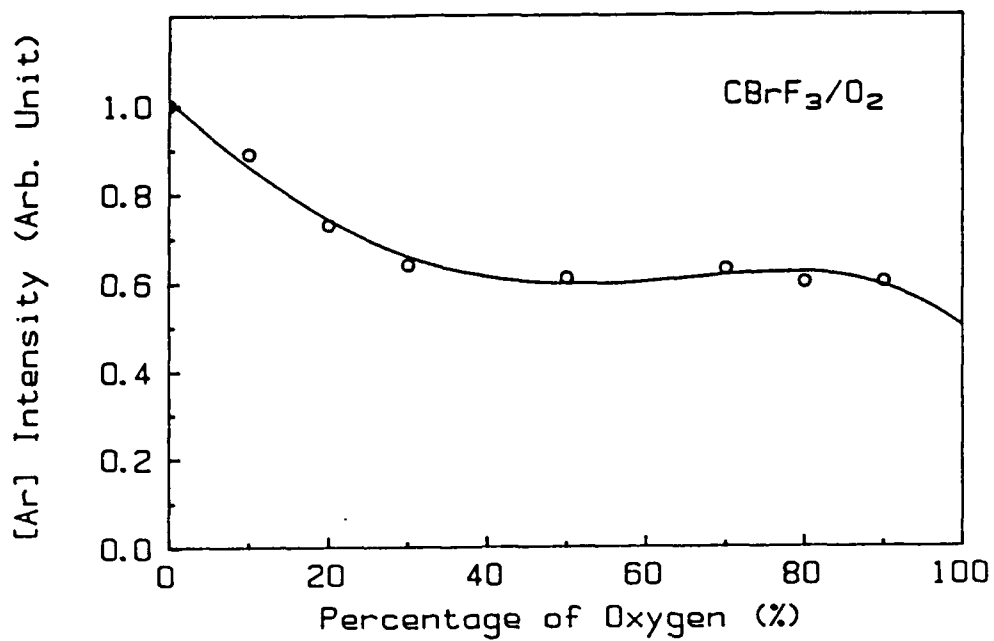
Figure 4.2.   Normalized Ar emission intensity as a function of percentage of oxygen in (c). $CBrF_3$, (d). CHF_3 plasma.

4.2 SF$_6$/O$_2$ Plasma

4.2.1 Percentage of O$_2$

First, the etch rates were determined as a function of oxygen percentage in SF$_6$ gas plasma. In Figure 4.3(a), the SF$_6$/O$_2$ plasma is investigated and the SiC, Si and SiO$_2$ etch rates are shown as a function of oxygen percentage (from 0% to 90%) at a pressure of 20 mTorr, a total flow rate of 20 sccm and power of 200W. The highest SiC etch rate measured is 53.3nm/min at 35%O$_2$, where the etch rates of Si and SiO$_2$ are 1.4μm/min and 60nm/min. The maximum etch rate of Si, 2.1μm/min, is at 10%O$_2$. No etch rate ratio of SiC to Si higher than unity was found in SF$_6$/O$_2$ plasma, even at 90%O$_2$. The SiO$_2$ etch rate is similar to that at SiC. In Figure 4.3(b) is shown the corresponding DC self-bias and the relative density of fluorine [F](703nm) and oxygen [O](777nm). A typical emission spectrum of SF$_6$/35%O$_2$ plasma at 200W, 20mTorr, 20sccm in RIE mode is shown in Figure 4.4, where a few plasma products, such as [SO](258nm), [SO$_2$](315nm), [Ar](750nm), [F] and [O], were marked at different wavelengths. The fluorine concentration reaches its maximum value at 30-40% O$_2$, then decreases as oxygen increases. The DC bias linearly increases from -285V at 0%O$_2$ to -400V at 90%O$_2$. Fixing the oxygen composition at 35%O$_2$, the pressure and power were varied to optimize the etching rate.
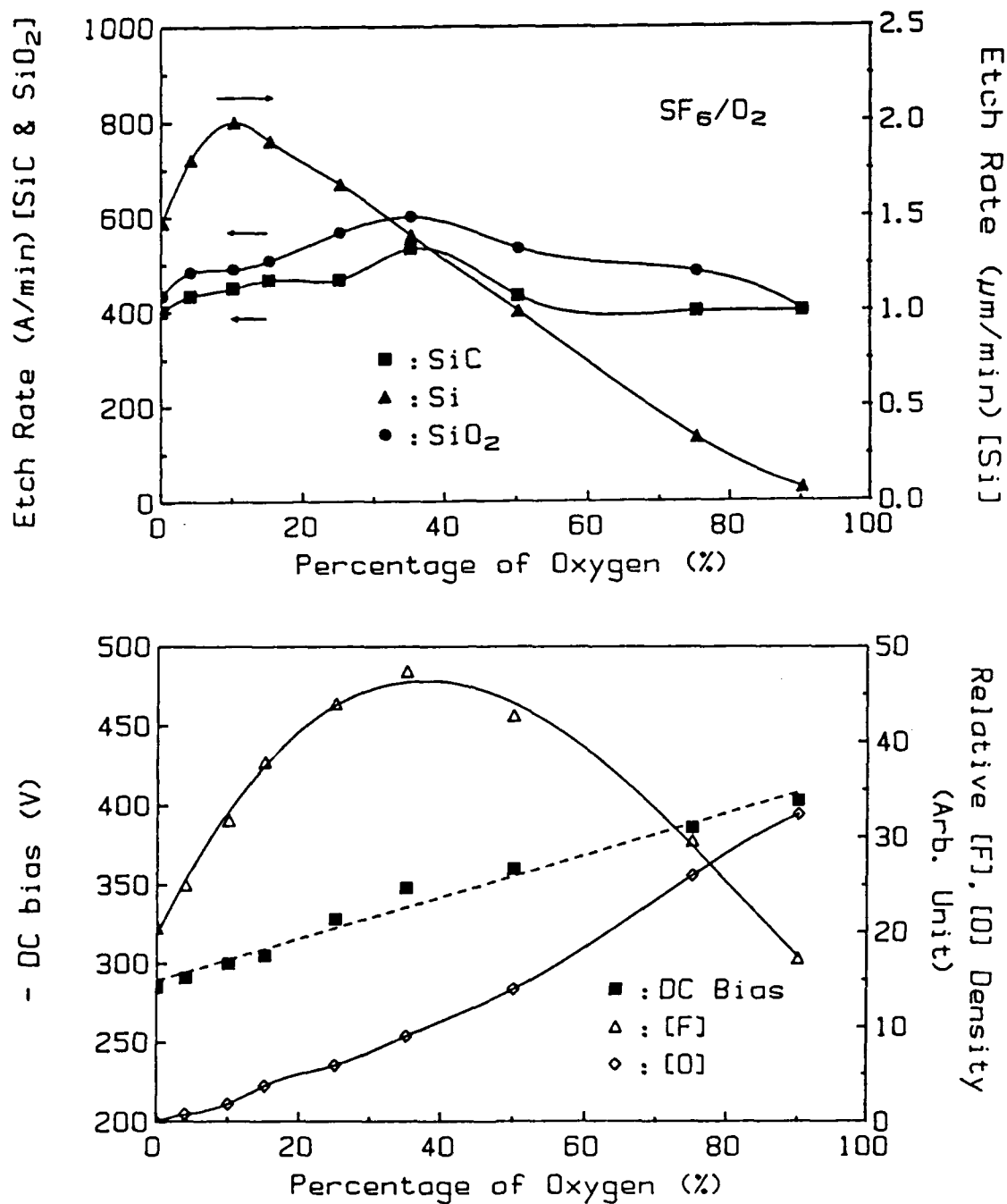
Figure 4.3. (a) Etch rates of SiC, Si and SiO_2, (b) -DC self bias and relative fluorine, oxygen density as a function of O_2 in SF_6 + % O_2.
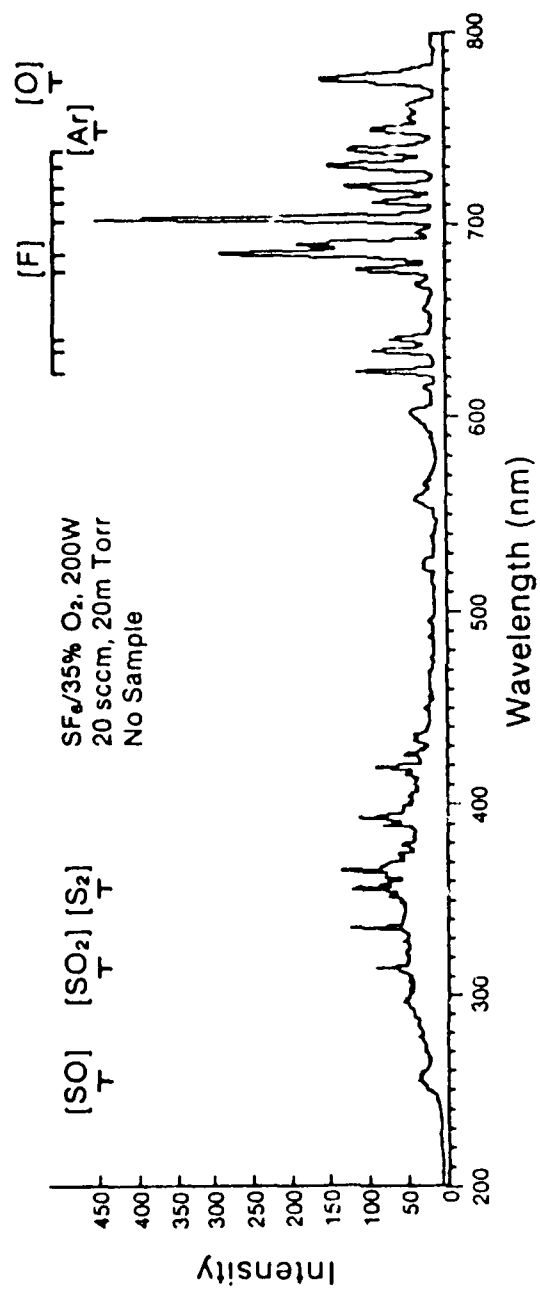
Figure 4.4. Plasma emission spectrum of $SF_6/35\%O_2$ for no sample situation

4.2.2 Pressure

In Figure 4.5(a) and (b), the etch rate versus pressure (from 20mTorr to 256 mTorr) is shown along with the DC self-bias and the [F] and [O] densities for an RF power of 200W and a flow rate of 20sccm at 35%O_2. The SiC etch rate and the DC bias decreased rapidly when the pressure increased. The Si etch rate followed the trend of the fluorine density reaching its maximum value of 5.34μm/min at 200mTorr. The highest reverse selectivity of SiC to Si is 1:267 at 200mTorr and the corresponding etch rate of SiC is 20nm/min. At 50mTorr, the etch ratio, 2.1:1, of SiC to SiO_2 is obtained, where the etch rate of SiO_2 reaches its highest value, 75nm/min.

4.2.3 Power

The effect of varying the power from 50 to 300W etching of SiC at 35%O_2 at 20sccm and 20mTorr is shown in Fig. 4.6(a) and (b). The etch rates of all samples increased linearly with increasing power up to an RF power of 250W. When the power is higher than 250W, the etch rate of Si and SiO_2 and the fluorine density saturate. However, the SiC etch rate continues to increase with power and reaches its highest value of 100nm/min. In spite of the saturation in fluorine concentration. In Figure 4.6(b), the variation of oxygen concentration with power is seen to be small, only 30% increase over the power range from 50W to 300W. However, an 83% change is obtained in the fluorine concentration under same conditions.
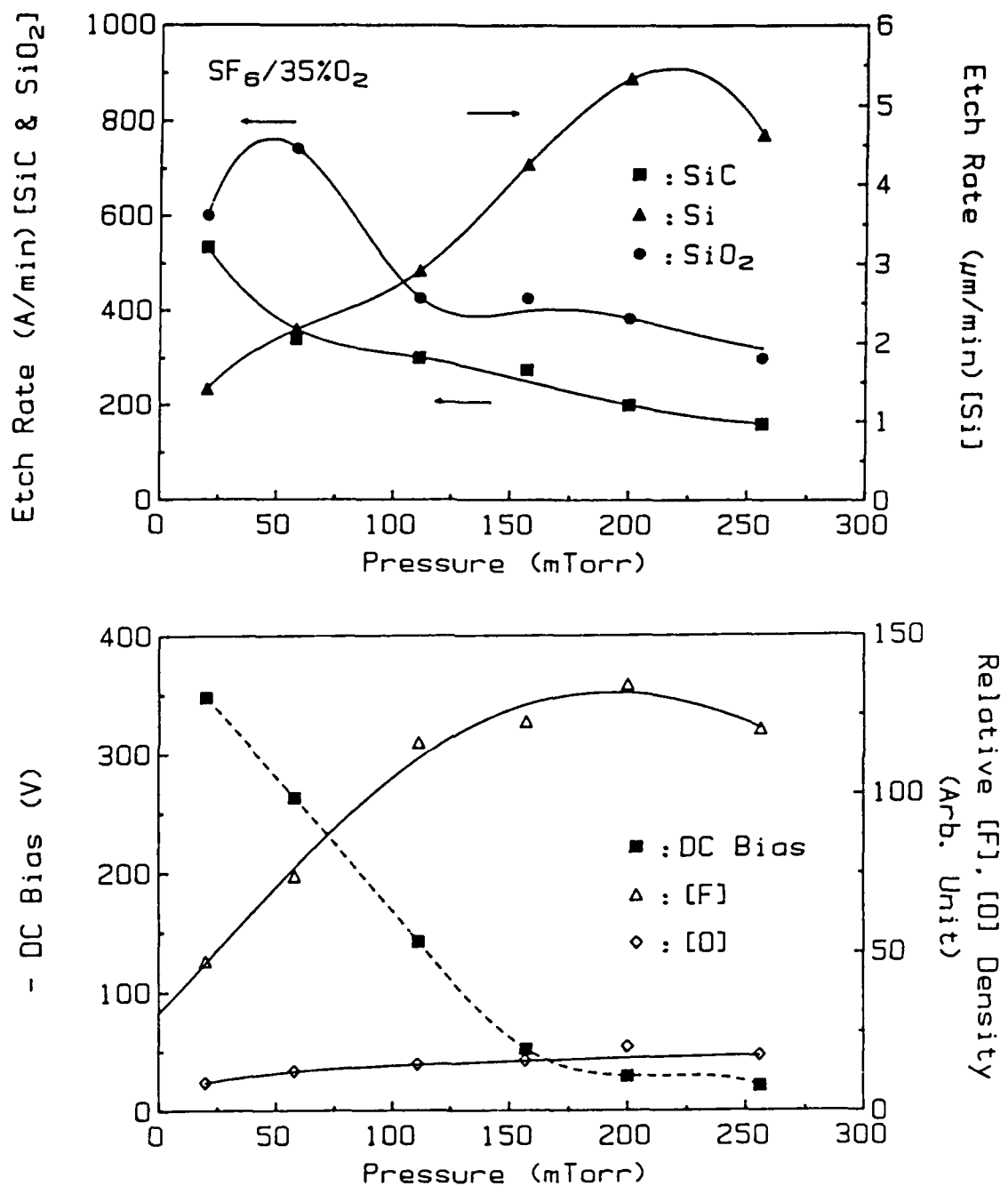
Figure 4.5. (a) Etch rates of SiC, Si and SiO_2, (b) -DC self bias and relative fluorine, oxygen density as a function of pressure in SF_6 + 35% O_2 at 200W.
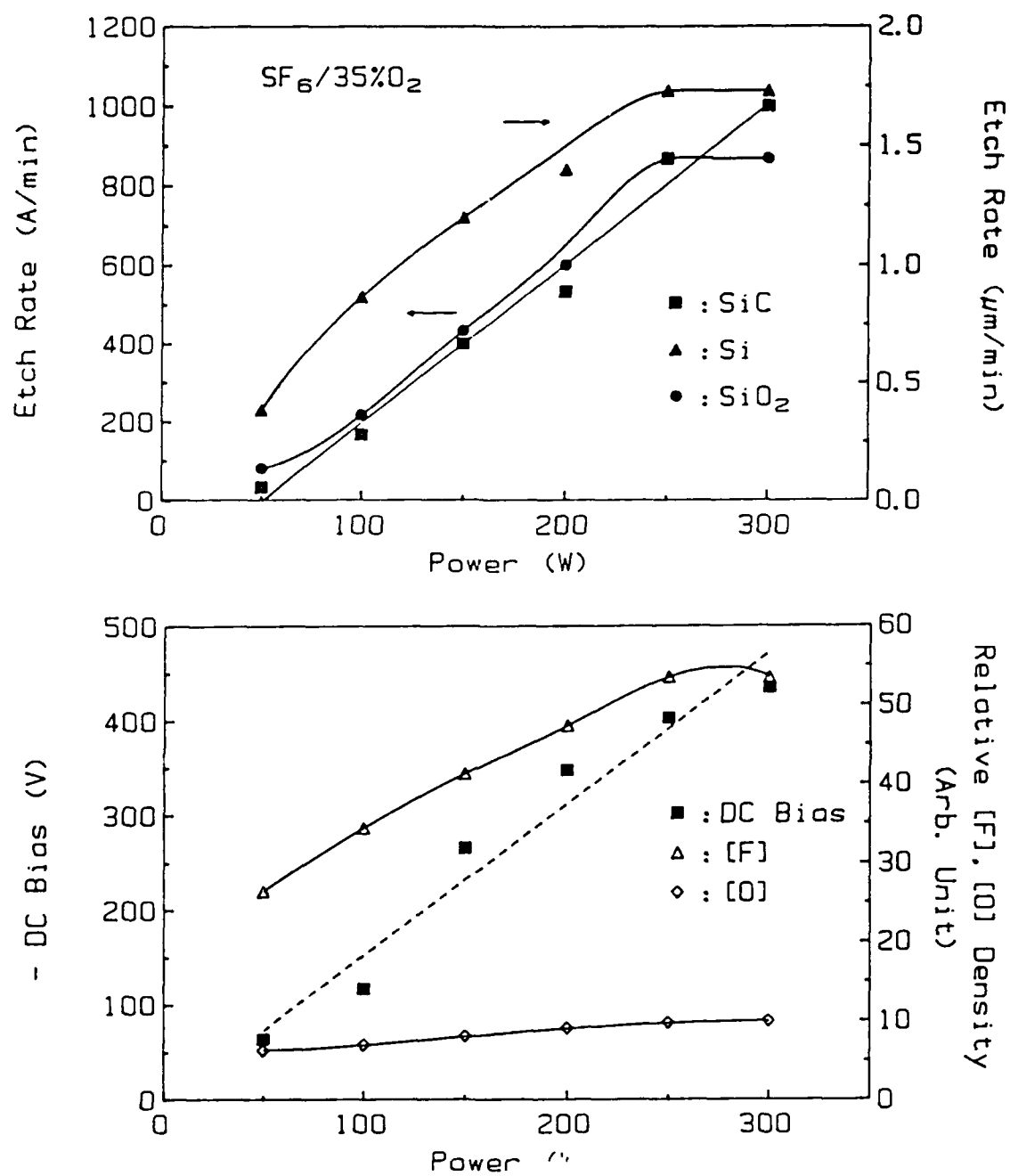
Figure 4.6. (a) Etch rates of SiC, Si and SiO_2, (b) -DC self bias and relative fluorine, oxygen density as a function of power in SF_6 + 35% O_2.

4.2.4 SF_6/90%O_2 Plasma

The pressure dependence experiment was repeated at high percentage of oxygen in SF_6 plasma. Results are shown in Figure 4.7(a) and (b) for SF_6/90%O_2 , 200W, 20sccm plasma conditions. The SiC etch rate reached its maximum etch rate, 50nm/min, at 68mTorr and then decreased as pressure increased. This behavior is quite different from pressure dependence experiment in 30%O_2 plasma. A maximum etch rate of 46nm/min is measured for SiO_2 at the same pressure. The etch rate of Si increases monotonically with the pressure, still basically following the variation of fluorine density even at such a high composition of oxygen. The DC bias decreases linearly, while both oxygen and fluorine density increase as pressure increases.
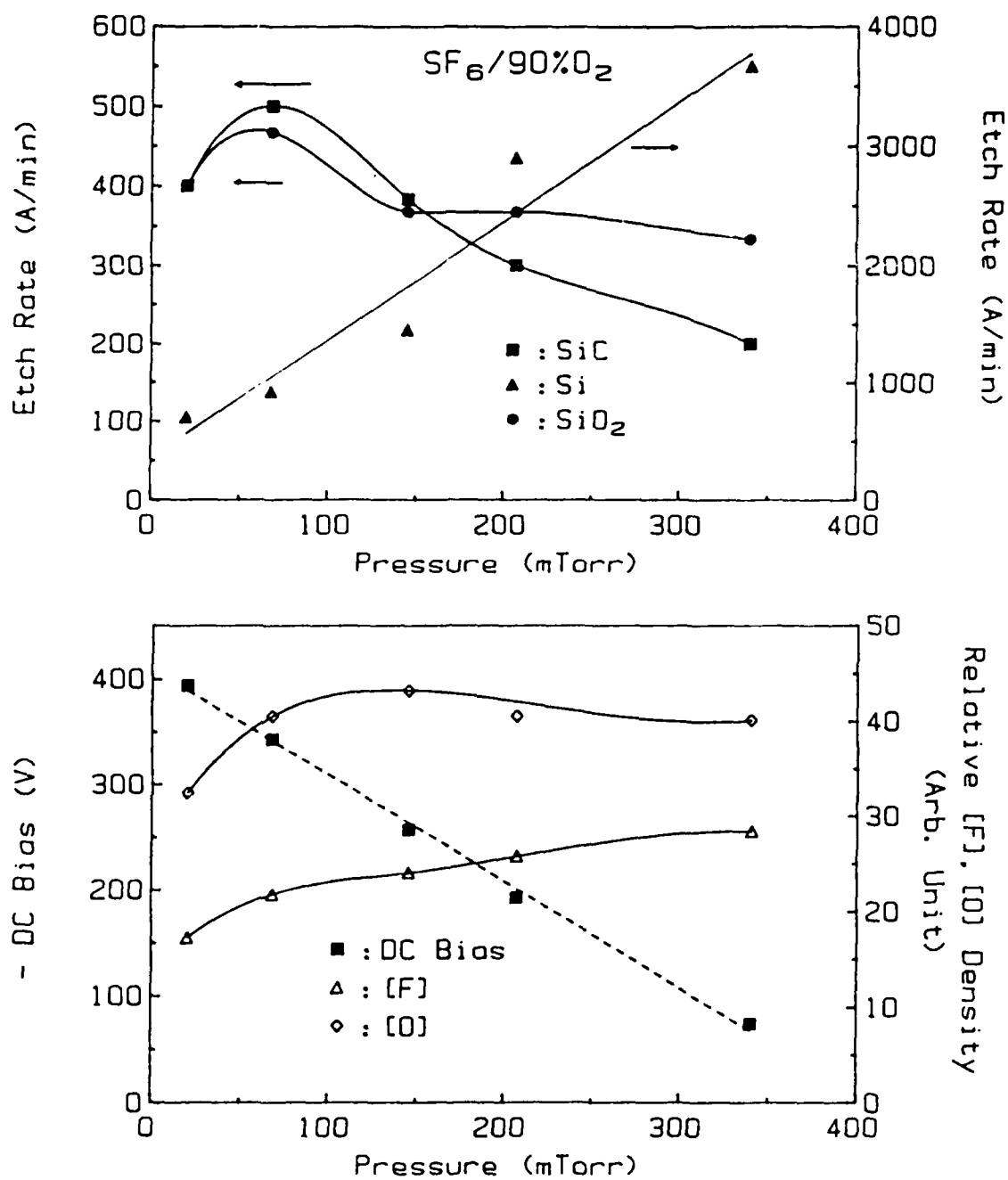
Figure 4.7.   (a) Etch rates of SiC, Si and SiO_2, (b) -DC self bias and relative fluorine, oxygen density as a function of pressure in SF_6 + 90% O_2 at 20sccm, 200W.

4.3 CBrF$_3$/O$_2$ Plasma

4.3.1 Percentage of O$_2$

The etching results of using CBrF$_3$ and O$_2$ mixtures in a similar etching experiment are shown in Figure 4.8(a). The SiC etch rate linearly increased with oxygen percentage until 75%O$_2$, which the Si etch rate decreased gradually after reaching its maximum value, 65nm/min, at 10%O$_2$. A SiC to Si etch rate ratio of 2:1 was reached at 75%O$_2$, where the etch rates of SiC and Si are 37.5nm/min and 18.8nm/min, respectively. The variation of SiO$_2$ etch rate was small, which was from 27nm/min at 0%O$_2$ to 28nm/min at 90%O$_2$. The DC bias and [F], [O] and [Br](336nm) density are presented in Figure 4.8(b). A typical emission spectrum from the CBrF$_3$/75%O$_2$ plasma at 200W, 20mTorr, 20sccm in RIE mode is shown in Figure 4.9, with a few plasma products, such as [CF$_2$](275nm, 289nm), [CO$_2^+$](289nm), [Br](336nm) [Ar], [F] and [O] indicated at different wavelengths.

4.3.2 Pressure

In Figure 4.10(a), the pressure dependence experiment, from 20mTorr to 215mTorr, is shown. The SiC etch rate reached its maximum value (40nm/min) at 50mTorr, then decreased with further increases in pressure. The SiC:Si etch rate ratio decreased from 2:1 at 20mTorr to 1:1 at 215mTorr. The SiC etch rate decreased when DC bias was smaller
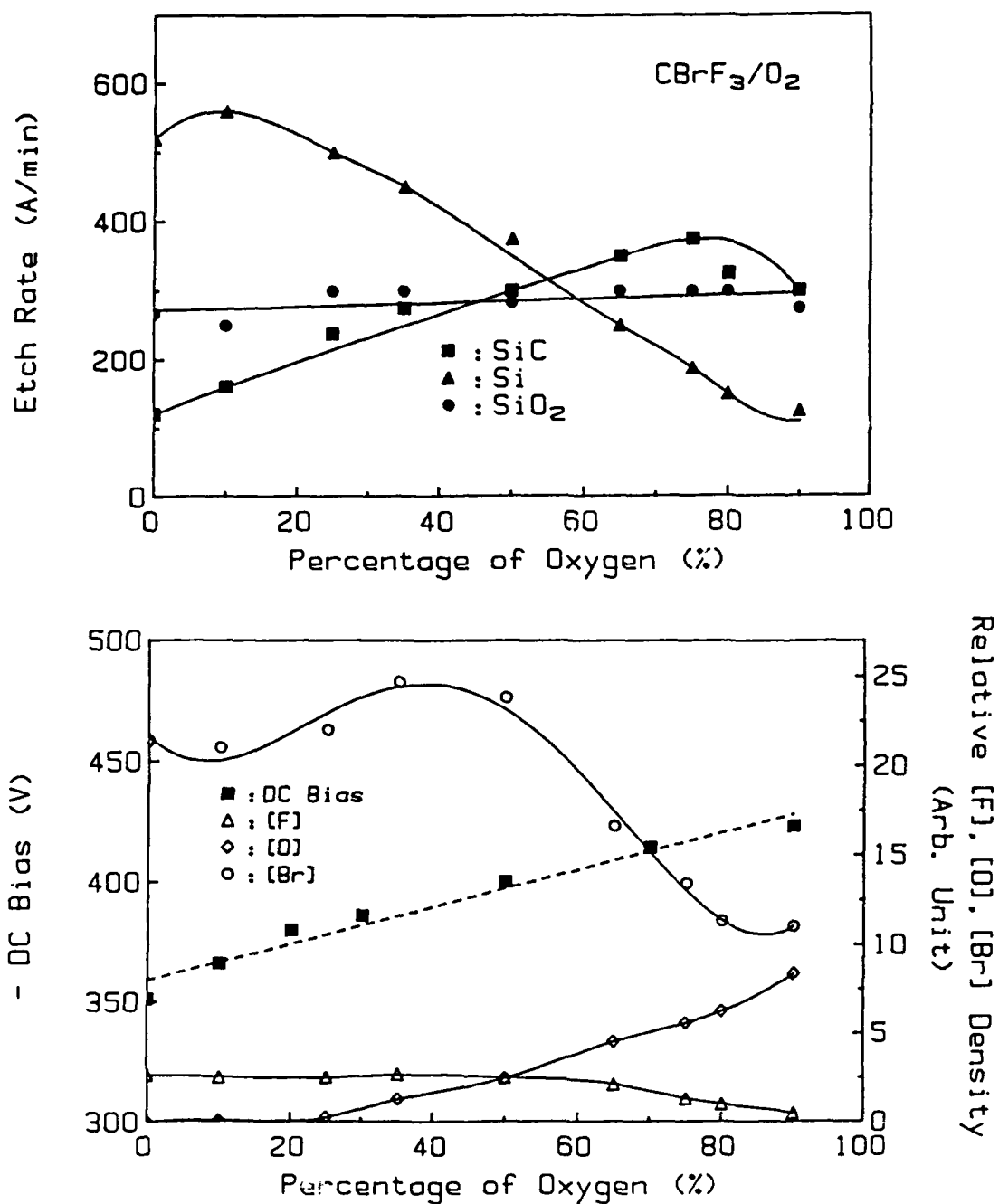
Figure 4.8. (a) Etch rates of SiC, Si and SiO$_2$, (b) -DC self bias and relative fluorine, oxygen, bromine density as a function of O$_2$ in CBrF$_3$ + % O$_2$.
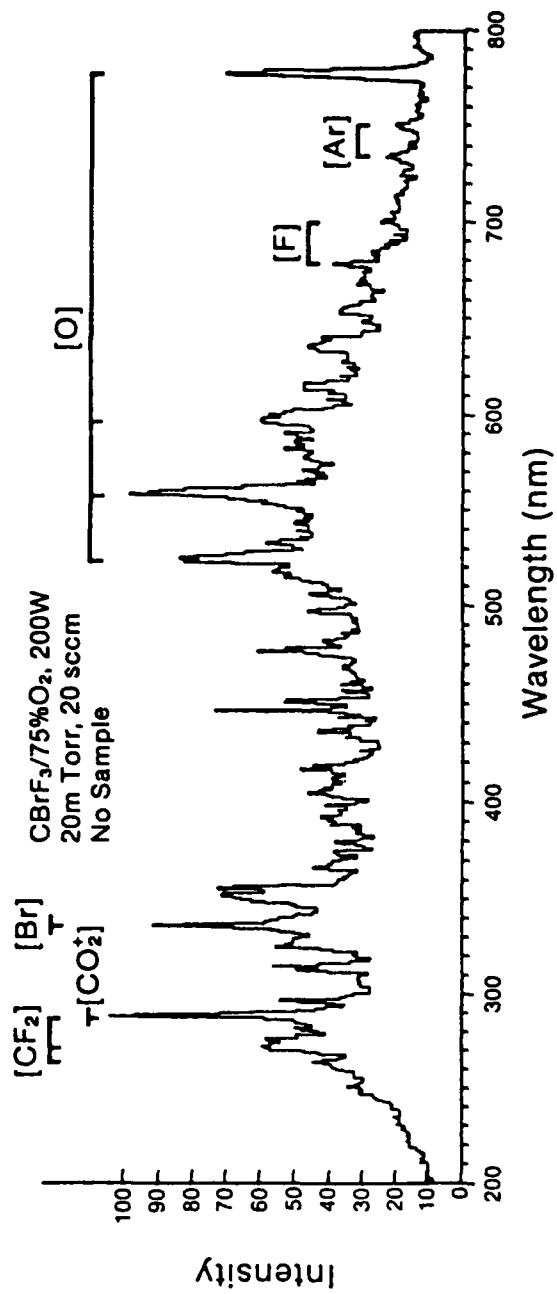
Figure 4.9. Plasma emission spectrum of $CBrF_3/75\%O_2$ at no sample situation

than -300V at 100mTorr, as shown in Figure 4.10(b). As the pressure is changed from 10 to 100mTorr, the variation of the SiC etch rate is less than 12%, bias was higher than -300V before 100mTorr. So, the SiC etching behavior may be dominated by such a critical value of DC bias. A high density of [Br] and low density of [F] and [O] are detected in high pressure region. The etch rate of SiO_2 is similar as SiC.

4.3.3 Power

In Figure 4.11(a) and (b), both the etch rate of SiC and SiO_2 are seen to increase monotonically with increasing power, which is equivalent to DC bias. A sub-linear increase in Si etch rate with power was observed. The selective ratio is not improved by changing power from low to high value. Except for [F] density, both [Br] and [O] densities are increased monotonically with power.
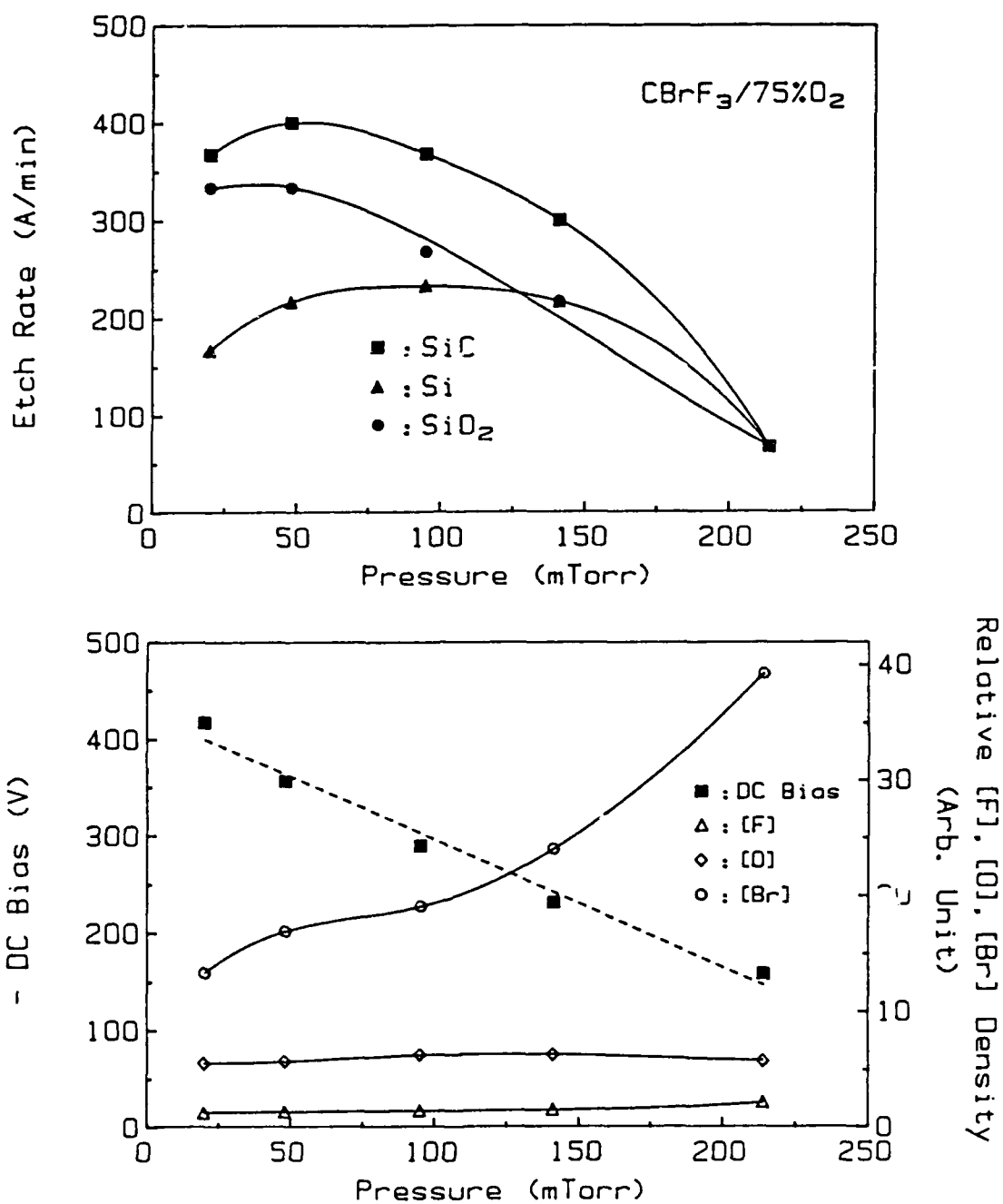
Figure 4.10. (a) Etch rates of SiC, Si and SiO_2, (b) -DC self bias and relative fluorine, oxygen, bromine density as a function of pressure in $CBrF_3$ + 75% O_2.
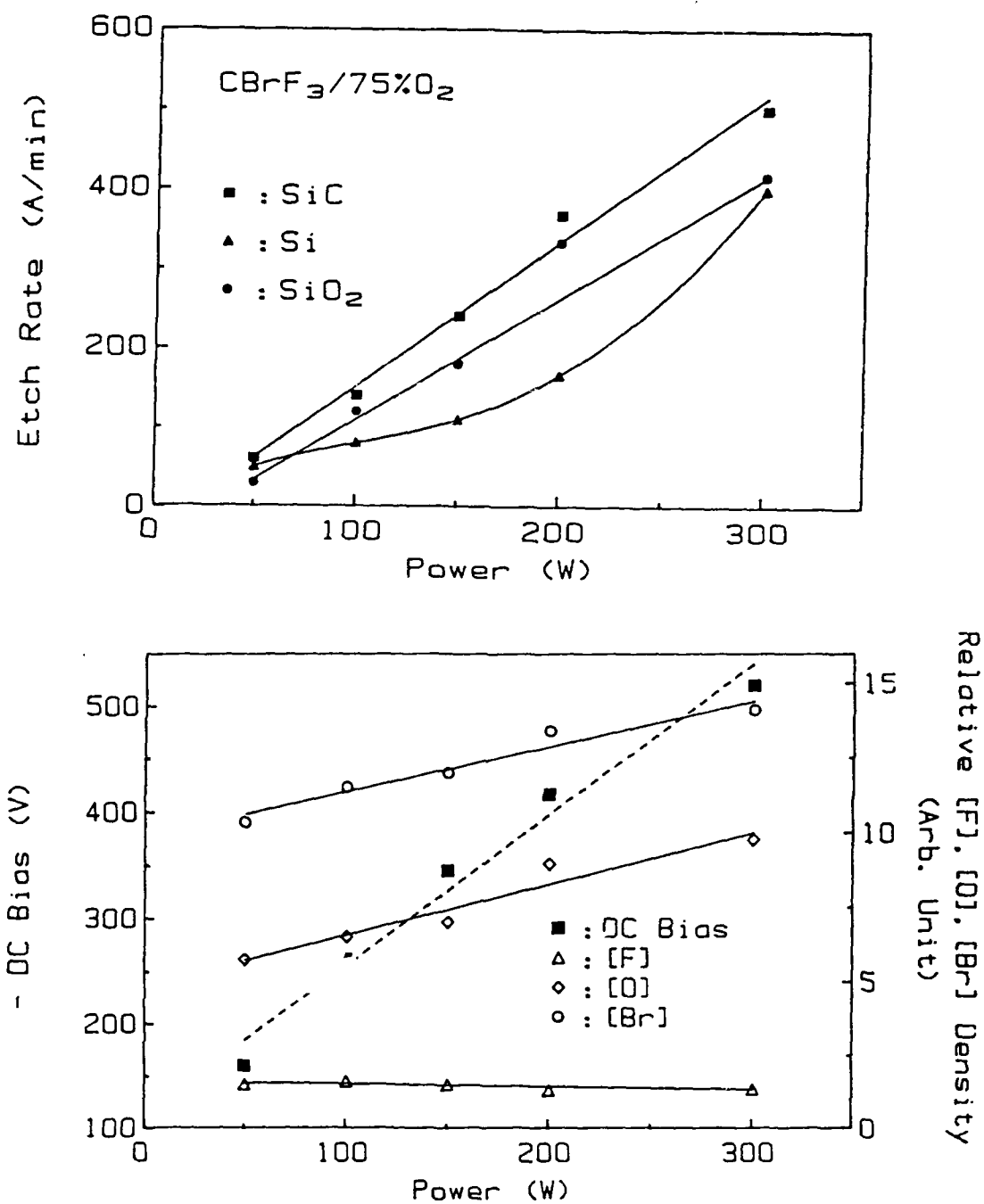
Figure 4.11.   (a) Etch rates of SiC, Si and SiO_2, (b) -DC self bias and relative fluorine, oxygen, bromine density as a function of power in $CBrF_3$ + 75% O_2 at 20sccm, 20mTorr.

4.4 CHF$_3$/O$_2$ Plasma

4.4.1 Percentage of O$_2$

The etching data obtained for CHF$_3$ and different percentages of O$_2$ mixture are shown in Figure 4.12(a) under the same plasma conditions as in previous experiments. The SiC etch rate increased with increasing of O$_2$ composition and reached the maximum value at 85%O$_2$, then decreased to zero for pure O$_2$ plasma. The Si etch rate has a similar trend with the maximum occurring at 70%$_2$. A maximum etch rate ratio of SiC to Si of 2:1 was obtained for CHF$_3$/90%O$_2$. For mixtures less than 90%O$_2$, the SiO$_2$ etch rate is close to 40nm/min. In a pure O$_2$ plasma, the etching rate is almost zero for all samples. The corresponding DC bias, [F], [O] and [H](486nm) density are shown in Figure 4.12(b). A typical emission spectrum for a CHF$_3$/90%O$_2$ plasma at 200W, 20mTorr, 20sccm in RIE mode is shown in Figure 4.13, with a few major plasma products, such as [CO](283, 297, 313nm), [CO$_2$$^+$](289nm), [H] [Ar], [F] and [O], identified at different wavelengths. The highest fluorine density occurred between 75% and 85%O$_2$ and a average value of -410V was obtained for the DC bias all values of oxygen percentage.

4.4.2 Pressure

Results of Pressure dependence experiments are shown in Figure 4.14(a) and (b). The selectivity ratio decreased from 2:1 at 20mTorr to
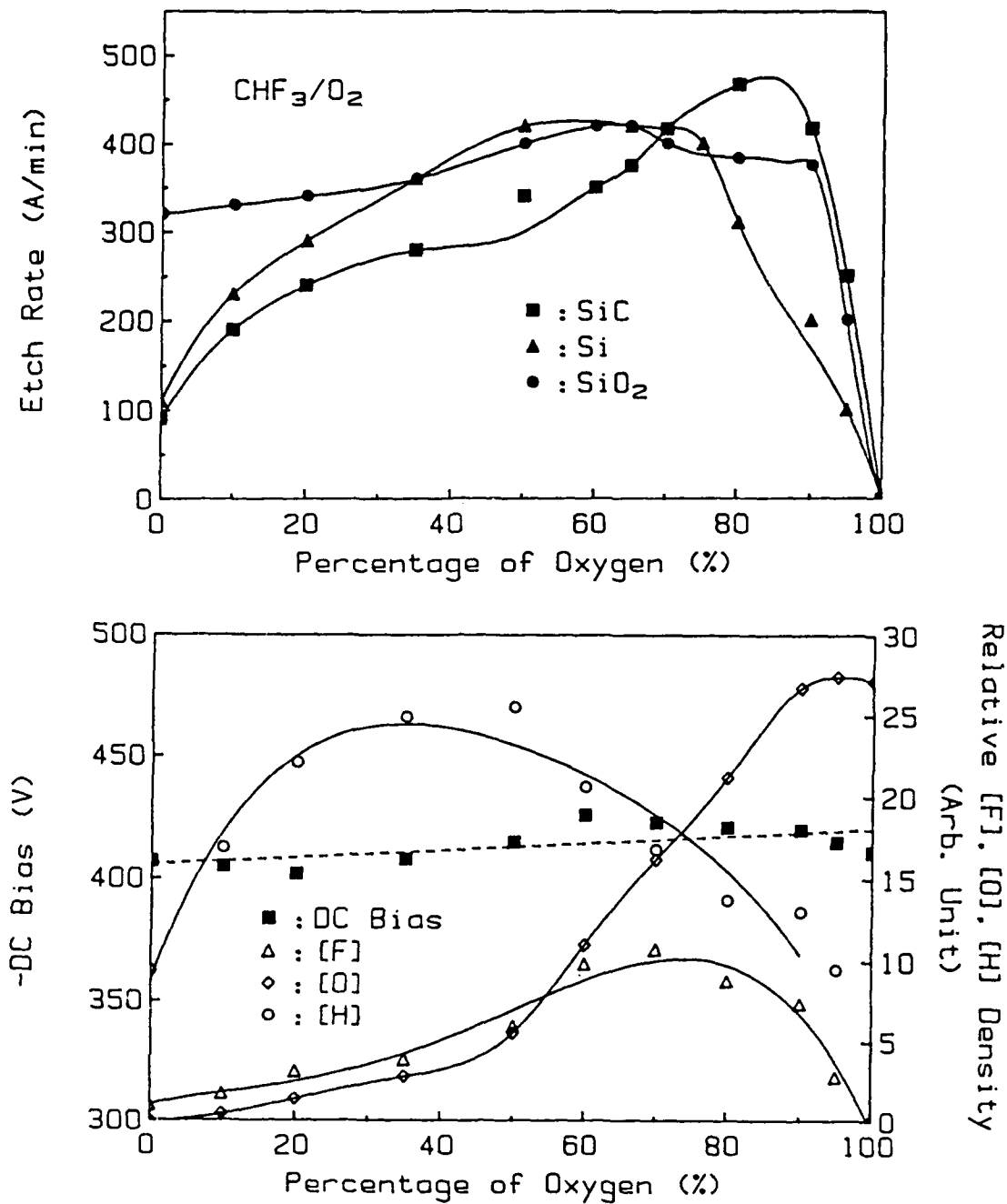
Figure 4.12.   (a) Etch rates of SiC, Si and SiO_2, (b) -DC self bias and relative fluorine, oxygen, hydrogen density as a function of O_2 in CHF_3 + % O_2.
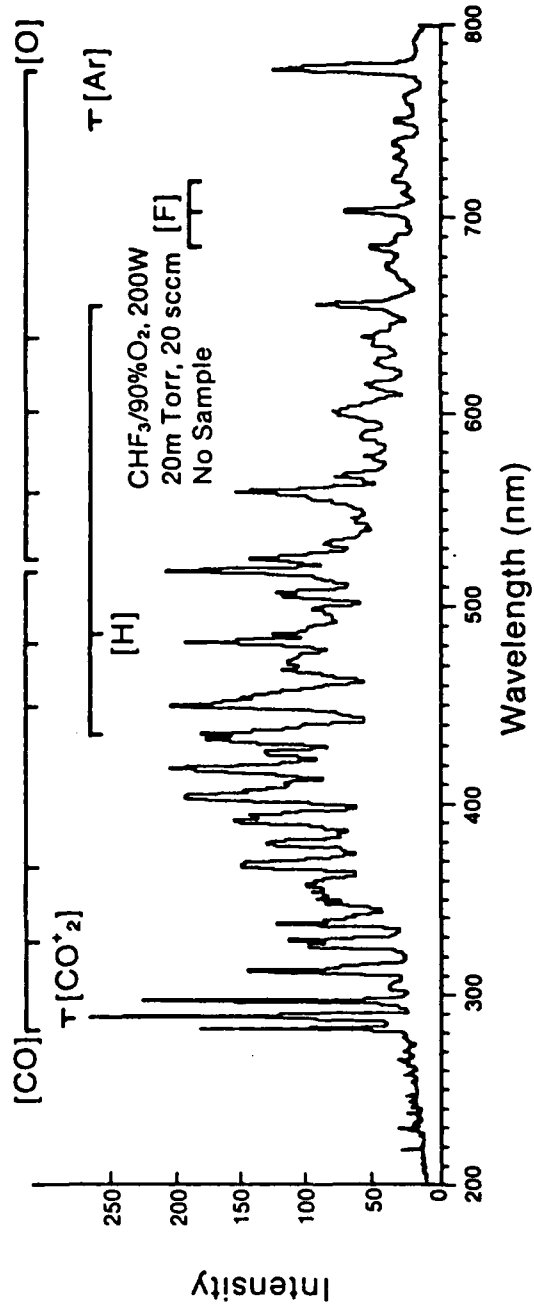
Figure 4.13. Plasma emission spectrum of $CHF_3/90\%O_2$ at no sample situation

1:1.1 at 315mTorr by varying pressure at 200W, 20sccm in Figure 4.14(a). The DC bias decreased monotonically as the pressure increased, as shown in Figure 4.14(b). On the contrary, the SiC etch rate shows a different behavior in the $CHF_3/90\%O_2$ pressure dependence experiment as compared to the use of $SF_6/35\%O_2$ and $CBrF_3/75\%O_2$ plasma. A small increase in the etch rate is first evident. Then, a gradual decrease, after 70mTorr, in the SiC etch rate was measured as the pressure was changed from 20mTorr to 315mTorr. The DC bias decreased from -420V to -250V and the same pressure range.

4.4.3 Power

As for other gas plasmas, varying the RF power for the CHF_3/O_2 case results in the monotonic increase in etch rate for Si, SiC and SiO_2, as shown in Figure 4.15(a). The selectivity ratio was close to 2:1 at all power level. The SiC etch rate of 75nm/min was measured at 300W, and a corresponding 33nm/min for Si. The corresponding DC bias and plasma densities are displayed in Figure 4.15(b).

4.5 Etching Profile

The edge profiles obtained using these fluorinated gases were examined by SEM. In general, no undercut was observed, but rather a tapered profile of the SiC film edge was found. In the microphotograph of Figure 4.16(a), it is shown that a vertical-to-lateral edge profile ratio,
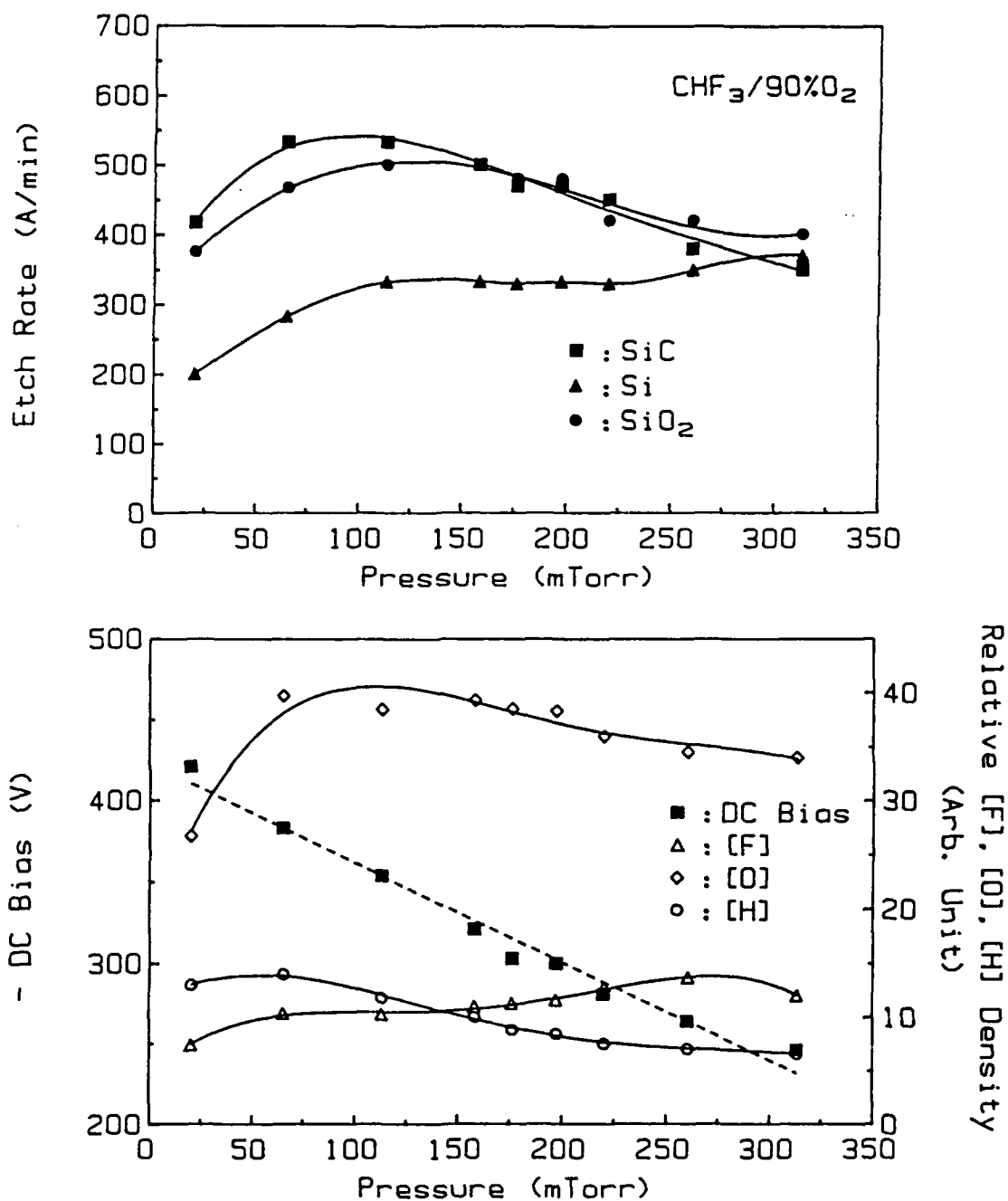
Figure 4.14.   (a) Etch rates of SiC, Si and SiO_2, (b) -DC self bias and relative fluorine, oxygen, hydrogen density as a function of pressure in CHF_3 + 90% O_2 at 20sccm, 200W.
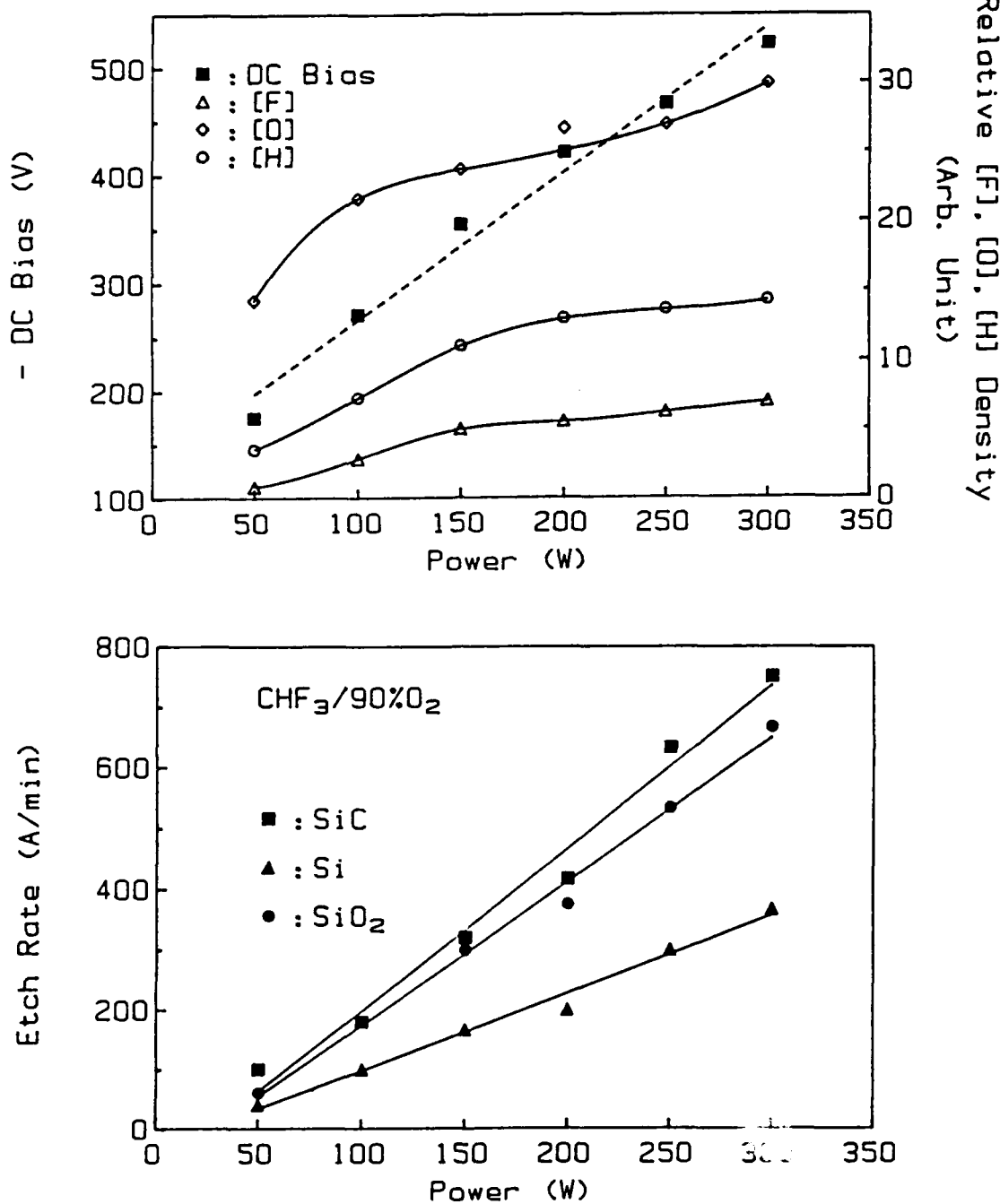
Figure 4.15. (a) Etch rates of SiC, Si and SiO$_2$, (b) -DC self bias and relative fluorine, oxygen, hydrogen density as a function of power in CHF$_3$ + 90%O$_2$ at 20sccm, 20mTorr.

which has been defined in Figure 2.3, of 10.3:1 has been obtained in a $SF_6/35\%O_2$ plasma at 200W, 20mTorr. The Si substrate underneath the SiC film was removed by isotropic etching and no backside etching of the SiC film was observed. In Figure 4.16(b), a top view of Figure 4.16(a) is shown and the basic etching phenomena were displayed clearly such as the undercut by involving a very strong chemical reaction to cause isotropic etching, and the edge trench effect due to ion reflection off the side of step under strong ion bombardment when using reactive ion etching mode.

The undercut of the Si substrate was not improved by increasing the power, since that will induce a higher fluorine concentration. However, it will be strongly reduced by using a high composition of oxygen in the plasma. In Figure 4.17(a), an etch ratio of 11:1 is shown to result from using $SF_6/90\%O_2$, 200W, 20mTorr and 20sccm plasma and a small undercut, 50nm, was measured after etching 400nm into Si substrate. Furthermore, in Figure 4.17(b), a ratio of 5:1 for SiC was obtained at $SF_6/90\%O_2$, 74mTorr, 200W. The reducing of anisotropic ratio was due to the increasing of pressure, which will reduce DC bias and increase fluorine concentration, and a 130nm undercut was formed by etching into 600nm Si substrate.

A tapered profile ratio of 6.3:1 was obtained by using $CBrF_3/75\%O_2$ plasma at 200W, 20mTorr, as shown in Figure 4.18(a), where the etching was stopped inside the SiC layer. The ratio was improved to 7.6:1 by increasing the pressure to 72mTorr, at $CBrF_3/75\%O_2$ 200W, 20sccm, as shown in Figure 4.18(b) A half-micron SiC line patterned with Al mask under these conditions is shown in
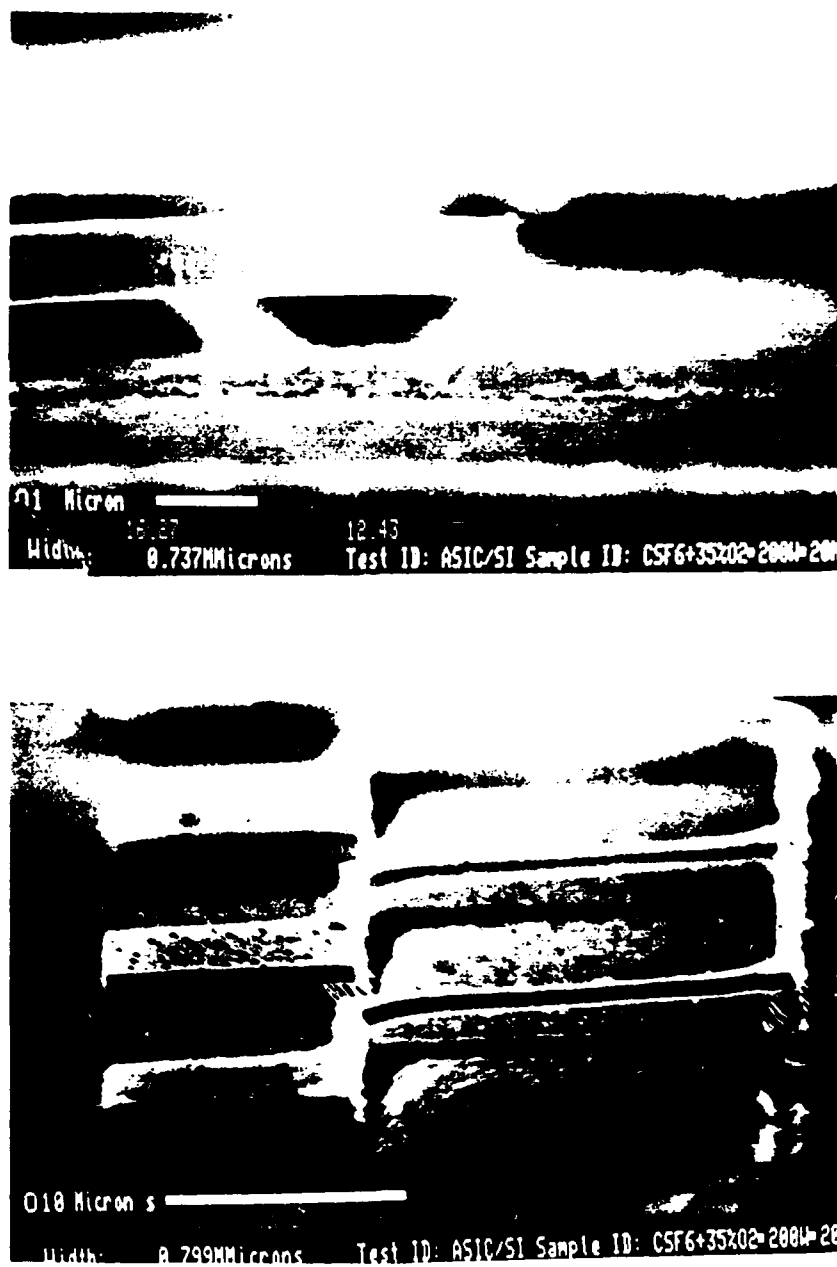
Figure 4.16. SEM photomicrograph of SiC layer on Si(100), RIE-etched by $SF_6/35\%O_2$, 20mTorr, 200W (a). Cross section of SiC layer, (b). **Whole view** of picture.
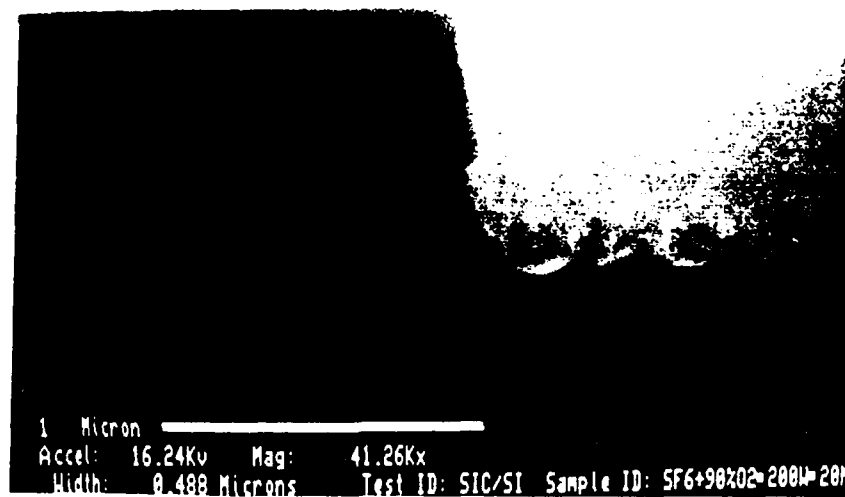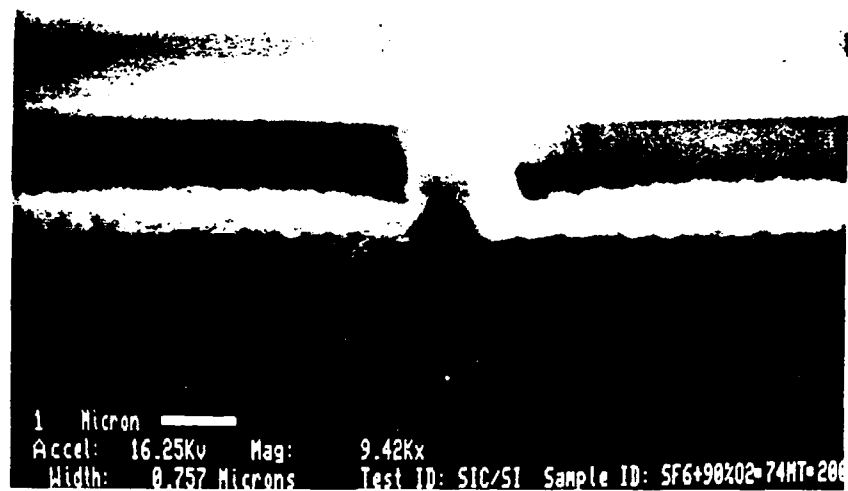
Figure 4.17. SEM photomicrograph of SiC layer on Si(100), RIE-etched by SF$_6$/90%O$_2$, 200W (a). 20mTorr, (b). 74mTorr.

Figure 4.19(a). Higher power conditions did not increase the profile ratio and a ratio of 4:1 was measured at 300W, 20mTorr, as shown in Figure 4.19(b).

In Figure 4.20(a), no undercut of SiC or Si is obtained with an anisotropic ratio of 12.5:1 by using a $CHF_3/90\%O_2$ mixture. In this microphotograph, the SiC film is shown with the Al thin film mask in place. The ratio was reduced to 5.5:1 when the pressure was increased to 74mTorr at same composition of plasma, shown in Figure 4.20(b). The highest ratio of 17:1 obtained at $CHF_3/90\%O_2$, 300W, 20mTorr is shown in Figure 4.21(a) & (b). The Si substrate has been etched down and a very clean and smooth surface was obtained after etching.

4.6 Discussions

For the case of reactive ion etching in SF_6/O_2 plasmas, the largest generation of fluorine concentration is observed compared to the other investigated gas mixtures. These results in the highest (by a factor 2-3) Si etch rate levels and in an etch rate dependence on oxygen percentage in the plasma which is related to, but dose exactly follow, the fluorine density. The main etching mechanism of Si in a SF_6 plasma involves the chemical reaction between silicon and fluorine atom with the formation of volatile compounds[4.6]. The chemisorption[4.7] of oxygen on the Si surface reduces the availability of etching sites and thus decreases the Si etch rate. Thus, the shift of maximum Si etch rate from $35\%O_2$ (maximum [F] density) to $10\%O_2$ is result of this effect. Oxygen chemisorption is not considered to have a strong effect in the case of SiC,
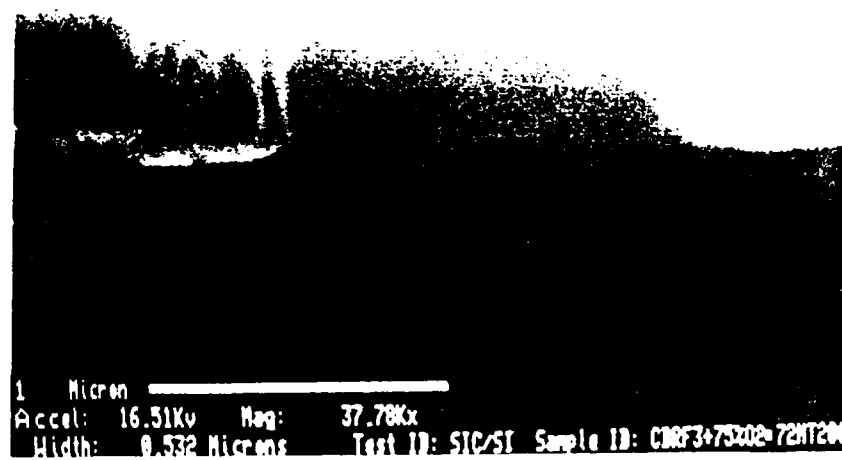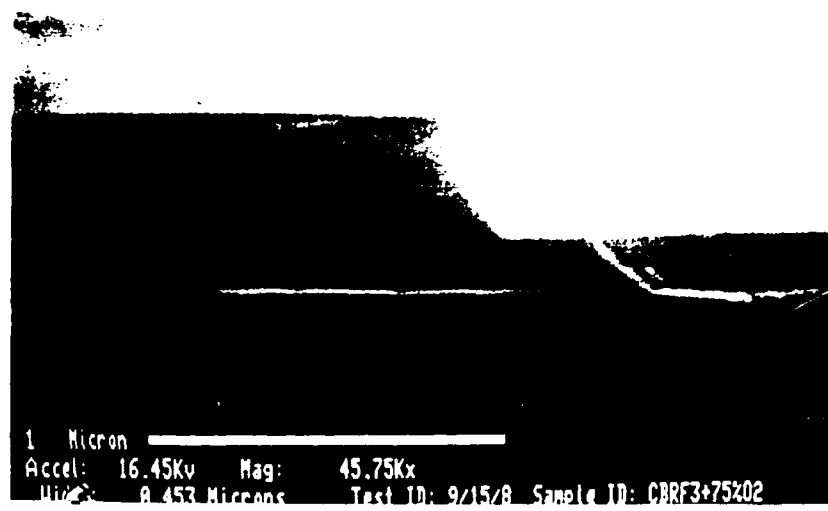
Figure 4.18. SEM photomicrograph of SiC layer on Si(100), RIE-etched by $CBrF_3/75\%O_2$, (a). 200W, 20mTorr, (b). 200W, 74mTorr.
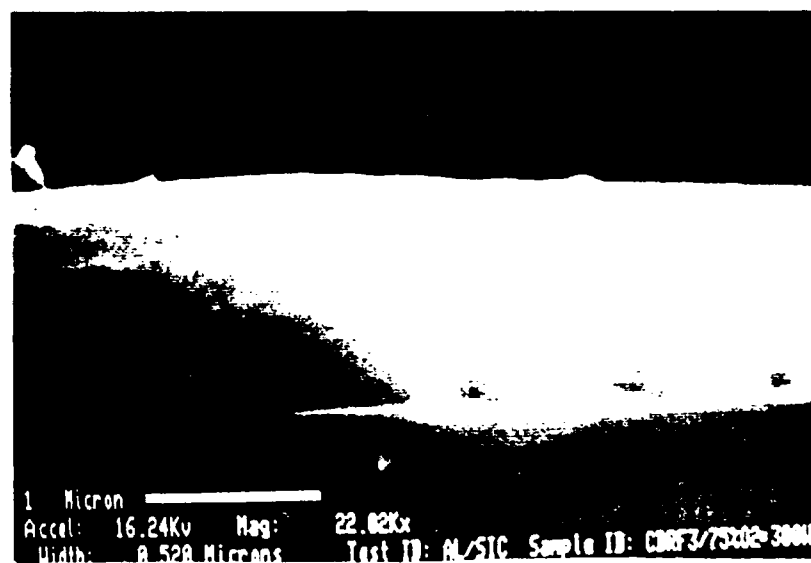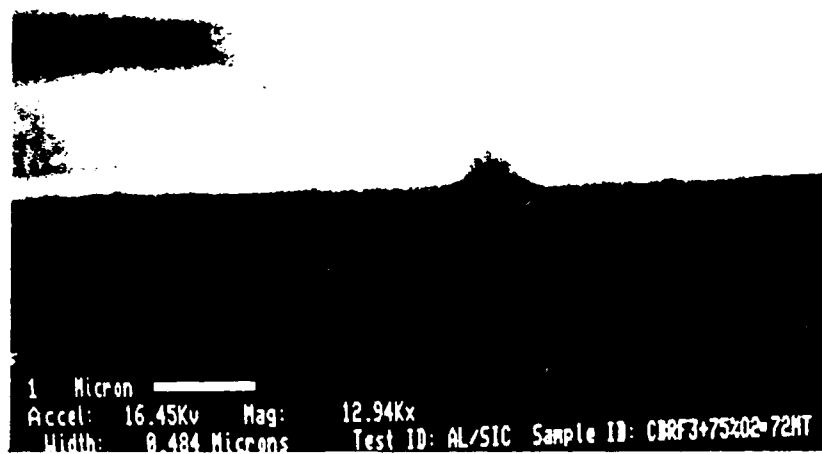
Figure 4.19. SEM photomicrograph of SiC layer on Si(100), RIE-etched by $CBrF_3/75\%O_2$, (a). 200W, 74mTorr,(b). 300W, 20mTorr.
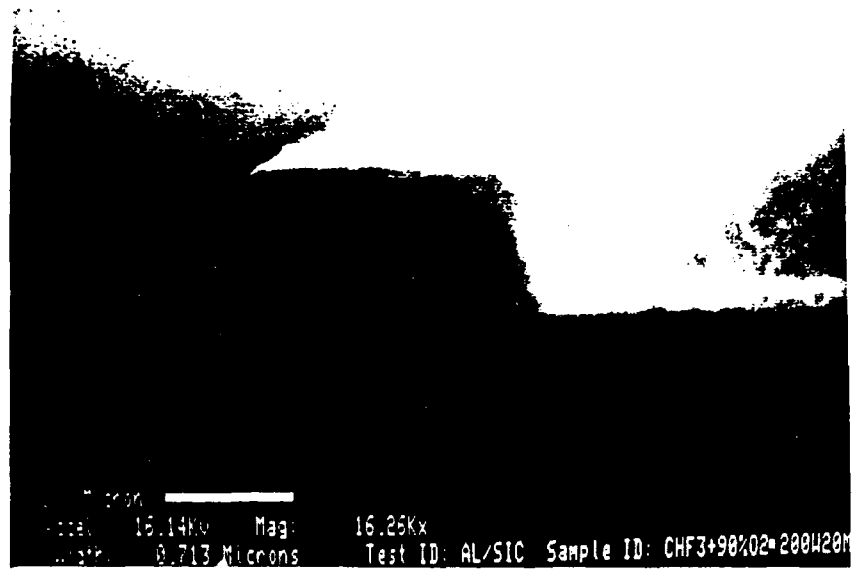
Figure 4.20. SEM photomicrograph of SiC layer on Si(100), RIE-etched by $CHF_3/90\%O_2$ (a). 20mTorr, 200W. (b). 74mTorr, 200W.

Figure 4.21. SEM photomicrograph of SiC layer on Si(100), RIE-etched by $CHF_3/90\%O_2$ 20mTorr, 300W (a) & (b).

since carbon can react directly with oxygen.

The SiC-to-Si etch rate ratio in SF_6/O_2 plasma is much smaller than unity for the entire range of parameters investigated. The compatible SiC etch rate, even higher, at low oxygen concentration and low DC bias (from 0% to 35%O_2 and 290V to 350V) was caused by the high concentration of fluorine atom required to penetrate the carbon layer and react with Si, then create more voids to help remove the carbon layer by physical sputtering under low energy ion bombardment. When the oxygen concentration and DC bias increased by using a high percentage of oxygen, the chemical reaction of carbon and oxygen was involved, but the fluorine penetration effect was reduced by the decrease of the fluorine concentration. A fairly high (10 to 1) etching anisotropy was observed for SF_6/O_2 etched SiC films, as shown in Figure 4.16(a). No etching of SiC film from unexposed areas observed (see Figure 4.16(b)) suggests that a protective carbon blocking layer was formed, which has no energetic ion bombardment for physically sputtering or producing the chemical reaction between carbon and oxygen.

When pressure was increased from 20 to 250mTorr (Figure 4.5), the DC bias decreased rapidly from 350 to 25V. The SiC etch rate strongly followed the change of DC bias even though both F and O concentrations also increased. A critical DC bias was observed in the $SF_6/90\%O_2$ pressure experiment (Figure 4.7). When the DC bias was higher than 300V, the etching rate of SiC was limited by the chemical reaction rate given sufficient abundant reactants, namely oxygen and fluorine. The SiC etch rate reached its maximum value of 50nm/min and stayed at a level about 40nm/min up to the point where the DC bias

dropped below 300V. Therefore, the DC bias is considered to be the key factor controlling the reaction between carbon and oxygen, while the reaction between fluorine and Si can take place at low ion energy. Increasing power level (Figure 4.6) indicates that higher reactant concentration and higher ion energy were induced by the plasma resulting in a higher etching rate for all samples. Almost no lateral etching was observed even when the percentage of oxygen was increased to 90%O_2, the anisotropic ratio was 11:1. The undercut of the Si substrate was improved by reducing the chemical reaction through low fluorine concentration and by increasing the higher DC bias.

In $CBrF_3$/O_2 plasmas, as shown in Figure 4.8, the density of [F] and [O] is much smaller than in the corresponding SF_6/O_2 plasma. Consequently, the Si etch rate is dramatically reduced, by a factor of approximately 10 to 30, compared to SF_6/O_2 plasma. The SiC etch rate was also reduced, but only by a factor of 1.5-2. Therefore, for oxygen percentage in the plasma greater than 60%, the relative abundance of oxygen compared to the near absence of fluorine, results in a SiC-to-Si etch rate ratio greater than unity. At $CBrF_3$/75%O_2, a selectivity of 2:1 is observed. Under these conditions, a SiC line edge anisotropy of 6.3:1 was measured [see Figure 4.18(a)]. The DC bias decreased from 420V to 160V, when pressure was increased from 20mTorr to 215mTorr, as shown in Figure 4.10. When the pressure was lower than 100mTorr, or the DC bias higher than 300V, the SiC etch rate ranged within a 5% band from 38nm/min (at 20mTorr). However, above 100mTorr, the SiC etch rate followed the same trend as the DC bias, which is similar to the SF_6/90%O_2 pressure experiment. The linearly increasing etch rate and

species density was caused by the increasing plasma power in the power experiment shown in Figure 4.11. The effects of bromine atoms in the etching process and on the line edge ratio are not quite clear yet and need further investigation.

In CHF_3/O_2 plasma, the presence of hydrogen mainly depresses the [F] intensity, with the oxygen intensity reaching levels similar to the SF_6/O_2 plasma. The peaks in [F] and [O] density occur for 70% and 90% O_2 mixtures, respectively. The Si etch rate variation with O_2% tracked the [F] density well and decreased very fast with lowered fluorine density and chemisorption of oxygen on surface in the high oxygen density region. On the contrary, the SiC etching conditions reaches the optimum conditions in this situation, such as high DC bias (high ion energy), sufficient fluorine density (to remove Si) and high concentration of oxygen (to remove carbon). The maximum SiC etch rate, 47nm/min, occurred at $80\%O_2$ mixture, while the maximum SiC:Si selectivity of 2 was measured at $90\%O_2$ mixture. The high (415V) and almost constant (with O_2%) DC bias found in this case produced the highest anisotropic ratio (12.5:1) achieved. A similar result of SiC etch rate compared to SF_6/O_2 and $CBrF_3/O_2$ gases was observed in Figure 4.14 by changing pressure from 20mTorr to 315mTorr at $CHF_3/90\%O_2$, 200W. For a DC bias higher than 300V, the SiC etch rate will be limited by the reaction rate between carbon and oxygen. In low DC bias case, the SiC etch rate was shown to be strongly dependent on DC bias rather than high density of reactants ([F] & [O]). Therefore, the selective ratio of SiC to Si was decreased from 2:1 at 20mTorr to 1:1.1 at 315mTorr. The linear relation between etch rate and DC bias was observed in the power experiment at $CHF_3/90\%O_2$

and shown in Figure 4.15(a). The higher ion energy enhanced almost all reactions, and thus no better selectivity ratio was obtained. A very high anisotropic ratio, 17:1, was, however, obtained (Figure 4.21) by using 300W instead of 200W power.

For selective etching of SiC to SiO_2, the maximum ratio of 1.3:1 was obtained in $CHF_3/80\%O_2$. The optimum reverse selectivity of 1:3.6 was measured in pure CHF_3 plasma. In SF_6/O_2 and $CBrF_3$ plasmas, the SiO_2 etch rate is quite similar to that of SiC and no selectivity was observed. A summary of results of selective and anisotropic ratios of SiC/Si and SiC/SiO_2 is shown in Table 4.1.

4.7 Other Effects

Different plasma conditions, such as addition of H_2 gas, gas flow rate and substrate temperature, have been investigated and the effects on SiC etching mechanism are considered.

4.7.1 Hydrogen effect

4.7.1.1 In $SF_6/35\%O_2$ Plasma

In Figure 4.22, varying amounts of hydrogen gas was added into a 20sccm $SF_6/35\%O_2$ gas plasma at 200W and 20mTorr. H_2 acts as a scavenger of fluorine atoms[4.8], forming HF molecules and reducing the fluorine concentration. This was expected to improve the

Table 4.1   SiC Reactive Ion Etching (RIE)

Gases	Power (W)	Pressure (mTorr)	Edge Profile Ratio *	Selectivity SiC : Si	Etch Rate SiC (nm/min)
CHF$_3$ +90%O$_2$	200	20	12.5 : 1	2.0 : 1	41.7
	200	74	5.5 : 1	1.9 : 1	53.3
	300	20	17.0 : 1	2.0 : 1	75
CBrF$_3$+75%O$_2$	200	20	6.3 : 1	2.0 : 1	37.5
	200	72	7.6 : 1	1.8 : 1	39
	300	20	4.0 : 1	1.3 : 1	50
SF$_6$ +35%O$_2$	200	20	10.3 : 1	1 : 26	53.3
	200	200	——	1 : 267	20
SF$_6$ +90%O$_2$	200	20	11.0 : 1	1 : 1.8	40

Gases	Selectivity SiC : SiO$_2$
CHF$_3$	1 : 3.6
CHF$_3$+80%O$_2$	1.3 : 1

* : Ratio of Vertical to Lateral etching

selectivity ratio of SiC to Si. However, as seen in Figure 4.22(a), the SiC etch rate kept a constant value of 41nm/min when changing the H_2 from 0sccm to 5sccm while the Si etch rate increased from $1.4\mu m$ to $1.6\mu m$. From Figure 4.22(b), the DC bias and [H] density are seen to increase linearly with increasing H_2. It is believed that the Si etch rate was rate-limited by the reaction between Si and fluorine, even though the fluorine density was suppressed by adding H_2. However, the roughly constant SiC etch rate observed was due to compensation between the effects of decreasing [O] density and the increasing DC Bias. The change of [O] density may be caused by : (1). the plasma chemical balance which includes the decreasing [F] density, dissociating of SF_6 gas and generating $[SO_x]$ products, and (2). redistribution of electron and ion energy in plasma. The increasing Si etch rate was caused by the increasing DC bias, which enhances the reaction rate between Si and fluorine and reduce the chemisorption of oxygen on surface.

4.7.1.2 In $CHF_3/90\%_2$ Plasma

Similar experiments were used to study the effect of hydrogen in $CHF_3/90\%O_2$ plasma. In Figure 4.23(a), all etch rates were decreased rapidly by adding only 1sccm H_2 into $CHF_3/90\%O_2$, 200W, 20sccm, 20mTorr plasma. The sensitivity of fluorine concentration was shown in Figure 4.23(b), the fluorine density almost vanished when 1sccm H_2 was added. The DC bias and [O]
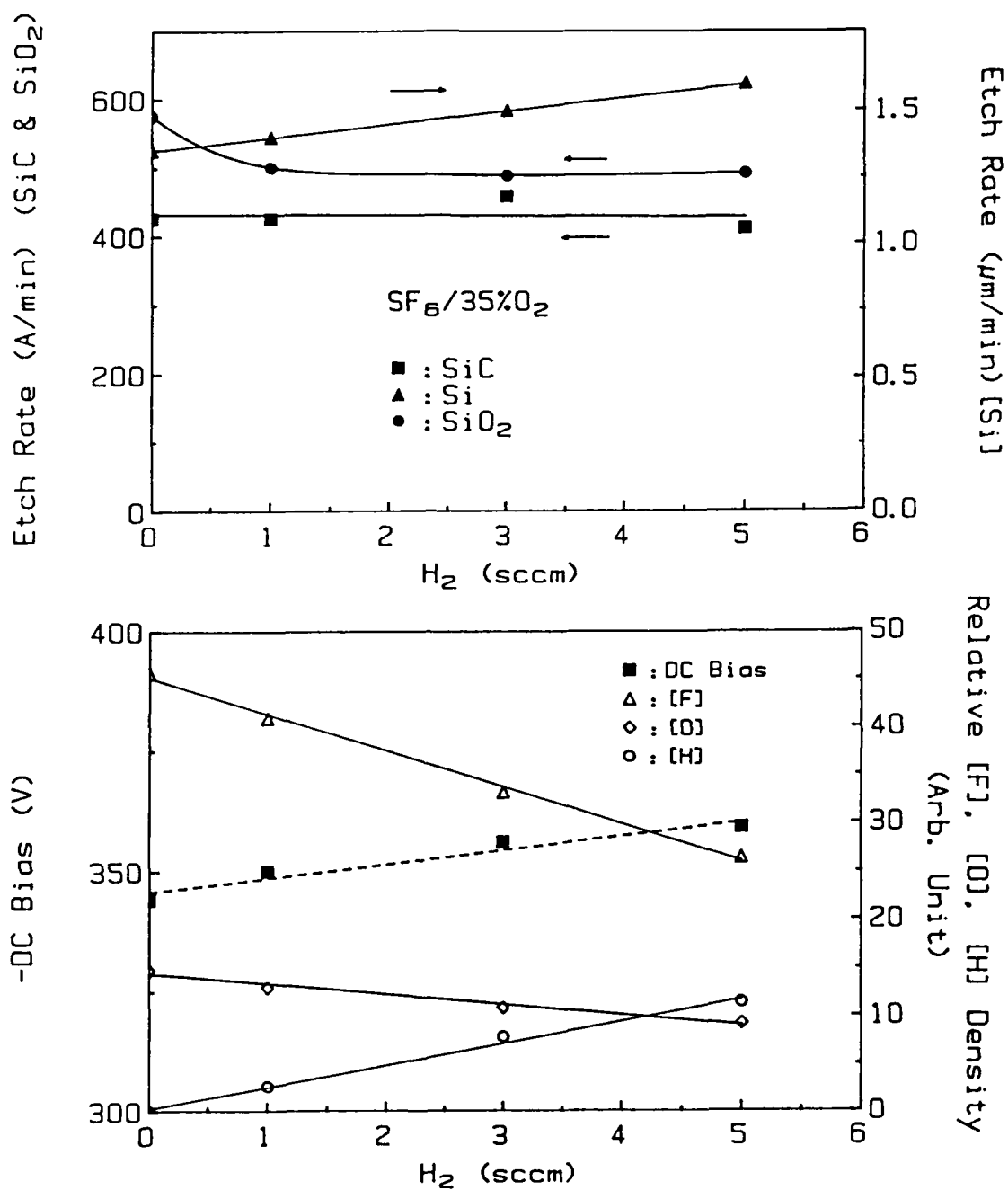
Figure 4.22.   The hydrogen effect in $SF_6/35\%O_2$, 200W, 20mTorr (a).
Etch rate of SiC, Si, and SiO_2, (b). -DC Bias and relative [F], [O] density.

density were not changed by the increasing of H_2. It could be concluded that the level of fluorine density was much more critical in $CHF_3/90\%O_2$ plasma than in $SF_6/35\%O_2$ plasma, since only a small amount of fluorine concentration was generated from plasma. Therefore, a mass-transfer limit of fluorine concentration was considered to dominate the reaction of silicon and fluorine in this case, which will affect the etching rate of SiC, Si and SiO_2 directly in $CHF_3/90\%O_2$ plasma.

4.7.2 Flow Rate Effect

The flow rate of processing gases was changed in $CHF_3/90\%_2$ at 200W, 20mTorr conditions. A slight decrease of all etch rates was observed in Figure 4.24(a), when the flow rate was increased from 10sccm to 40sccm. However, the [O] density, the DC bias, [F] and [H] density are decreased slightly and are shown in Figure 4.24(b). It can be explained that the SiC etch rate was not rate-limited by oxygen concentration under this high oxygen composition (90%) plasma, but affected by the DC bias and fluorine concentration mainly.

4.7.3 Temperature effect

The increasing of substrate temperature from 25°C to 97°C during etching is shown in Figure 4.25(a). There was almost no variation in SiC etch rate. The Si etch rate remained constant below 60°C, then increased
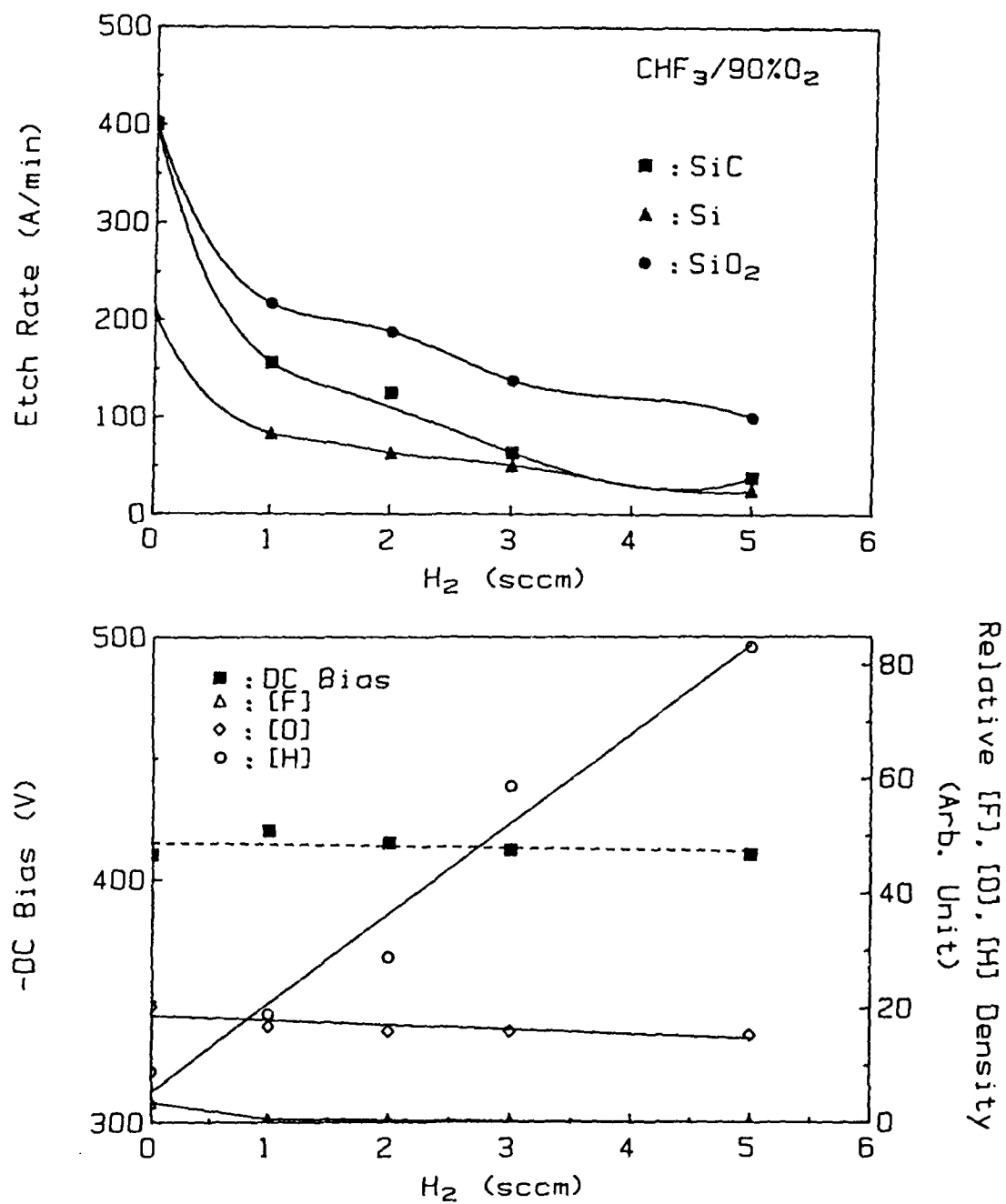
Figure 4.23. The hydrogen effect in $CHF_3/90\%O_2$, 200W, 20mTorr (a). Etch rate of SiC, Si, and SiO_2, (b). -DC Bias and relative [F], [O], [H] density.
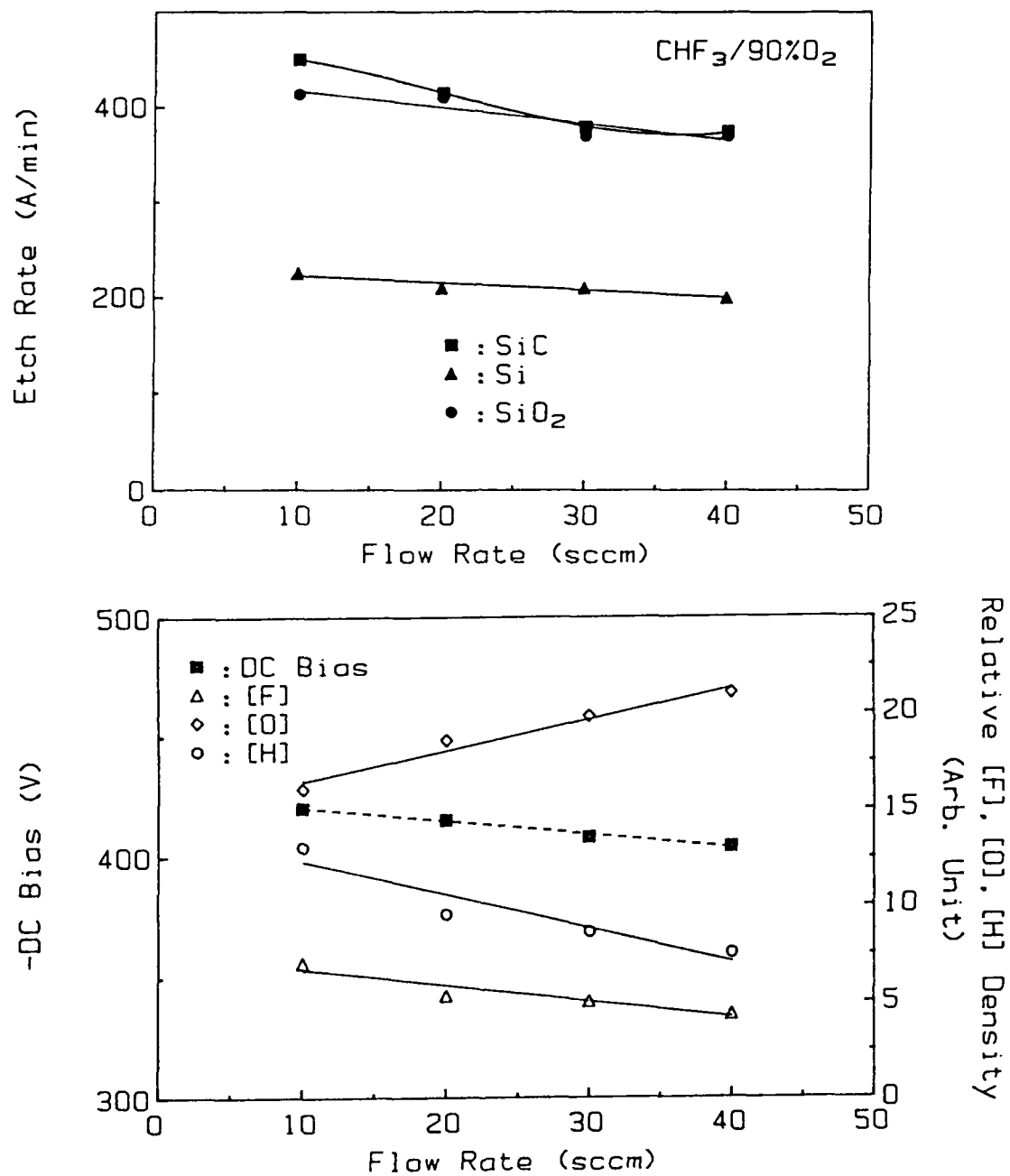
Figure 4.24.   The flow rate effect in $CHF_3/90\%O_2$ at 200W, 20mTorr, (a). Etch rate, (b). -DC bias and relative [F], [O], [H] density.

for higher temperature. In Figure 4.25(b), DC Bias, [F], [O], [H] density, were kept the same for all different substrate temperatures. Therefore, the reduction of oxygen chemisorption on the Si surface by a thermal effect will be the main factor to increase the Si etch rate. The chemisorption mechanism of oxygen on Si surface has been discussed in the above section.

4.8 Etching Mechanisms

4.8.1 Carbon Rich Surface

The surfaces of SiC films, prepared by 3min etching at 200W, 20mTorr, 20sccm plasma conditions under different compositions of oxygen in each gas, have been analyzed by Auger electron spectroscopy (AES). The average sputtering rate, 1.2nm/min, of 5keV Ar ion beam in AES was measured. The peak-to-peak intensity of every element (Si, C, O, F, Al, etc.) measured is illustrated in Figure 4.26 by different etching gases, such as $SF_6/\%O_2$, $CBrF_3/\%O_2$ and $CHF_3/\%O_2$ in different percentage of O_2 from 0% to 100%.

After being normalized to the system sensitivity and calibrated by thermal oxide (SiO_2), the results of AES depth profiles for each element were replotted and are shown in Figure 4.27 for $SF_6/\%O_2$, Figure 4.28 for $CBrF_3/\%O_2$, Figure 4.29 for $CHF_3/\%O_2$. A carbon rich surface was found at different concentration levels of oxygen in all gases. The atomic ratio of Si to C was close to unity before and after RTA (or FA)
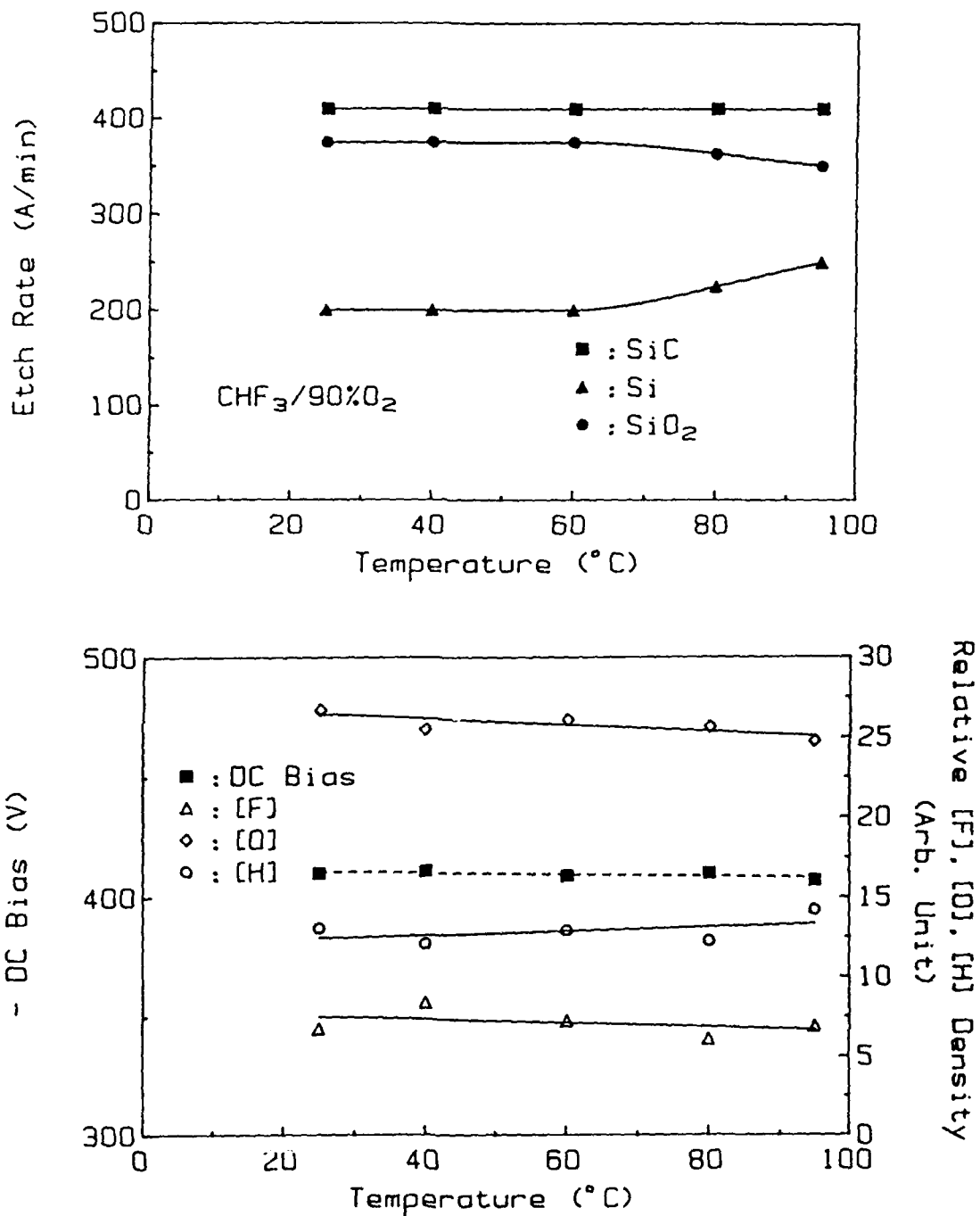
Figure 4.25. Temperature effect to SiC, Si and SiO_2 in $CHF_3/90\%_2$, 200W, 20mTorr, 20sccm, (a). Etch rate, (b). -DC Bias and [F], [O], [H] density.
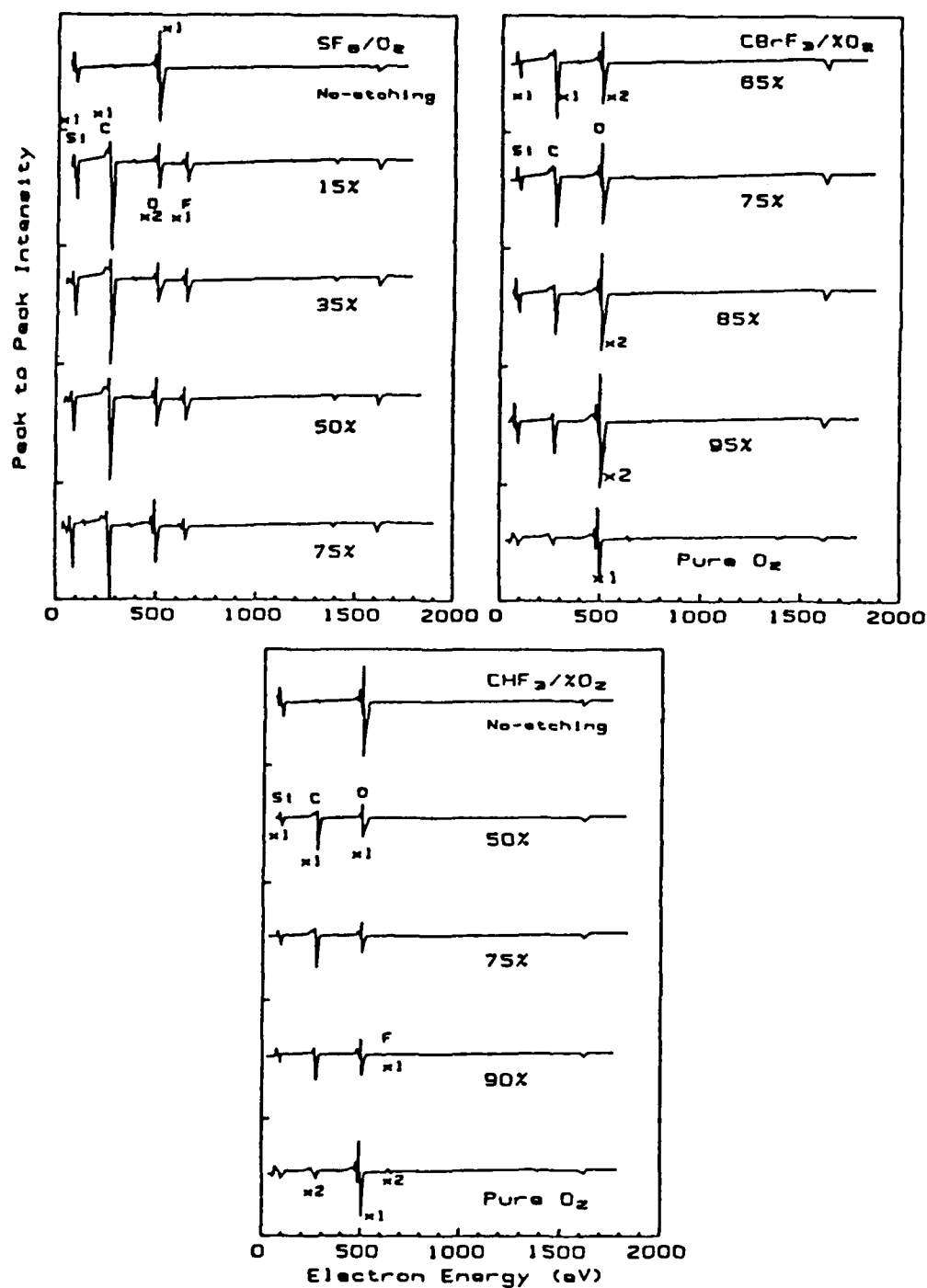
Figure 4.26. The AES spectra of SiC surface etched by (a). $SF_6/\%O_2$ (b). $CBrF_3/\%O_2$, (c). $CHF_3/\%O_2$ in different composition of O_2.

annealing for SiC thin films. The surface carbon concentration was reduced by increasing oxygen concentration in the plasma. When pure oxygen plasma was used, the surface was oxidized. Therefore, removing the carbon layer from the etching surface is believed to be the rate-limiting step for etching SiC. A high intensity [F] was found only in SF_6/O_2 plasma No measurable [Al] intensity was observed in all cases. Therefore, the use of an Al electrode and an Al mask for experiments were not considered to have a contamination effect under these plasma conditions, unlike the observation reported by Palmour et al.[4.9] on Al micromask effects causing a rough etching surface.

4.8.2 Chemical Reaction Model

The etching mechanism of each gas has been investigated by exposing large area of SiC wafers in chamber. The surface coverage was from 10% to 40%. The backside samples used in this experiment was covered by an aluminum film to avoid reaction from the backside surface, which was extremely important for the chemical reaction between Si and [F] atom. The changes of species density in the plasma caused by consuming large amount of reactants[4.10], such as [F](703nm) and [O](777nm), and generating byproducts, such as [CO](297nm) and $[CF_2]$(289nm), were easily detected from optical emission spectra. As usual, the [CO] and $[CF_2]$ products could be formed by the process gases themselves in the plasma, such as in $CBrF_3$ and CHF_3. Therefore, a comparison spectrum was used to eliminate this effect from the experiments. Carbon products believed were, therefore, considered to be
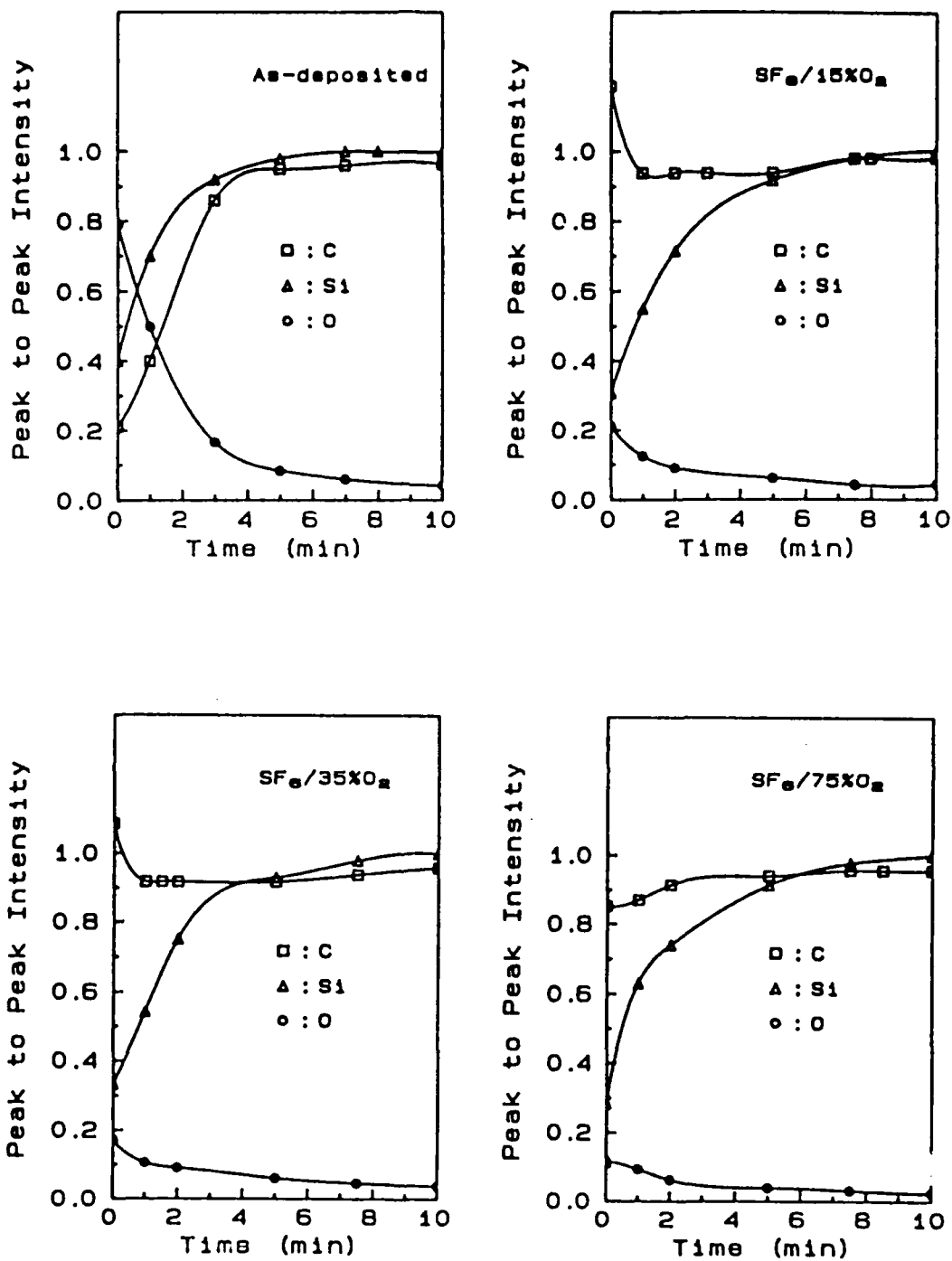
Figure 4.27.   The AES depth profile of SiC etched by $SF_6/\%O_2$ (a). as-deposited, (b). 15%, (c). 35%, (d). 75%.
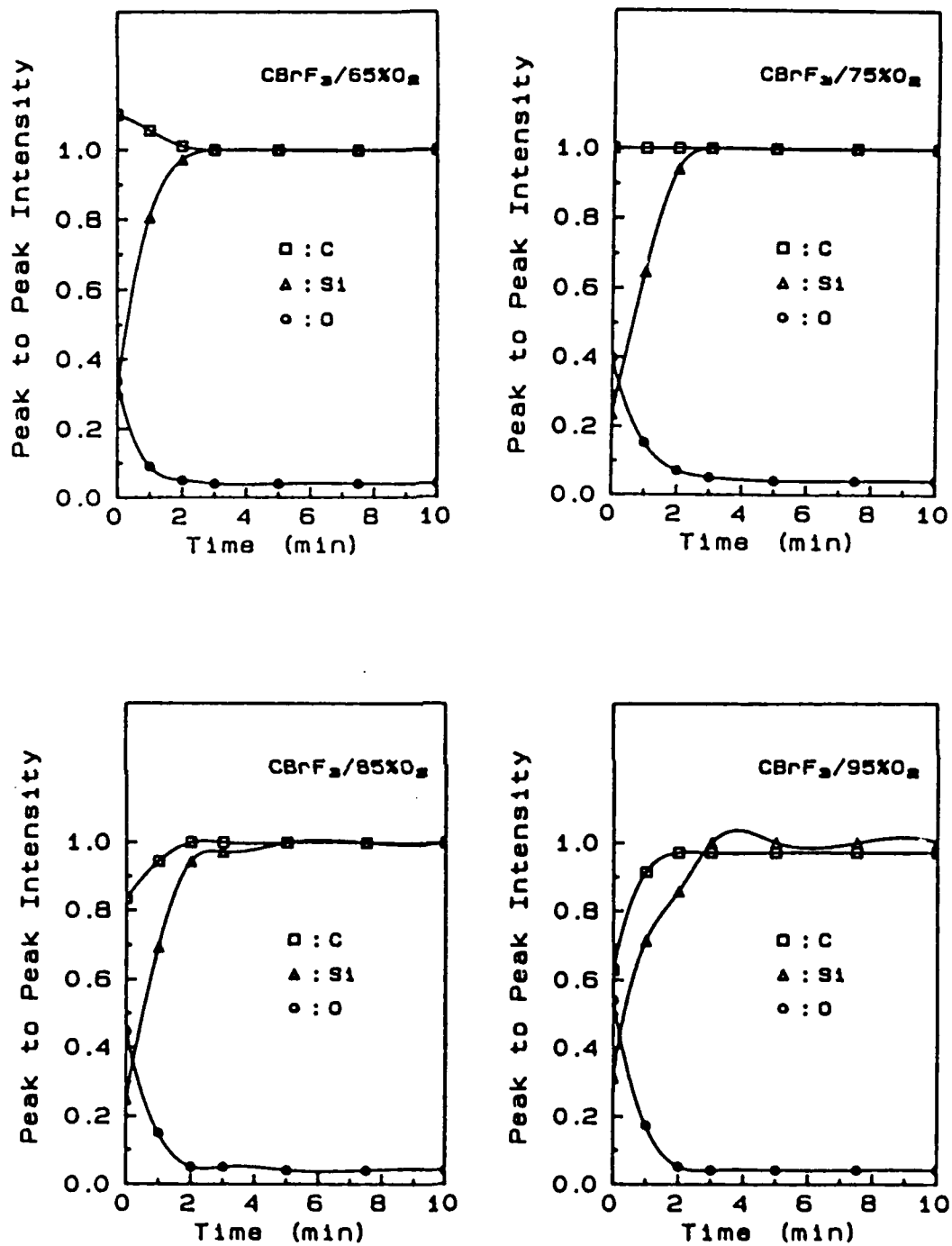
Figure 4.28.   The AES depth profile of SiC etched by $CBrF_3/\%O_2$ (a). 65%, (b). 75%, (c). 85%, (d). 95%.
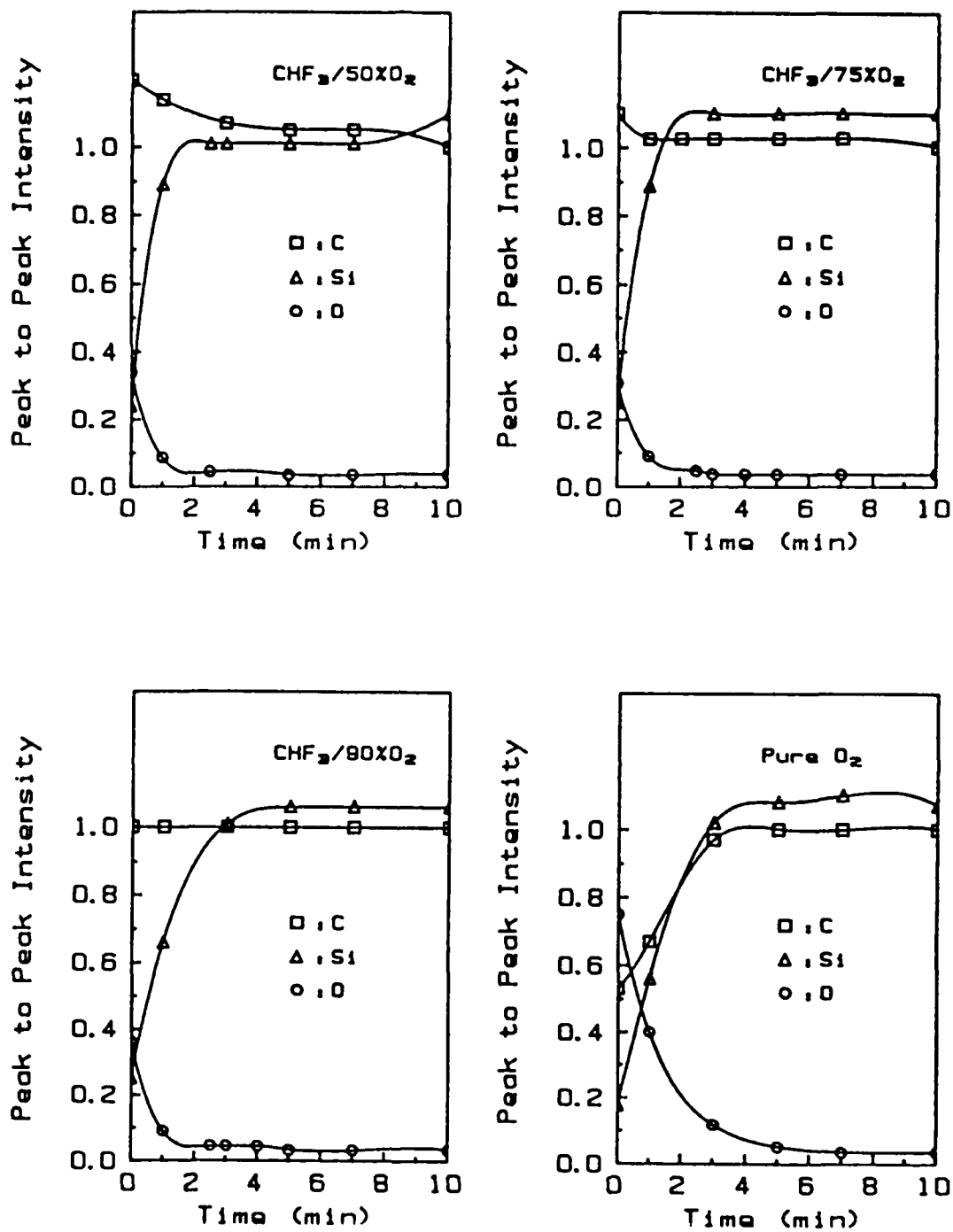
Figure 4.29. The AES depth profile of SiC etched by $CHF_3/\%O_2$ (a). 50%, (b). 75%, (c). 90%, (d). pure-O_2.

contributed by SiC only. The $[CO_x]$ and $[CF_x]$ intensity could be detected at many different wavelengths, such as 283nm, 297nm, 313nm for [CO], 290nm for $[CO_2^+]$, 275nm, 262nm, 290nm for $[CF_2]$, etc., and the choice of each monitor wavelength depended on the variation of intensity during etching by each processing gas. In general, once a particular product has been observed in the plasma, all the relative wavelengths should be identified by the spectrum map. In Figure 4.30(a), the spectrum results of loading zero to four 3" SiC/Si wafers were shown by using $SF_6/35\%O_2$ plasma at 200W, 20mTorr, 20sccm. The [F] and [O] density were monitored. The same experiment is shown in Figure 4.30(b) for $CHF_3/90\%O_2$ under the same plasma conditions and [F], [O] and [H] were monitored. The variation of each reactant described its role in the etching mechanism.

The etching mechanism of SiC in SF_6 and O_2 mixture plasmas at RIE mode was obtained by etching four 3" SiC samples (40% coverage) and monitored the DC bias , [F](703nm), [O](777nm), $[CF_2]$(289nm) and [CO](297nm) intensity during the etching by $SF_6/35\%O_2$ at 200W, 20sccm, 20mTorr. In Figure 4.31(a), the intensity of comparison spectrum was shown and the differences between "no sample" plasma (positive part) case and SiC sample loaded plasma (negative part) are displayed. The main reactants and products are marked. The data for [F] and [O] density versus etching time was recorded in Figure 4.31(b), which started with unloaded plasma (before 0min), then etched SiC film from 0 to 3.5min, and finished at Si etching. The [CO] density was measured from the comparison spectra. Both [F] and [O] density decreased. The [CO] density has a remarkable change during the etching of the SiC film,
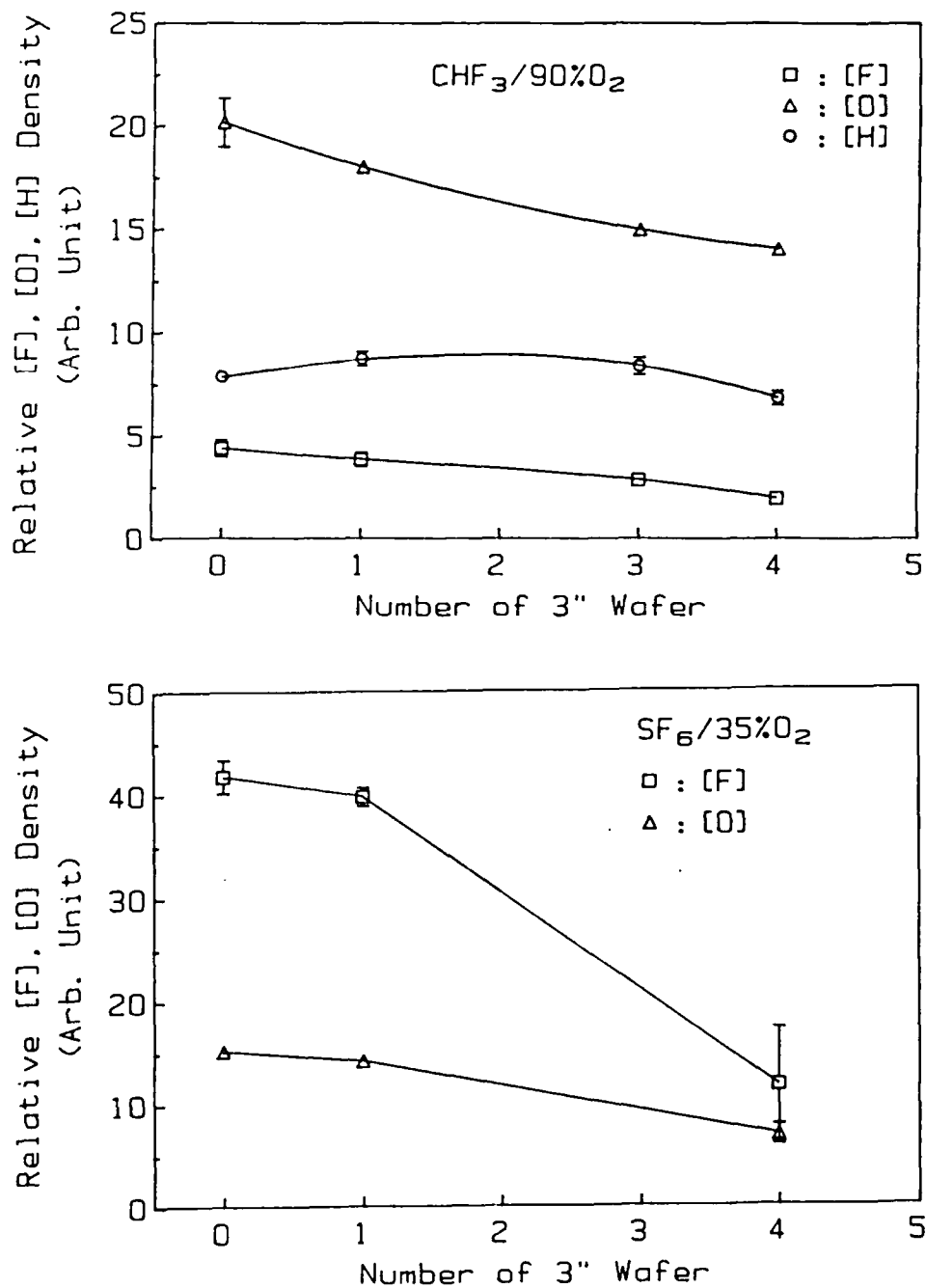
Figure 4.30.   The loading effect of SiC by (a). $SF_6/35\%O_2$, (b). $CHF_3/90\%O_2$ at 200W, 20mTorr and 20sccm.

compared to non-SiC etching plasma. No $[CF_2]$ peak was found.

In Figure 4.32, the high concentration of oxygen was used at $SF_6/90\%O_2$, 200W, 20mTorr to etch two 3" $SiC/SiO_2/Si$ samples. The comparison spectrum was shown in Figure 4.32(a) and the consumption of [F] and [O] during the SiC etching was believed to be the main etchants to react with Si and C and form volatile products, as SiF_4 and CO gases. A compatible [CO] density was observed by etching only two 3" SiC sample. In Figure 4.32(b), the variation of reactants and product ([CO]) concentration were shown clearly as a function of etching time.

The comparison spectrum of $CBrF_3/75\%O_2$ is shown in Figure 4.33(a) by etching only one 3" SiC sample from 0 to 9min at 200W, 20mTorr plasma. Because of its low induced fluorine density, no fluorine density is detected by loading more samples. The changes of [F] and [O] were small and uncertain and the [Br] did not show evidence of its role in SiC etching. In Figure 4.33(b), the $[CO_2^+]$(287nm) was the monitor product, which increased rapidly during the SiC etching but had no intensity for etching into Si substrate.

A similar experiment and results were observed using CHF_3 and oxygen mixture. The [F], [O], [H] density were measured and [CO] density was recorded from the comparison spectrum by etching three 3" SiC samples at $CHF_3/90\%O_2$, 200W, 20mTorr, shown in Figure 4.34(a) and (b). Both [F] and [O] were decreased when etched SiC from 0 to 16min. After 16min etching, the SiO_2 layer was reached.

In the etchant-unsaturate model described by reactions (4.1) to (4.4)[2.82], specific chemical species derived from electron collisions with etchant gases are considered.
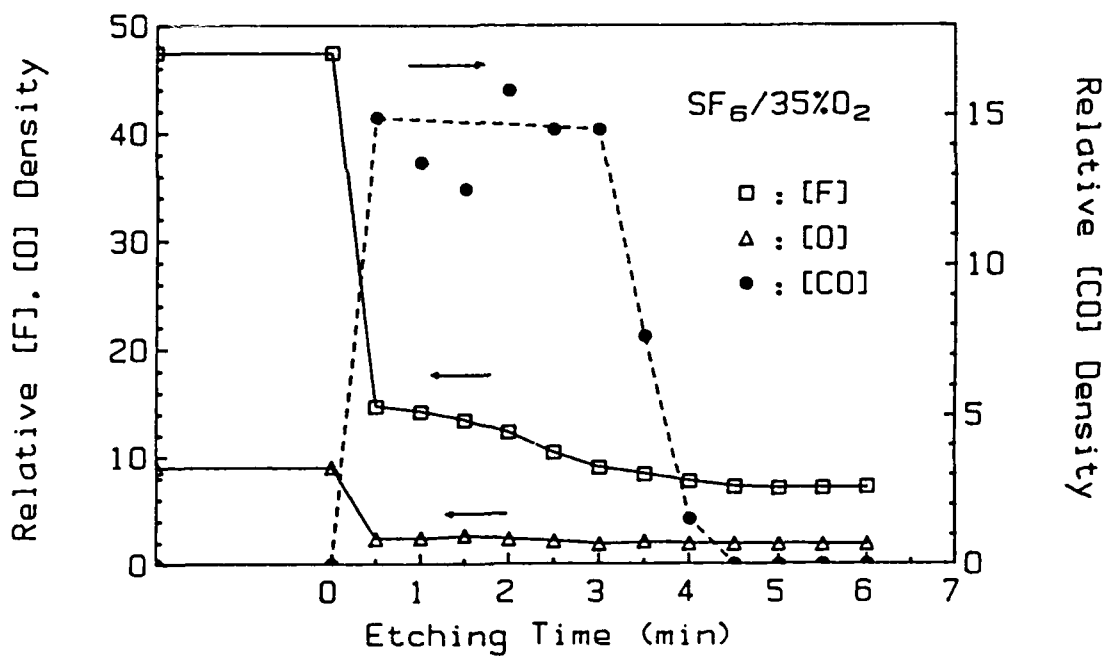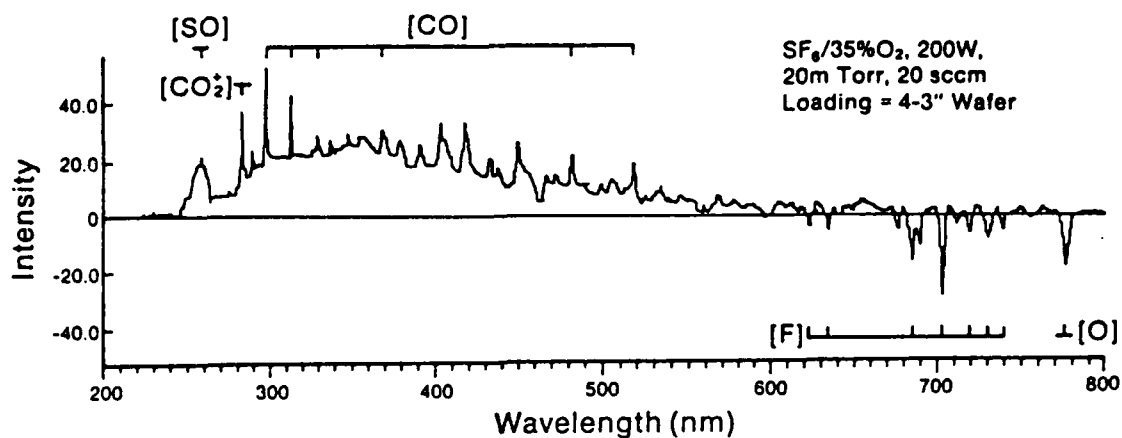
Figure 4.31. Loading experiment of etching four 3" SiC wafers at $SF_6/35\%O_2$ (a). comparison spectrum(b). Relative [F], [O], [CO] density.
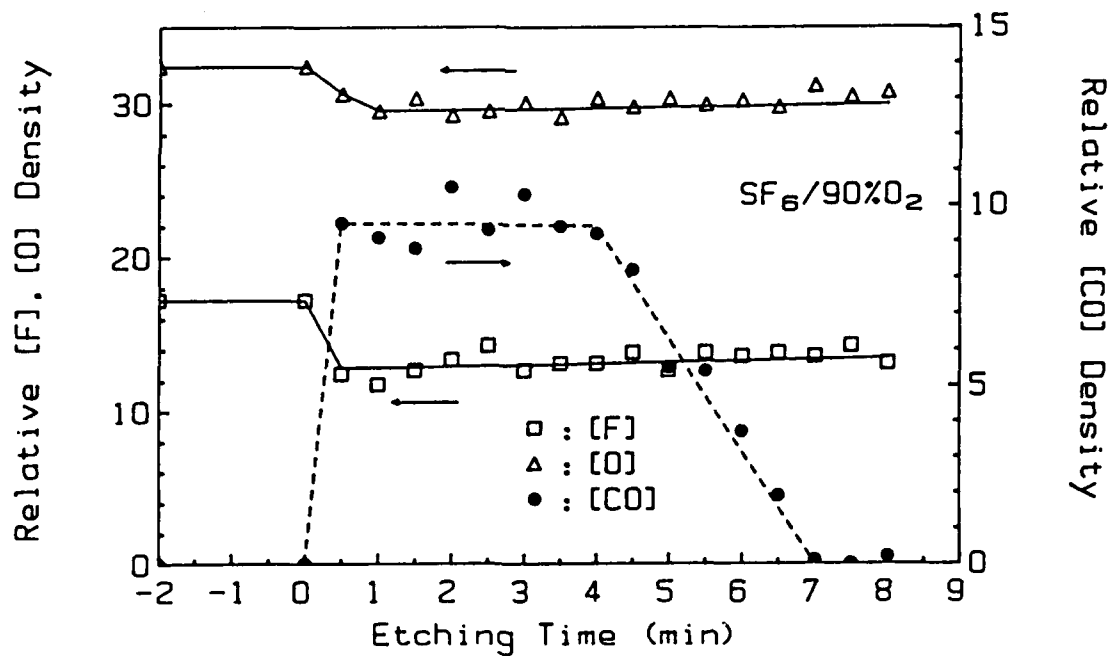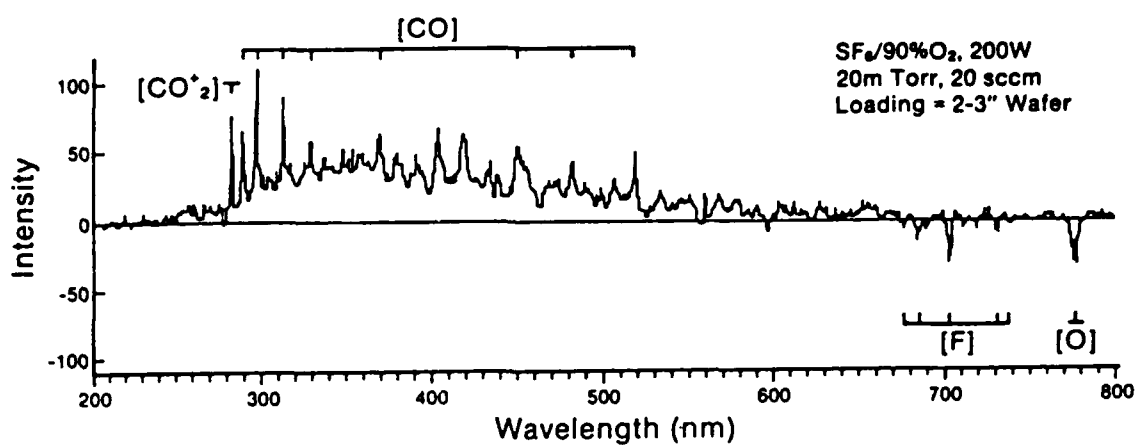
Figure 4.32.   Loading experiment of etching two 3" SiC wafers by $SF_6/90\%O_2$ (a). comparison spectra (b). Relative [F], [O], [CO] density.
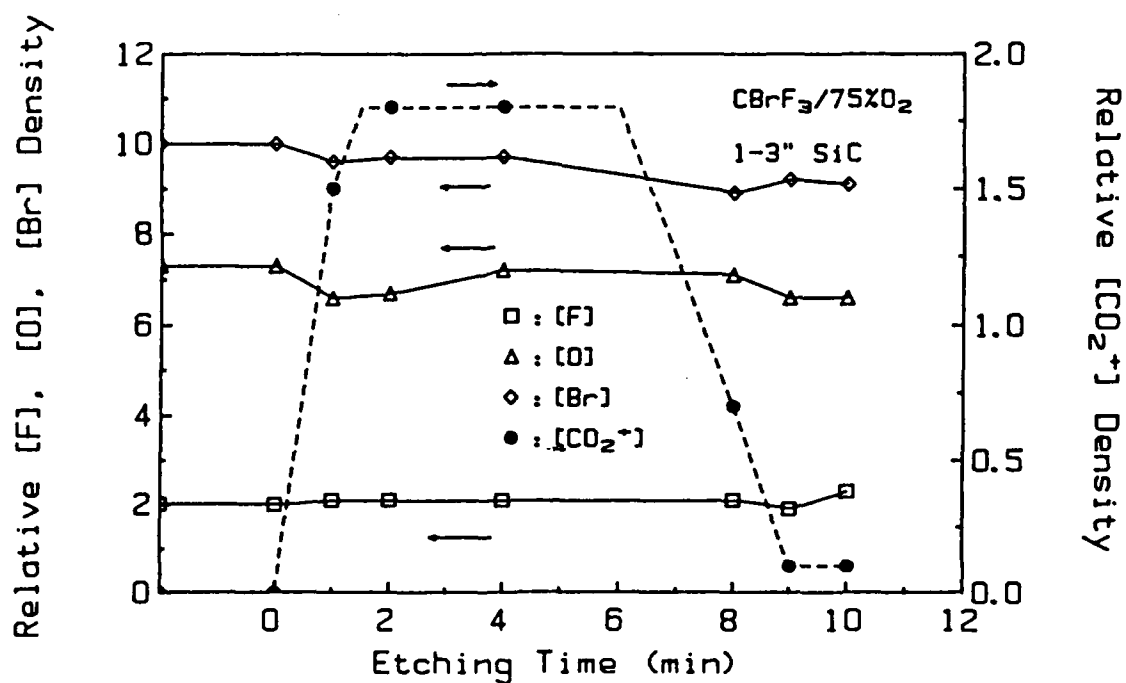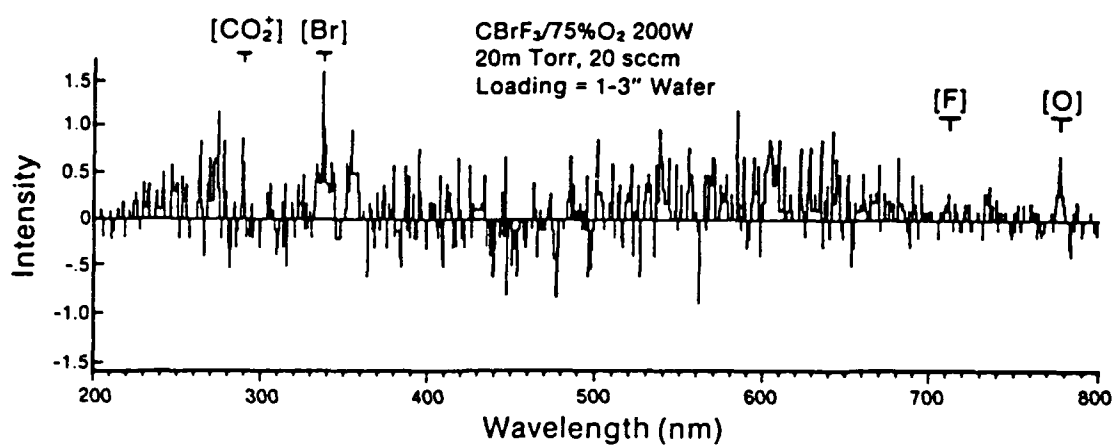
Figure 4.33. Loading experiment of etching one 3" SiC wafers at $CBrF_3/75\%O_2$ (a). comparison spectra (b). Relative [F], [O], [Br], $[CO_2^+]$ density.
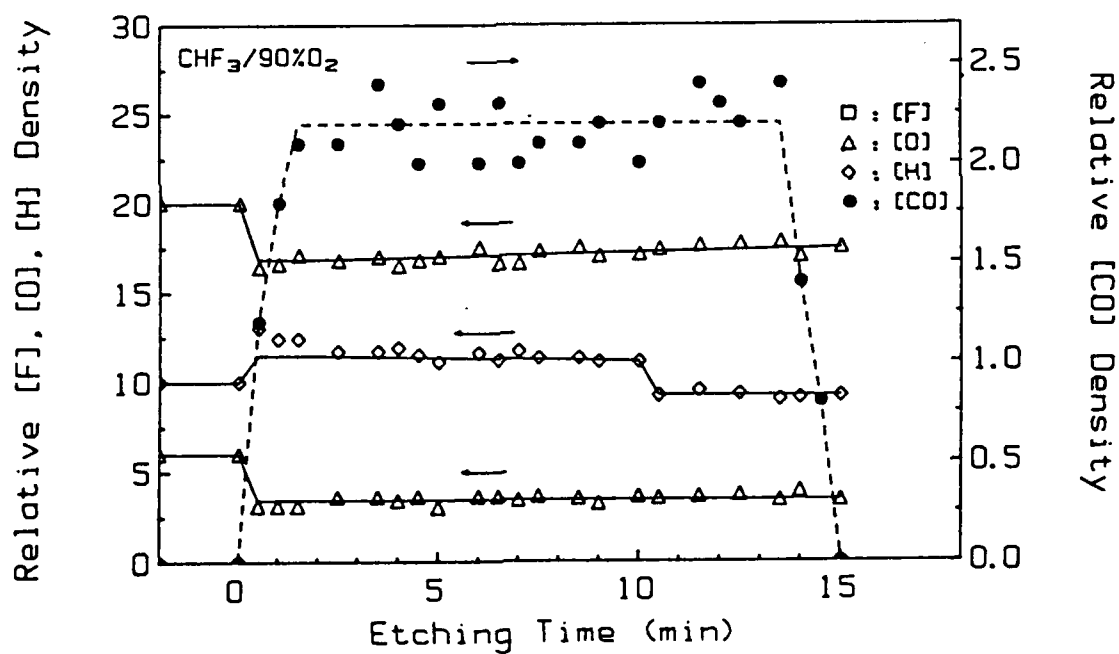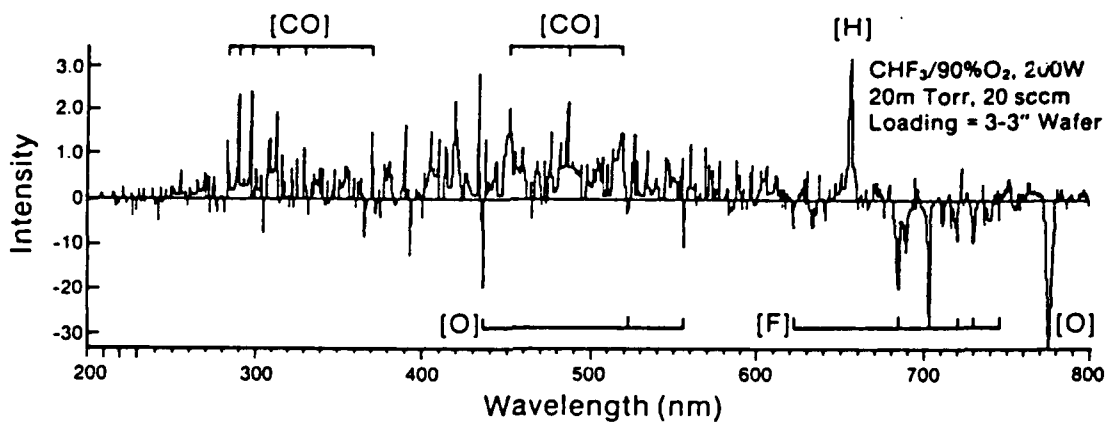
Figure 4.34. Loading experiment of etching three 3" SiC wafers at $CHF_3/90\%O_2$ (a). Comparison spectra (b). Relative [F], [O], [H], [CO] density.

(4.1) e- + Processing Gases ---> Saturated Radicals +

Unsaturated Radicals + Atoms

(4.2) Reactive Atoms & Molecules + Unsaturates ---> Saturates

(4.3) Atoms + Surface ---> Chemisorbed layer

or Volatile Products

(4.4) Unsaturates + Surfaces ---> Films

As an example, the CF_3 is saturated radicals in CF_4 plasma, the CF_2 is unsaturated radical, the SiF_4 is volatile product, and the $(CF_2)_n$ is chemisorbed film on surface.

Hence, the possible products for each gas mixture in these plasma experiments can be simply summarized in reactions (4.5) to (4.7) as shown below :

(4.5) SF_6 + O_2 ---> SF_x + SO_y + [F], [O] (x = 1 to 4, y = 1,2)

(4.6) $CBrF_3$ + O_2 ---> CF_x + CO_y + [Br], [F], [O] (x = 1 to 3, y = 1,2)

(4.7) CHF_3 + O_2 ---> CF_x + CO_y + [H], [F], [O] (x = 1 to 3, y = 1,2)

The [F], [O], [H] and [Br] atoms were the main reactants in Si and SiC etching. The etching of SiC in the reactive ion etching process is considered to consist of two basic mechanisms : chemical and physical reactions, which are based on the above experimental results. For SiC and Si etching in fluorinated gases the most likely chemical reactions are given below :

(4.8) $Si + 4F \rightarrow SiF_4$

(4.9) $C + xO \rightarrow (CO, CO_2)$

(4.10) $SiC + xF + yO \rightarrow SiF_4 + (CO, CO_2)$
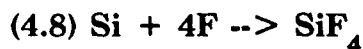
In reaction (4.8), Si is removed mainly by reacting with fluorine to form SiF_4 volatile gas[4.6] at room temperature. The required energy for this reaction (4.8) is believed to be much lower than the energy needed for oxygen and carbon in reaction (4.9). In Figure 4.3(a) & (b), the Si etch rate followed the variation of fluorine density, even though the DC bias was as low as 25V. It should be assumed that carbon can react with both fluorine and oxygen atoms and the products carbon mono- or di-oxide were observed directly from etching experiments by previous loading experiments. However, no carbon fluoride product was identified from emission spectra even in abundant fluorine concentration gases, such as the $SF_6/35\%O_2$ loading experiments. Hence, only oxygen is considered

in reaction (4.9) and the reaction between carbon and fluorine is suggested to occur at a very low rate.

The mechanism of reaction (4.9) could be suggested by both ways, such as chemisorbed oxygen on surface and gained the reaction energy from other ion, or bombarded by energetic oxygen ion and reacted with carbon directly. Therefore, the carbon layer could be removed by the combination of ion bombardment and chemical reaction with oxygen during these reactive ion etching experiments.

A typical DC bias, 300V, is concluded from previous experiments for the dependence of SiC etch rate and physical reaction. When DC bias is higher than 300V, the SiC etch rate is strongly determined by the chemical reaction, which is related to the concentration of reactive species, such as [F] and [O] under high composition oxygen condition.

Therefore, in the etching of SiC, a two-step etching process, shown in reaction (4.10), is considered to be an appropriate etching model, wherein silicon and carbon atoms are removed separately. Under most conditions, the Si etch rate is higher than that of SiC. This is due to comparatively higher removal rate of Si atoms than C atoms. As a result, a carbon-rich surface is formed on the SiC film during etching, becoming a potentially rate-limiting step under certain conditions. The C-rich surface has been verified by Auger electron spectroscopy (AES) in section 4.8.1 and could be reduced by increasing oxygen concentration and DC bias.

For SiC etching phenomena, the SiO_2/Si substrate was used and the etching situation was observed through the quartz window of chamber and stopped when a small amount of SiC film still remained.

The color change from green (SiC) to dark red (SiO_2) was used to recognize the end-point of the experiment. The SiO_2 background layer was preferable to use plain Si substrates. The relationship between the electrodes, sample position, gas flow direction and plasma are shown in Figure 4.1(b). The thickness and refractive index of the SiC film after annealing were measured by ellipsometry from edge to edge for a 3-inch wafer, and shown in Figure 3.5. The thickness at the wafer edge was 10% thinner than in the center region, due to a sputtering effect. The etching results were replotted at Figure 4.35 by using $SF_6/35\%O_2$, $SF_6/90\%O_2$, $CBrF_3/75\%O_2$ and $CHF_3/90\%O_2$ plasma at 200W, 20mTorr and 20sccm. For the low concentration oxygen case, such as $SF_6/35\%O_2$, when a 3" SiC wafer was loaded, the oxygen concentration was depleted along the direction of flow. Thus, the etching of SiC was dominated by mass-transfer limit and the the etch rate of the wafer edge close to the gas inlet was faster than the edge close to the exhausting hole (center). In the high concentration oxygen case, the reaction-limit will dominate the etching and because of the variation of thickness, the etching pattern was round and symmetric. The effect of the carbon rich surface in SiC etching is shown to be the limiting step. The oxygen has a strong effect to remove this carbon layer and improves SiC etch rate. Fluorine was shown not to be a major reactant for removing carbon in these etching conditions.
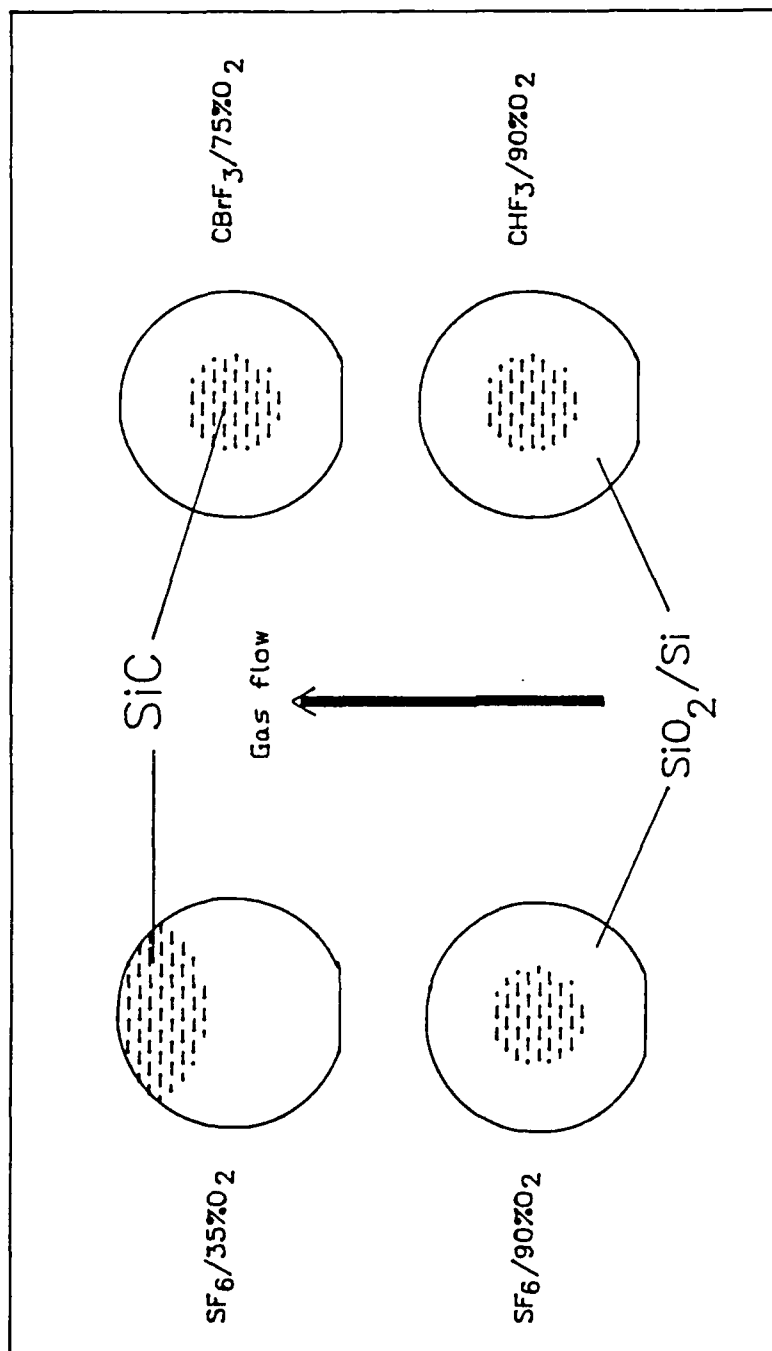
Figure 4.35. SiC etching phenomena by different gases and composition of oxygen at 200W, 20sccm, 20mTorr in RIE mode.

4.8.3 Anisotropic Etching Model

A carbon sidewall blocking model has been proposed in Figure 4.36(a) to understand the physical etching mechanism in reactive ion etching of SiC. In general, the surface damage and inhibitor mechanisms[4.11, 4.12] have been used to understand the anisotropic etching caused by ions in plasma etching. The result of ion bombardment caused by the plasma-induced DC bias on the electrode carrying the samples will cause a more directional etching and will generate more etching sites and more energetic ions to damage, react and remove inhibitor from the surface by physical and chemical means. However, ion bombardment is less effective at removing material from the sidewall (parallel to the ion direction). Therefore, a carbon-rich surface remains on the SiC sidewall reducing the lateral etching, thus, resulting in a more highly anisotropic etching. The carbon layer was assumed to be the only type of inhibitor. In Figure 4.36(b), the carbon blocking layer model was used to explain the etching phenomena in the strong undercut situation of Si substrate in Figure 4.16(a), in which the SiC layer was protected by this carbon layer and no etching from backside, especially by undirectional neutral fluorine atom, was observed and suggested that fluorine atom will not react with the carbon layer.

In general, discharges in halocarbon gases will produce unsaturated fragments that can react rapidly on surfaces to produce polymeric films. Especially, for CHF_3 plasma, the polymer film formed on Si and SiO_2 surface even in RIE mode was observed by Cardinaud et al.[4.13]. However, using such high percentage of oxygen mixture in our case, the
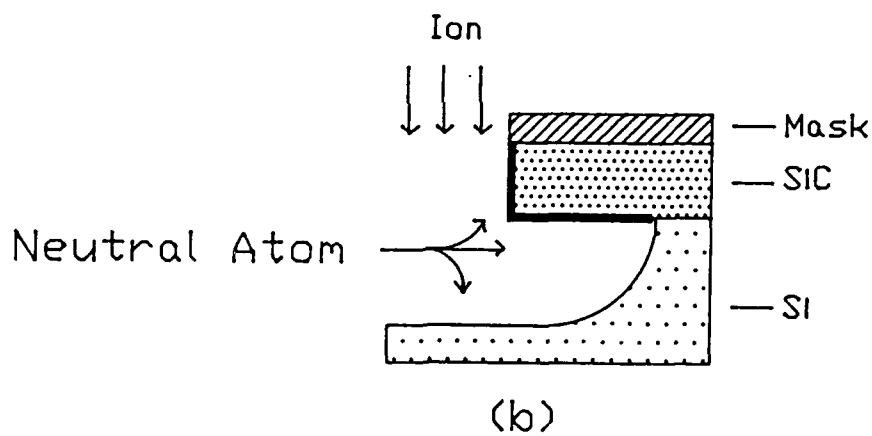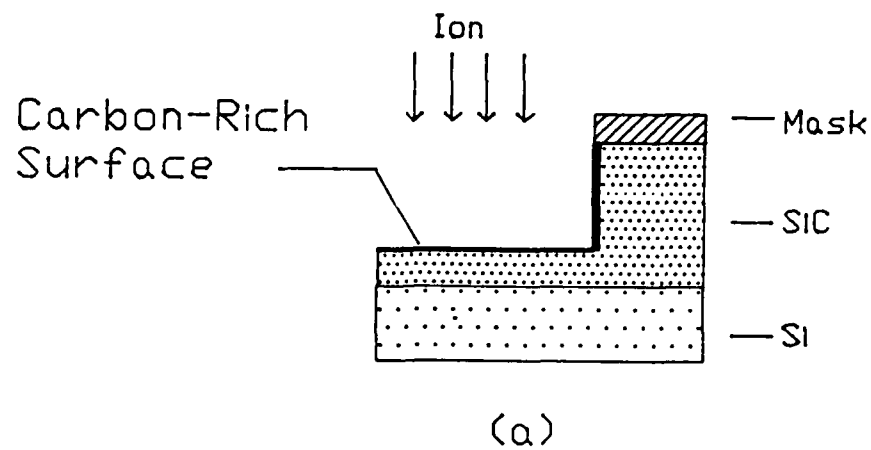
Figure 4.36. Carbon-blocking model (a). SiC anisotropic profile (b). strong undercut of Si substrate situation.

CHAPTER 5

REACTIVE ION ETCHING : TUNGSTEN

5.1 Experimental Procedure

Tungsten films of 300 to 500nm were deposited on Si and SiO_2 for annealing and etching experiments. RTA was found to be very effective at reducing the resistivity of the W films by changing annealing time and temperature. The lowest resistivity value of 13μohm-cm was obtained for 1100°C, 60sec for films annealed in Ar ambient, shown in Figure 3.13(b). X-ray diffraction patterns of W thin films deposited on oxidized Si (100) wafers were taken for each annealing temperature and compared to the as-deposited films. It was found that with increasing temperature the W films became strongly (110) oriented. More details on this topic are described in Section 3.2.5. For the etching experiments, W films were prepared by the above described conditions.

The reactive ion etching rates were determined as a function of oxygen percentage in CF_4, SF_6, $CBrF_3$ and CHF_3. The Ar actinometry technique was used to convert the emission intensity to its relative density.

5.2 $CF_4/\%O_2$ Plasma

In Figure 5.1(a), the W etch rate for CF_4 plasma, along with the etch rates of Si and SiO_2, is shown as a function of oxygen percentage

125
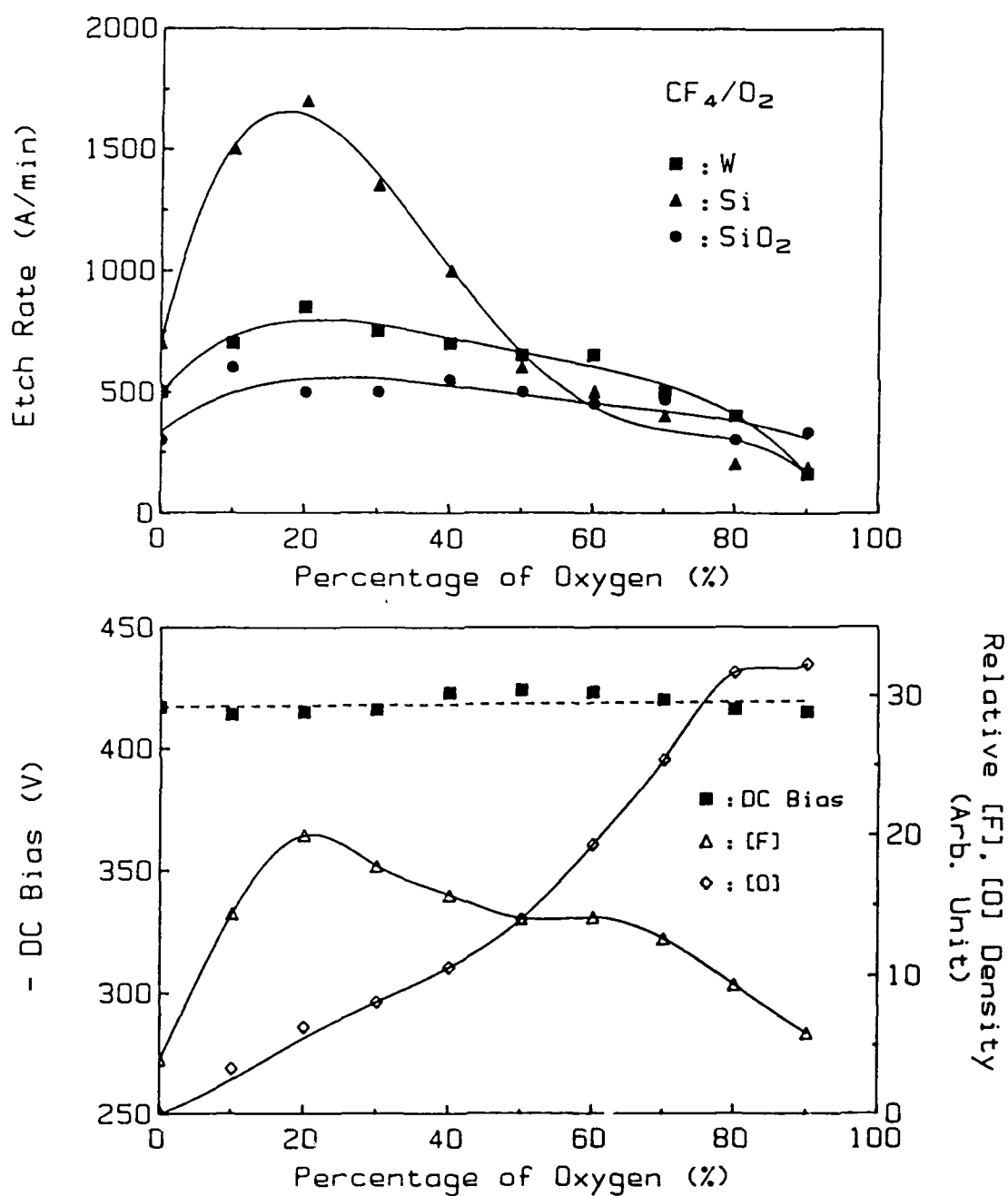
Figure 5.1.   (a) Etch rate of W, Si and SiO_2 (b) -DC self bias and relative [F], [O] atomic density versus percentage of O_2 in CF_4 and O_2 plasma.

(from 0% to 90%) at a power of 200W, a pressure of 20mTorr and a total flow rate of 20sccm. In Figure 5.1(b) is shown the corresponding DC self-bias and the plasma density of fluorine [F] and oxygen [O]. The addition of relatively small amounts of oxygen to CF_4 increases the Si etch rate as the oxygen consumes fluorocarbon radicals and liberates additional fluorine species[4.5]. Beyond a certain concentration, however, increasing amounts of oxygen have the opposite effect, as the oxygen-rich mixture dilutes the CF_4 gas and also lowers the energy of electrons in the plasma, which in turn reduces the electron-induced dissociation rate of CF_4. Another important effect at high O_2 concentrations is the competition for active etching sites on the surface between [F] and chemisorbed O atoms[4.6]. In general, however, the variation of the [F] density with O_2% is roughly mirrored in the Si etch rate.

The W etch rate behavior with O_2% in the CF_4 plasma appears to follow the [F] density, but the relationship is much less pronounced. However, all three parameters (Si and W etch rates, [F] density) exhibit a peak value for a 20% oxygen mixture. In our RIE-mode experiments, the shift of maximum etch rate from maximum [F] is reduced by the presence of a fairly high self-bias voltage (> 400V) which produces more energetic ions, capable of removing some of the chemisorbed oxygen or oxyfluorides from the surface. At high O_2 concentrations, tungsten oxyfluorides (WOF_x) which can form in plasma are less volatile than tungsten hexafluoride (WF_6), as shown in Table 2.9, and can retard the etching process through the formation of a surface oxyfluoride layer[5.1]. Indeed, Picard and Turban have reported[2.107] that W etching in CF_4/O_2 plasma at high pressure generates substantial ionized tungsten

oxyfluorides. For the CF_4/O_2 RIE process, the W:Si etch rate selectivity is considerably less than unity for O_2 mixtures of less than 50%. For O_2 mixtures greater than 50%, the selectivity does increase above unity (for example, 2:1 at 80% O_2), but under the restriction of rather low etch rates (40 and 20 nm/min for W and Si, respectively, at 80% O_2).

5.3 $SF_6/\%O_2$ Plasma

The etch rates of W, Si and SiO_2 in SF_6/O_2 mixtures are shown in Figure 5.2(a). The corresponding DC self-bias and the relative density of fluorine and oxygen in the plasma are shown in Figure 5.2(b). The greater abundance of fluorine species in SF_6/O_2 mixtures results in a much greater Si etch rate. The maximum Si etch rate of 2.2μm/min occurs at 10% O_2 concentration, even though the peak [F] density takes place for 30% O_2. This result is very similar to that reported by Pinto et al. [5.2] for Si RIE at 10mTorr, 50sccm and $0.4W/cm^2$, namely a peak etch rate of 1.3μm/min at 10% O_2. The offset between the maximum Si etch rate and the peak [F] density present in SF_6 etching versus its absence in CF_4 plasma can be explained by the considerably lower (approximately a factor of 2) DC bias found in the former case at small oxygen percentages, which is probably less effective in removing chemisorbed oxygen from the surface. Indeed, Pinto et al.[5.2] report that as the power density (and consequently the DC bias) is lowered the resulting etch rate is not only lowered, but the peak in the etch rate vs O_2 shifts to lower oxygen concentrations. The maximum etch rate of

180nm/min occurs for pure SF_6 gas and etch rate decreases as O_2 increases, which is similar to the results reported by Randall and Wolfe [2.105]. The SiO_2 etch rate is almost constant value of 51nm/min in all range of oxygen.

5.4 $CBrF_3/\%O_2$ Plasma

In Figure 5.3(a), in $CBrF_3$ and O_2 mixtures, the maximum etch rate of Si occurs at 10% O_2, which coincides with the maximum [F] peak. The maximum etch rate for W is much lower than that achieved in non-bromine-containing fluorinated gases. One possible explanation for the low etch rate in $CBrF_3$ lies in the properties of the tungsten bromides as compared to tungsten hexafluoride, as shown in Table 2.10. The W bromides and chlorides have much higher melting and boiling points than the fluoride[2.111]. It is, therefore, very likely that the W bromides have a vapor pressure similar to the W chlorides, which in turn are known to have a much lower vapor pressure than WF_6[5.1]. Further, the tungsten oxybromide also has higher melting and boiling points than the oxyfluoride. Therefore, it is reasonable to explain the lower $CBrF_3$ etch rate as being due to the formation of less volatile compounds. The DC bias and density of [F], [O] and [Br] (at 336nm) measured during W etching in $CBrF_3$ are shown in Figure 5.3(b). The selectivity of W to Si has a maximum of only 1.2:1 at 90%O_2, since it is restricted by very low etch rates for W (14nm/min) and Si (12nm/min). In the work of Schattenburg et. al.[2.108], lower pressure (10mTorr) was shown to improve the etching profile, but it is unlikely to improve the selectivity.
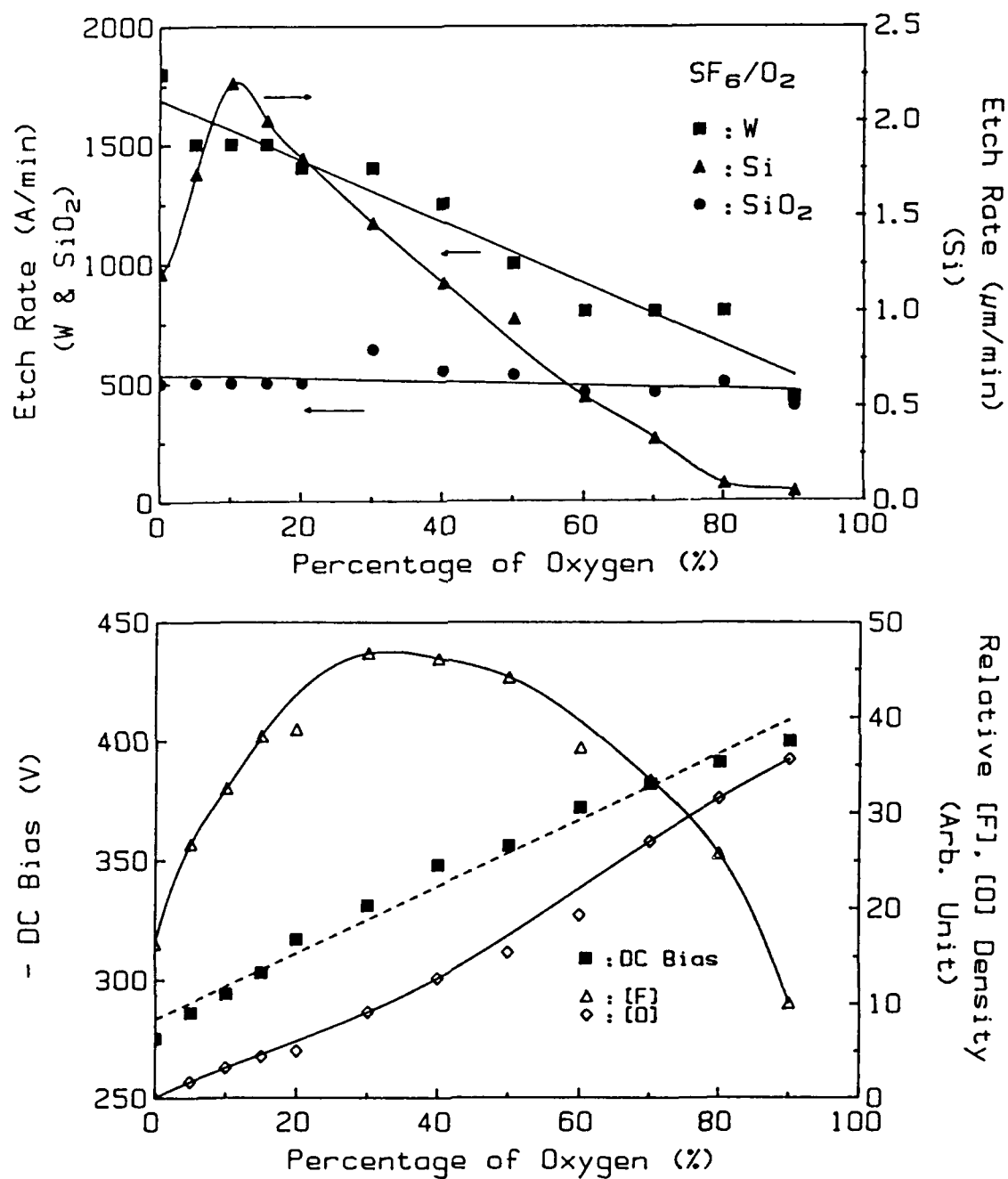
Figure 5.2. (a) Etch rate of W, Si and SiO_2, (b) -DC self bias and relative [F], [O] atomic density versus percentage of O_2 in SF_6 and O_2 plasma.

Finally, data for pure O_2 RIE, shown in Figure 5.3(a), indicates that almost no etching takes place for all materials investigated in the absence of the halogen gas.

5.5 CHF_3/O_2 Plasma

5.5.1 Percentage of O_2

The reactive ion etching rates using CHF_3 and O_2 mixtures are shown in Figure 5.4(a) and the corresponding DC bias, [F], [O] and [H] density (based on emission at 486 nm) are shown in Figure 5.4(b). In the pure CHF_3 plasma, the fluorine species concentration is diluted because of the high hydrogen concentration and by direct reaction with H forming HF molecules[5.3]. This decrease in [F] reduces the Si etch rate considerably, while the presence of HF increases the SiO_2 etch rate[5.4]. In Figure 5.4(b), we show that addition of large amounts of O_2 does result in a slight increase in the [F], with a peak at approximately 65% O_2. The Si etch rate peaks at 50% O_2 with a value of 55nm/min. By comparison, the maximum Si etch rate in SF_6 is 2.2μm/min or 40 times larger.

The W film etch rate in CHF_3/O_2 plasma is also strongly affected by the lower [F] concentration, especially at low O_2 % levels, where the [H] concentration is quite high. However, in the vicinity of the [F] peak at 60 - 70% O_2 mixtures, the W etch rate increases substantially . The highest W etch rate was 66.7nm/min at 70%O_2 and the corresponding
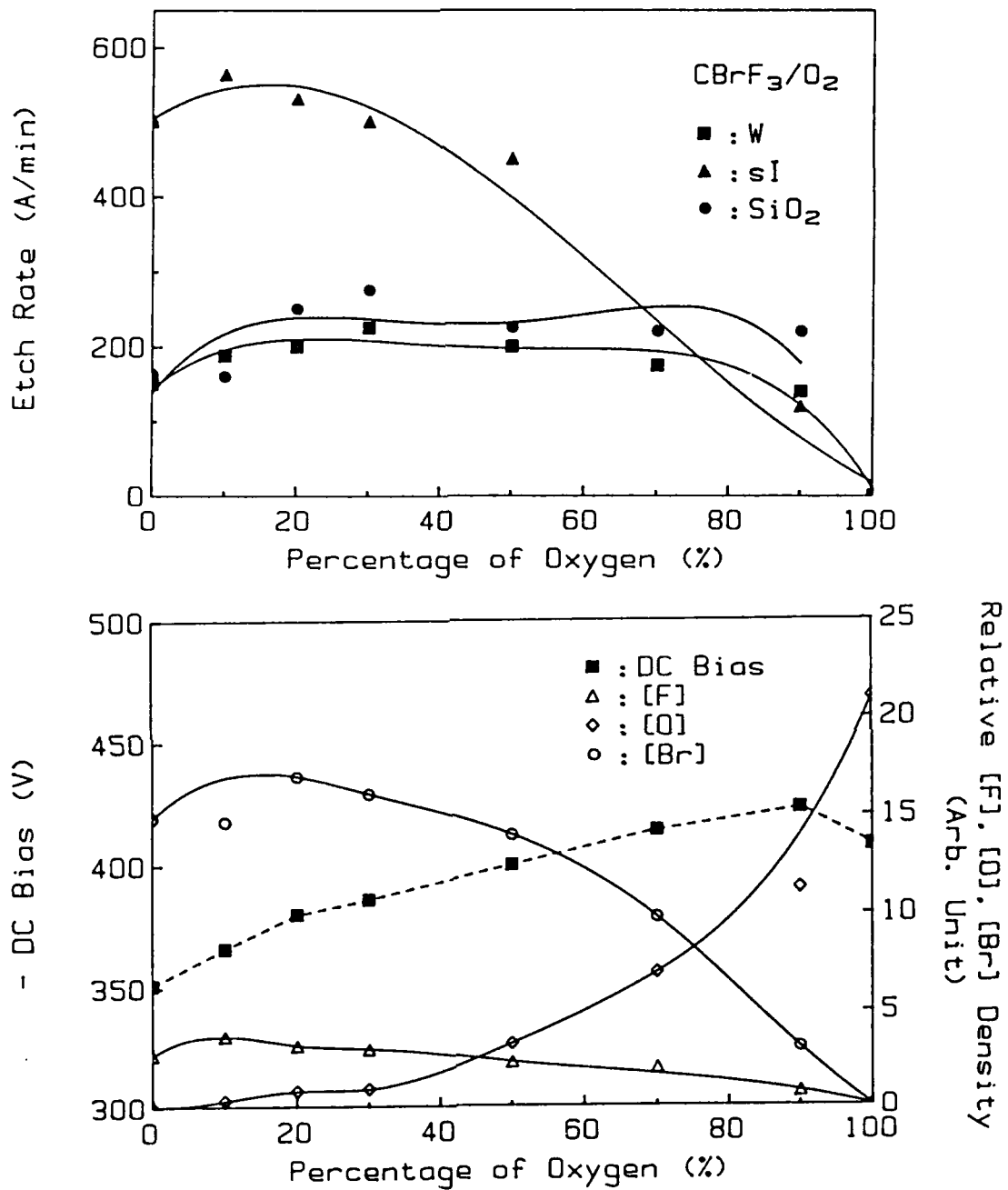
Figure 5.3. (a) Etch rate of W, Si and SiO_2, (b) -DC self bias and relative [F], [O], [Br] atomic density in $CBrF_3$ and O_2 plasma.

etch rate ratios for W to Si and SiO_2 are 1.6 and 1.8. For reverse selectivity, the optimum etching takes place in pure CHF_3, where the following etch rate ratios are obtained: W to Si and SiO_2 of 1:3.2 and 1:4.6.

5.5.2 Pressure

To optimize the W-to-Si etching selectivity, the pressure in the reactor chamber has been varied from 20 to 260mTorr for CHF_3 plus 70%O_2, 20sccm, 200W plasma conditions. The resulting pressure dependence of the etch rates are shown in Figure 5.5(a). Error bars are used to indicate the range of measurements at each pressure. Initially, the W etch rate increases rapidly with pressure, from 67nm/min at 20mTorr to 170nm/min at 88mTorr. At pressures higher than 100mTorr, the W etch rate exhibits substantial saturation. The Si etch rate increases monotonically with pressure, while the SiO_2 etch rate has a broad maximum at around 100mTorr pressure. The optimum W-to-Si selectivity of 3.6:1 and 4.8:1 for W:SiO_2 are measured at 88mTorr and 260mTorr respectively. The corresponding DC bias and [F], [O] and [H] concentrations are shown as a function of pressure in Figure 5.5(b). As expected, the DC bias decreases monotonically with increasing pressure due to increasing number of collisions within the plasma. The corresponding lower plasma electron energy reduces the efficiency of dissociation process. On the other hand, increasing the pressure increases the molecular density of the gas. Therefore, the net effect of two factors determine the pressure dependence of the various species in the plasma.
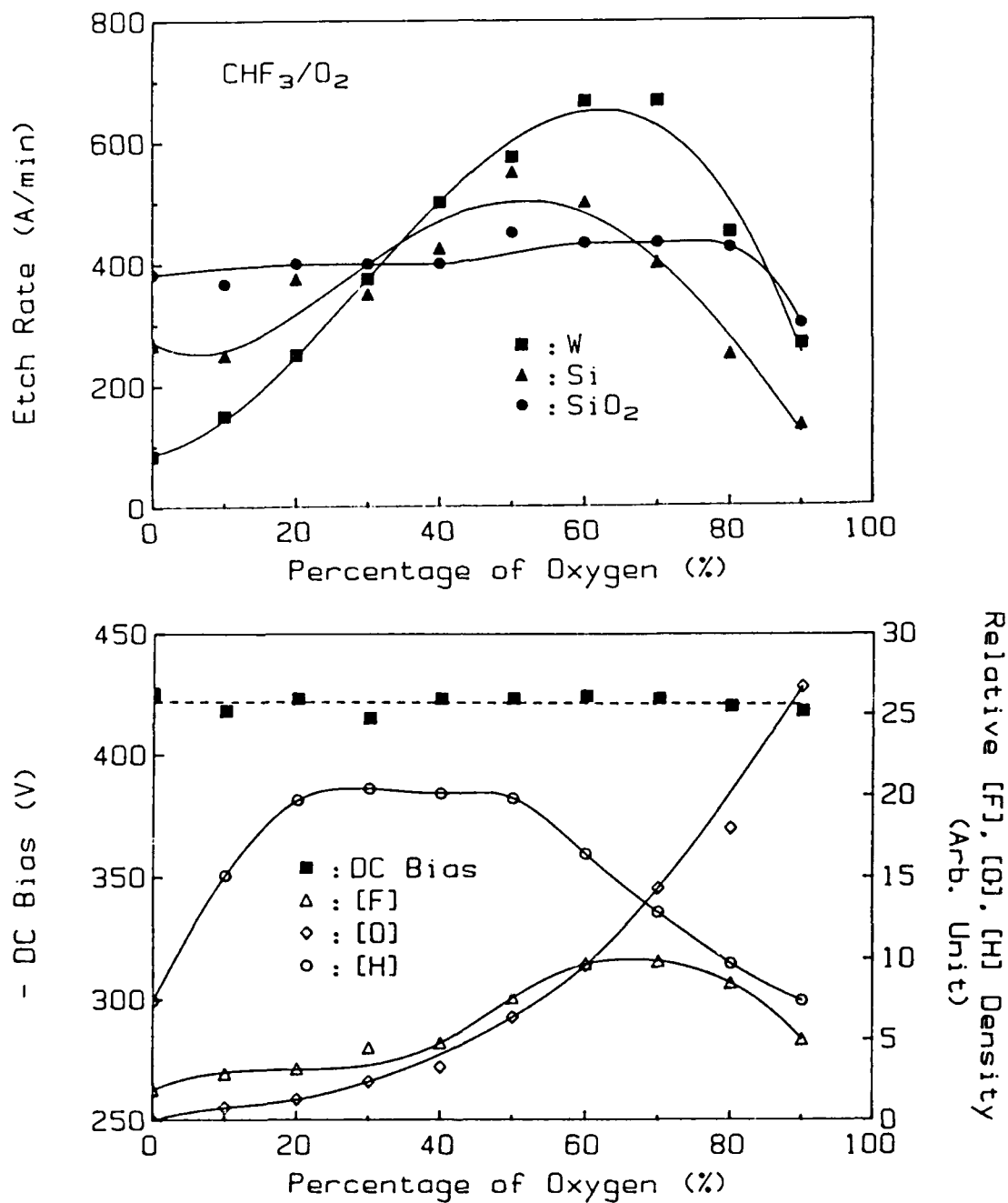
Figure 5.4.   (a) Etch rate of W, Si and SiO_2, (b) -DC self bias and relative [F], [O], [H] atomic density versus percentage of O_2 in CHF_3 and O_2 plasma.

The oxygen concentration is seen to increase rapidly with pressure up to 60mTorr, followed by a much more gradual rise at higher pressure. The fluorine concentration also increases with pressure, up to 110mTorr and thereafter maintains a constant value. Finally, the hydrogen density follows a non-monotonic behavior with a peak occurring at 60mTorr. While the Si etch rate appears to closely follow the [F] concentration, the W etch rate has a more complicated dependence, combining the effect of both [F] and [O].

5.5.3 Power

The effect of varying RF power on the etch rate is shown in Figure 5.6(a). The power is varied from 100 to 300W at 70%O_2, 20sccm, 60mTorr. The W, Si and SiO_2 etch rates exhibit a monotonically increasing dependence on plasma power. At an RF power of 150W, the W etch rate is 120nm/min and etching selectivity of W to Si is 4.0:1. The optimum selectivity of W to SiO_2 is 3.9:1 at 150W. In Figure 5.6(b) the DC bias is shown to increase linearly with RF power. However, both the [F] and [O] concentrations saturate beyond a certain power level. It is, therefore, likely that at high power levels physical mechanisms dominate the etching process by removing low volatility product, such as WOF_x, which can form on the surface under high percentage oxygen conditions[2.107].

The optimum selectivities of reactive ion etching are summarized in Table 5.1. A W:Si etch rate ratio greater than unity was shown for the
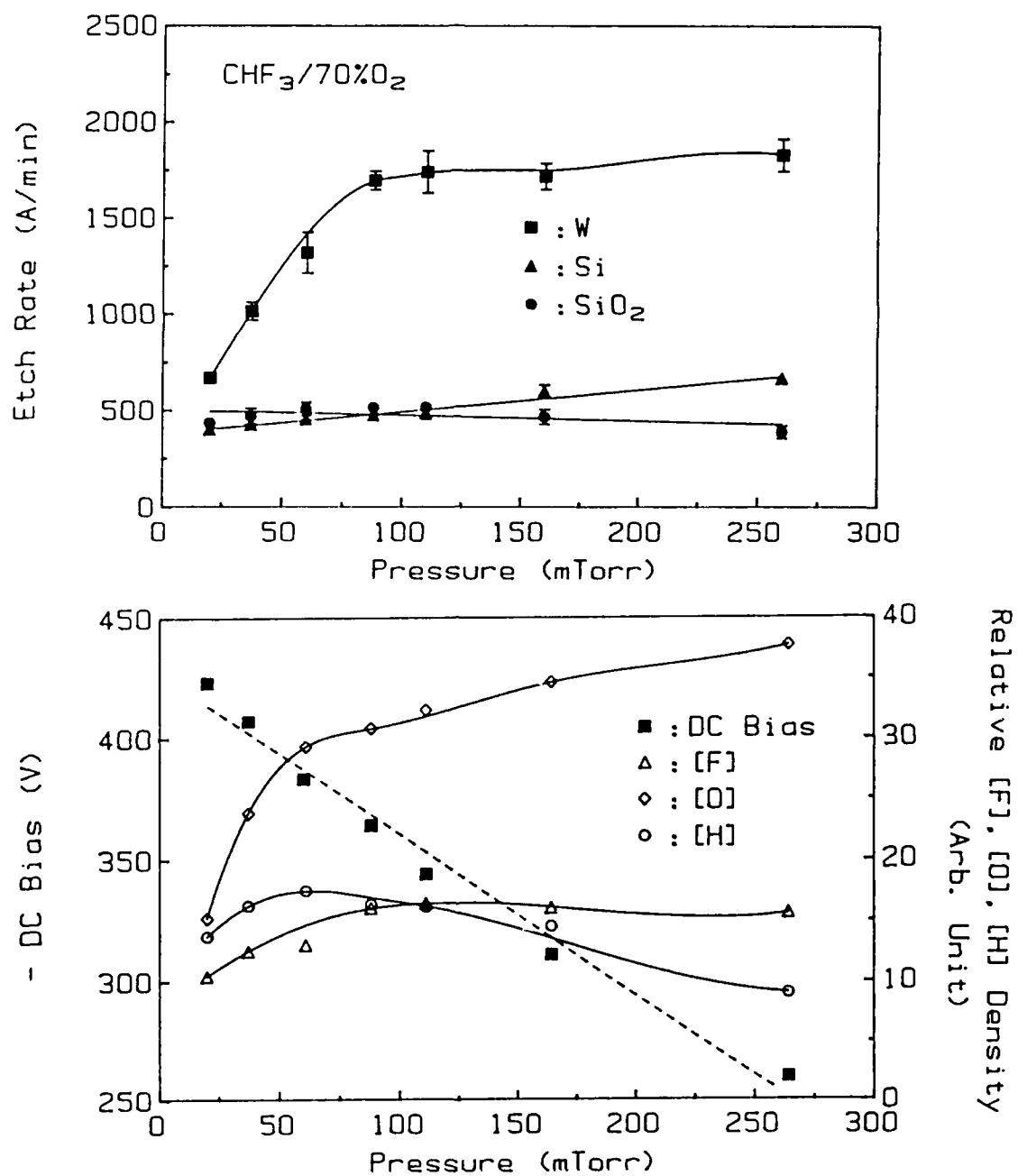
Figure 5.5. (a) Etch rate of W, Si and SiO_2, (b) -DC self bias and relative [F], [O], [H] atomic density versus pressure in CHF_3 / 70%O_2 plasma.
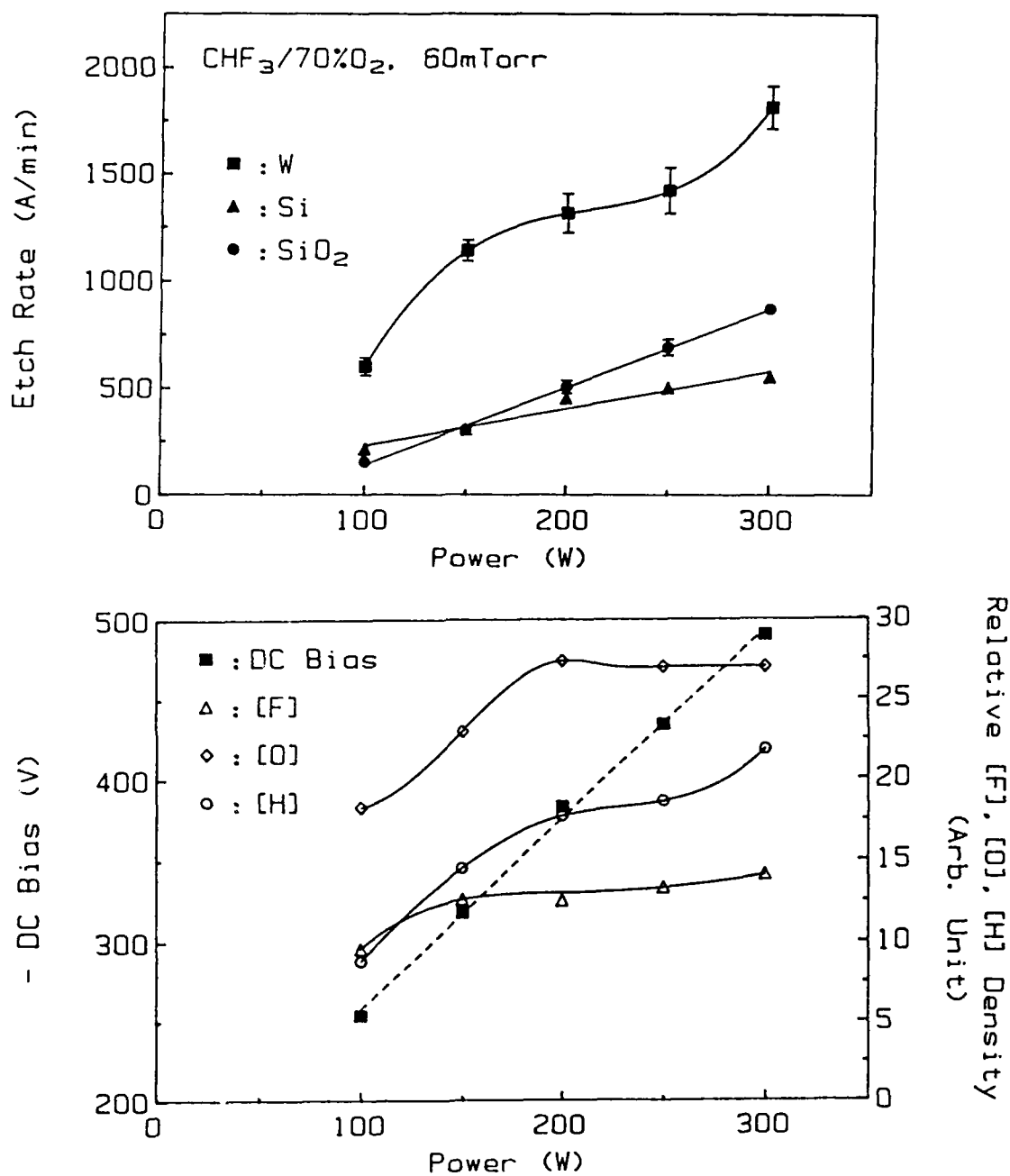
Figure 5.6.   (a). Etch rate of W, Si and SiO_2, (b) -DC self bias and relative [F], [O], [H] atomic density versus power in CHF_3 and 70%O_2 plasma at 60mTorr.

first time to be achievable using $CHF_3/70\%O_2$, 200W, 20mTorr where a selectivity of 1.6:1 was measured. The selectivity can be increased to 4.0:1 by adjusting the plasma pressure and power. The highest reverse W:Si selectivity of 1:11.6 was obtained with $SF_6/5\%O_2$, 200W, 20mTorr. For $W:SiO_2$ selectivity, the optimum value of 4.8:1 was obtained at $CHF_3/70\%O_2$, 200W, 260mTorr, while the optimum reverse selectivity is found in pure CHF_3 plasma.

The selectivity of W:SiC was given and the direct and reverse selectivies of etch rate will be considered for an in-situ patterning W and SiC in fabrication processes.

5.6 Etching Profile

The edge profile of W films etched by reactive ion etching was preliminarily investigated for different gases and plasma conditions. For comparison, the etching profile of W film by using high (CF_4, SF_6) and low (CHF_3) induced fluorine concentration gases was performed. In Figure 5.7, the SEM microphotograph showed an isotropic etching profile was obtained, which $CF_4/50\%O_2$, 200W, 20mTorr, 20sccm conditions was used to etch $0.5\mu m$ W film and stopped at Si surface. A similar result was observed in Figure 5.8(a) by using $SF_6/5\%O_2$ plasma. Both W and Si were etched away under an abundant induced fluorine concentration plasma and the Al mask was still in place, which was clear to show the size of original pattern. The reaction rate of fluorine atoms with Si was faster than W, which can be concluded by comparing the lateral etching length and exposure time. The undercut of Si substrate can be improved by

139

Table 5.1 Maximum Direct and Reverse Selectivies Observed
W:Si, W:SiO$_2$ and W:SiC

Gases / Selectivity	CHF$_3$/70%O$_2$	CHF$_3$	SF$_6$/10%O$_2$	CBrF$_3$/10%O$_2$
W : Si	1.6 : 1	1 : 3.2	1 : 15	1 : 3.8
W : SiO$_2$	1.8 : 1	1 : 4.6	3 : 1	—
W : Si	88mT* 3.6:1 / 150W** 4.0:1	—	—	—
W : SiO$_2$	260mT* 4.8:1 / 150V** 3.9:1	—	—	—

Gases / Selectivity	CHF$_3$/90%O$_2$	SF$_6$	CBrF$_3$/75%O$_2$	CF$_4$/20%O$_2$
W : SiC	1 : 1.5	4.5 : 1	1 : 2.3	2.1 : 1

RIE Etching Conditions : 200W, 20sccm, 20mTorr

* RIE, 20sccm, 200W
** RIE, 20sccm, 60mTorr

using high percentage of oxygen to dilute the fluorine concentration in SF_6, as shown in Figure 5.8(b), but the isotropic etching profile of W film was not improved at all. So, for high induced fluorine concentration gases, such as CF_4 and SF_6, the control of W etching profile was not easy even in the RIE mode, because of the reaction between neutral fluorine atoms and W.

Under the conditions to produce optimum W-to-Si and W-to-SiO_2 selectivity, W films, $0.53\mu m$ thick, were etched mainly in $CHF_3/70\%O_2$ gases. A $5\mu m$ line on Si patterned with $CHF_3/70\%O_2$, (at 20sccm, 200W and 20mTorr) is shown in Figure 5.9(a) with the Al mask layer still in place and in Figure 5.9(b) after removing Al mask. A $0.22\mu m$ undercut of the W film was measured when the etching is stopped at the Si substrate. The vertical-to-lateral etch ratio of the W film shown in Figure 5.9(a) & (b) is 2.3:1.

The etching directionality disappeared when the pressure is increased from 20mTorr to 60mTorr, as shown in Figure 5.10(a), or increased the power from 200W to 300W at 60mTorr in Figure 5.10(b). From the etching experiments in Figure 5.5 and 5.6, the increasing of fluorine concentration is the main reason to cause the loss of etching profile. It seems that increasing the power, DC bias, didn't affect the etching profile under this conditions, which was -380V at 200W, 60mTorr and -480V at 300W, 60mTorr.

However, a vertical-to-lateral etch ratio of 4:1 is measured when the pressure is reduced to 10mTorr, as shown in Figure 5.11(a) (with Al mask) and Figure 5.11(b) (no mask). This is due to the fact that the chemical reaction component of the W etch rate is reduced by the decreasing amount
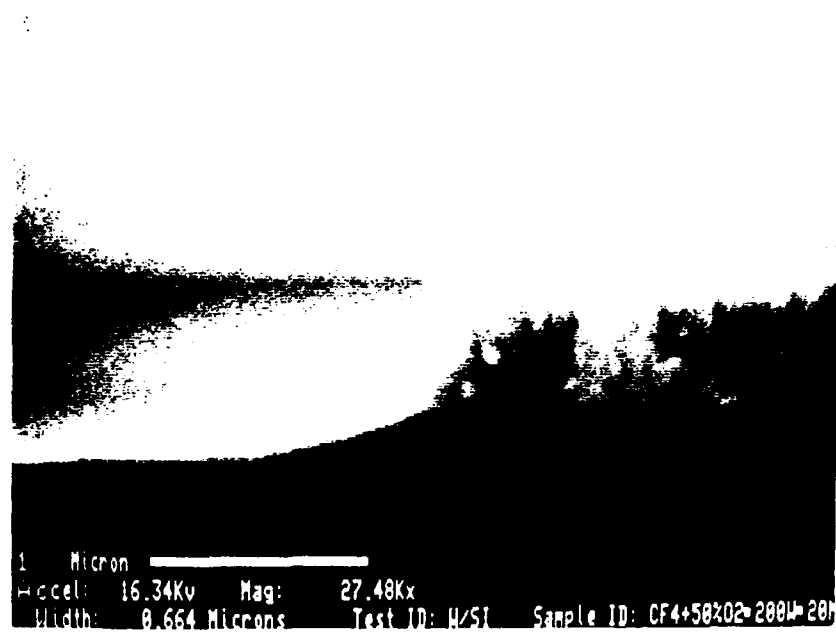
Figure 5.7. SEM picture of edge profile of 500nm W film etched by $CF_4/50\%O_2$, at 200W. 20mTorr.
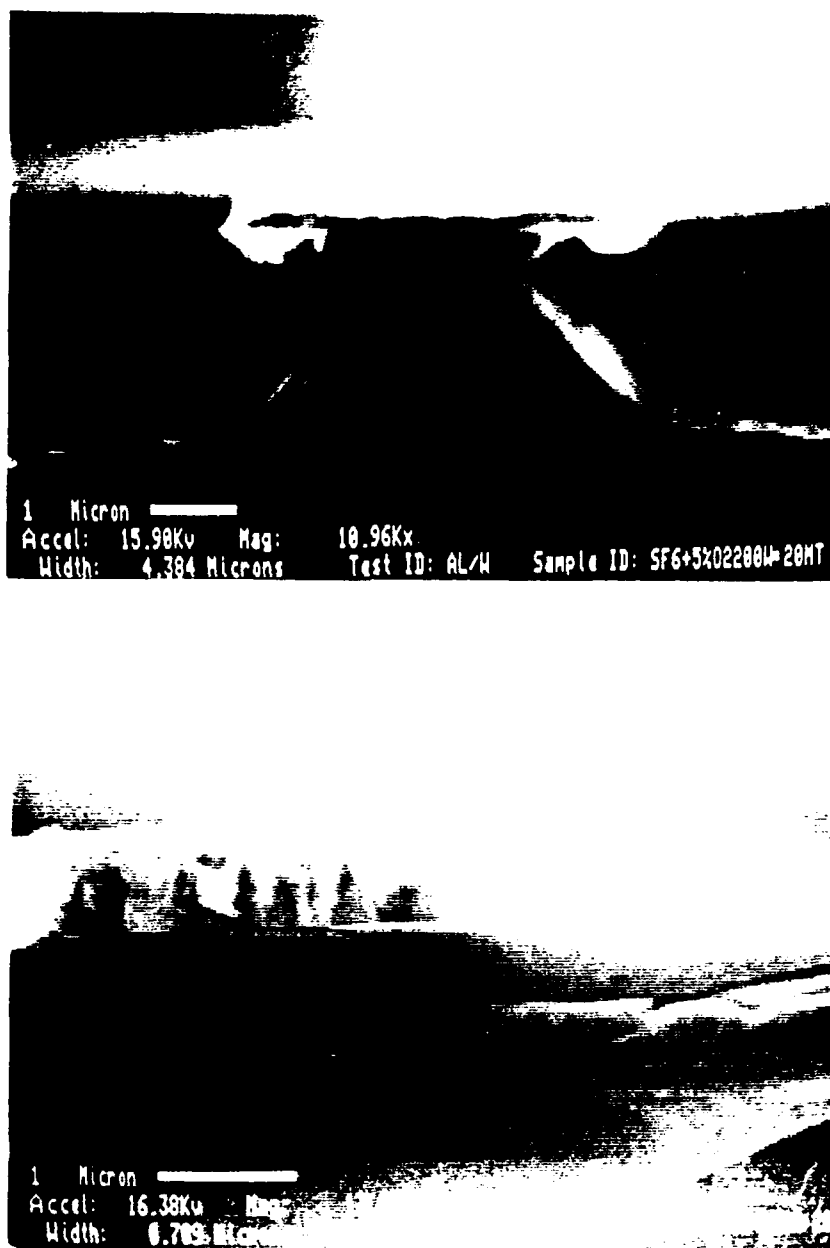
Figure 5.8. SEM picture of edge profile of 500nm W film etched by (a). $SF_6/5\%O_2$, (b). $SF_6/90\%O_2$ at 200W, 20mTorr.

1 Micron
Accel: 16.58Kv   Mag: 9.87Kx
Width: 4.552 Microns   Test ID: AL/W/S Sample ID: CHF3+70%02=200W=20

1 Micron
Accel: 16.17Kv   Mag: 17.59Kx
Width: 4.556 Microns   Test ID: W/SI   Sample ID: CHF3+70%02=200W=20
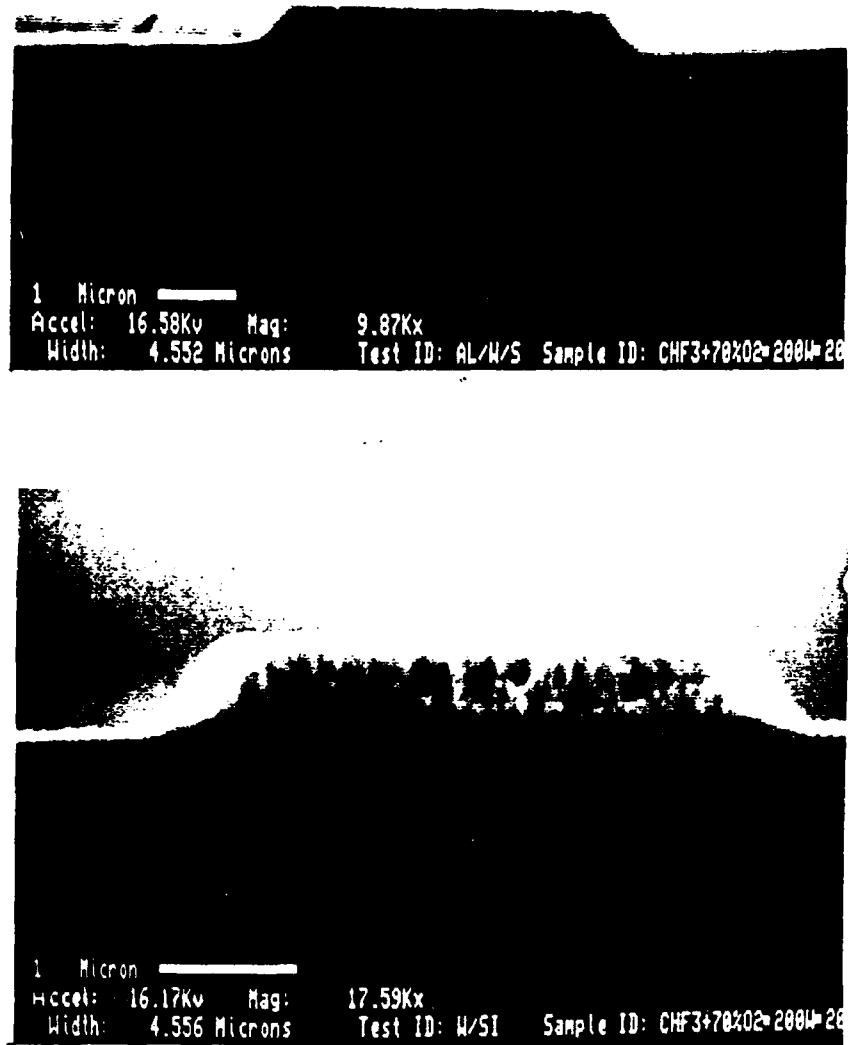
Figure 5.9. SEM picture of edge profile of 530nm W film etched by $CHF_3/70\%O_2$, at 200W, 20mTorr. (a). with Al mask. (b). no mask.
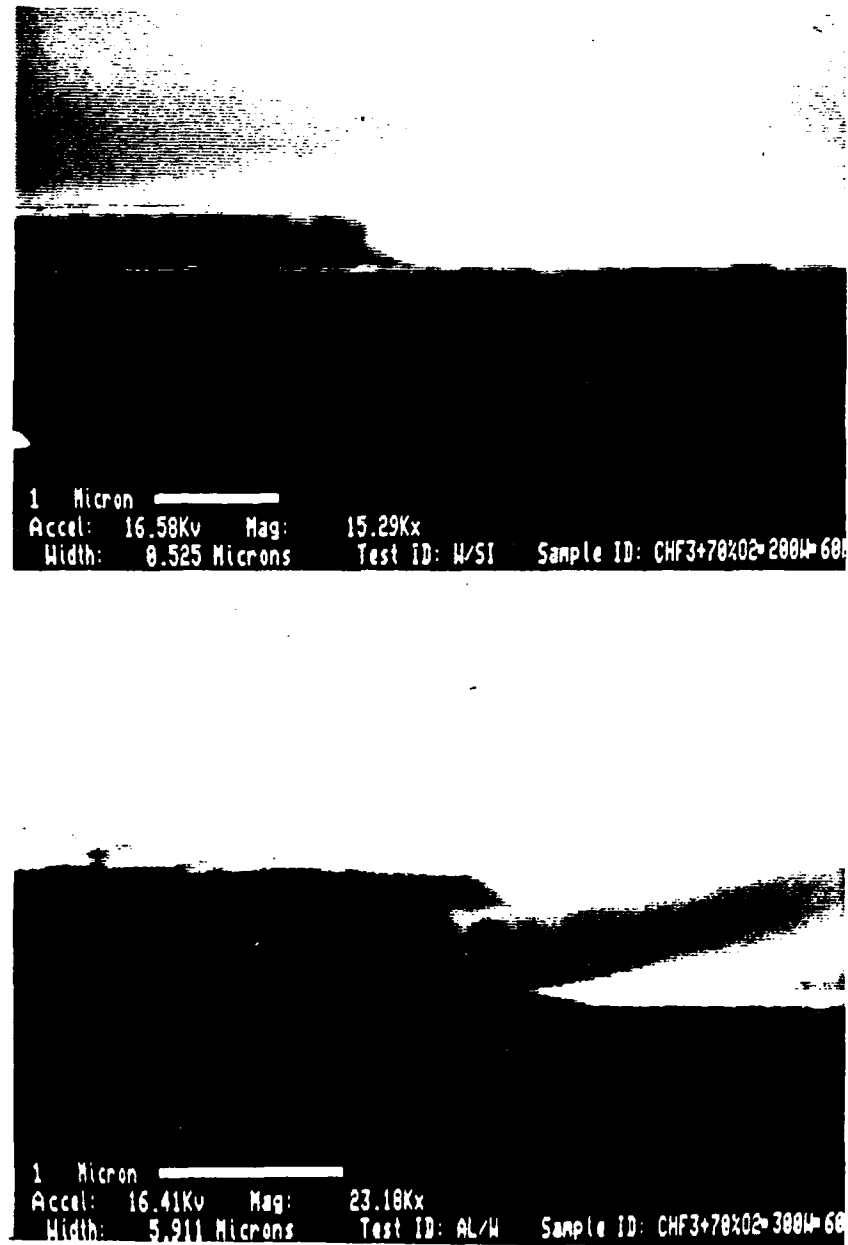
Figure 5.10. SEM picture of edge profile of W on Si etched by $CHF_3/70\%O_2$, at (a). 200W, 60mTorr, (b) 300W, 60mTorr.

of reactive species at lower pressure, while the physical component is enhanced by the increasing self-induced DC bias.

Thus, it is suggested that a good anisotropic etching profile could be obtained by reducing the reaction rate between fluorine and W and increasing the DC bias simultaneously, which could be reached by using low-induced fluorinated gas, and reducing reaction pressure, flow rate and increasing power, etc.

5.7 Discussions

In this work, the fluorinated gases diluted with oxygen in a plasma reactor operating in the RIE mode at a generally fixed pressure, flow rate and power. As discussed in the previous section, a very strong, but complex, relationship is evident between the amount of oxygen in each of the four fluorinated gases (CF_4, SF_6, $CBrF_3$ and CHF_3), the fluorine concentration and the resulting W and Si etch rates. In Table 5.2, the effect of oxygen on our results is compared with those of related work from the literature by indicating the O_2 percentage in the gas mixture at which the [F] density, and Si or W etch rates reach their maximum value. For comparison purposes, the corresponding plasma etching results are also included from the literature.

In the case of CF_4/O_2 mixtures, both our results with W RIE and those of others for W and Si plasma etching[2.106, 2.107] indicate a [F] peak at 20-23% O_2 mixtures. However, under our RIE conditions the W and Si etch rate maximum are coincident with the [F] peak, whereas the PE results published indicate a shift in the maximum etch rate to lower
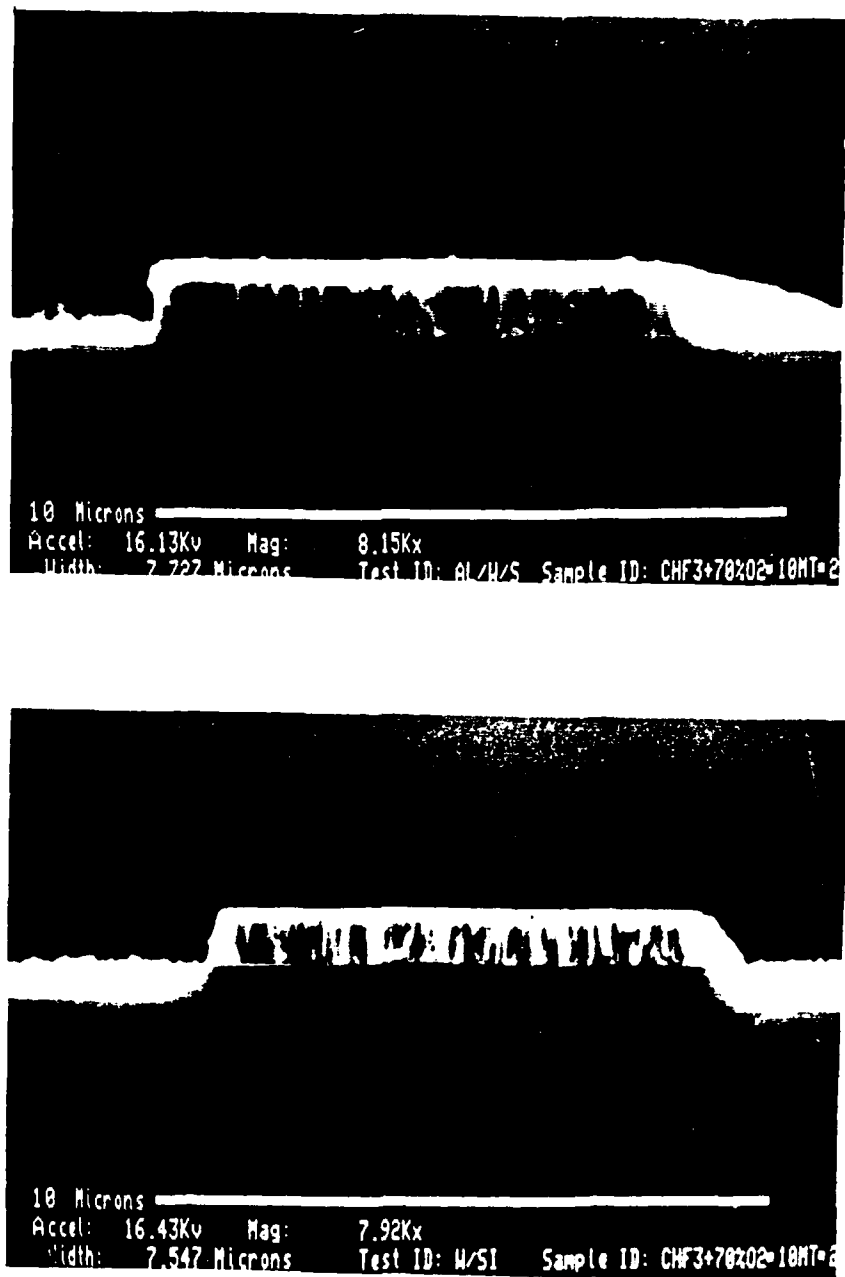
Figure 5.11. SEM picture of edge profile of W on Si etched by $CHF_3/70\%O_2$, at 200W, 10mTorr (a), with Al mask, (b), no mask.

Table 5.2 Comparison of Results for Fluorine/Oxygen-based
Plasma-Assisted Etching of Si and W

Gases	CF₄/ O₂	SF₆/ O₂		CHF₃/ O₂	CBrF₃/ O₂
Mode, Pressure & Power Density	[a] PE 350mT 0.16W/cm² [b] PE 200mT 0.2W/cm² [c] RIE 20mT 0.42W/cm²	[b] PE 200mT 0.2W/cm² [d] PE 1T ~1.8W/cm²	[c] RIE 20mT 0.42W/cm² [e] RIE 10mT 0.4W/cm² [f] RIE 10mT	[c] RIE 20mT 0.42W/cm²	[c] RIE 20mT 0.42W/cm²
[F] peak	** 20%[a] 20%[b]	20%[c]	30%[b] 30%[d]	30%[c]	65%[c]	20%[c]
Si E.R.* peak	12%[a]	20%[c]	30%[d]	10%[c] 10%[e]	50%[c]	10%[c]
W E.R.* peak	10%[b]	20%[c]	0%[b]	0%[c] 0%[f]	65%[c]	30%[c]

[a] Mogab et al.[4.7]

[b] Tang & Hess[2.115]   {W as-deposited at 350°C}

[c] Pan & Steckl[this work] {W RTannealed at 1100°C}

[d] d'Agostino & Flamm[5.5]

[e] Pinto et al.[5.2]

[f] Randall & Wolf[2.114]   {W as-deposited at 25°C}

* E.R. peak : Maximum Etch Rate

** O₂ percentage in processing gases

oxygen percentage (10-15%). In the case of SF_6/O_2 etching, both W PE and RIE of W and Si exhibit this shift. For $CBrF_3/O_2$ etching, shift is found only in W. Finally, in the case of CHF_3/O_2, a shift is observed for Si RIE but not for W etching.

To understand the role of fluorine radicals in the reactive ion etching process, We plot in Figure 5.12, 5.13, 5.14, the etch rates of Si, W and SiO_2 as a function of measured fluorine density obtained at various oxygen mixtures. As can be seen, most cases, with SiO_2 being a major exception , exhibit a substantial hysteresis effect, where for the same [F] concentration two widely different etch rates can result. This effect has been previously observed in the plasma etching of Si in CF_4/O_2[4.7] and SF_6/O_2[5.5] mixtures. As mentioned in above, this effect has been attributed to the competition between fluorine and oxygen atoms for chemisorption sites on the Si surface. Thus, the availability of increasing amounts of [F] does not necessarily result in an increasing etch rate, if it is accompanied by an equal or greater increase in oxygen concentration. In the case of W RIE, our data also exhibit hysteresis, indicating that a similar mechanism is at work. The situation is quite different for SiO_2, since oxygen forms an intrinsic part of the material to be etched. Consequently, no hysteresis effect is observed, but rather a generally increasing trend in etch rate with [F], with a similarly large scatter in the data as reported by Mogab et al.[4.7] for SiO_2 plasma etching in CF_4/O_2 mixtures.

To further elucidate the competing roles of fluorine and oxygen we have plotted in Figure 5.15 the self-normalized Si and W etch rates as a function of the ratio of [F] to [O] concentrations in all four gas mixtures.

149
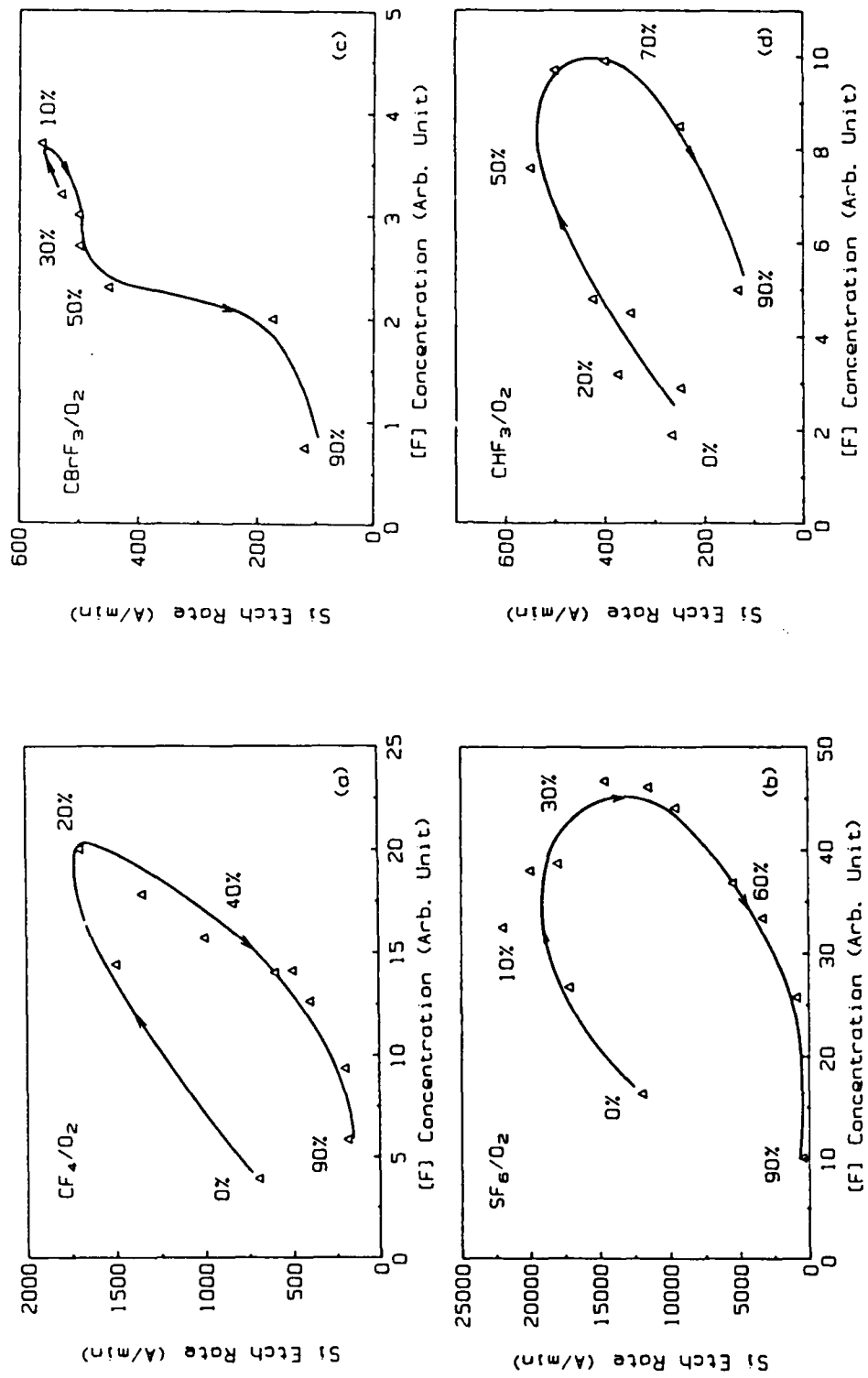
Figure 5.12. Etch rate of Si versus [F] density in (a). CF$_4$, (b). SF$_6$, (c). CBrF$_3$, (d). CHF$_3$ with O$_2$ plasma under RIE mode.
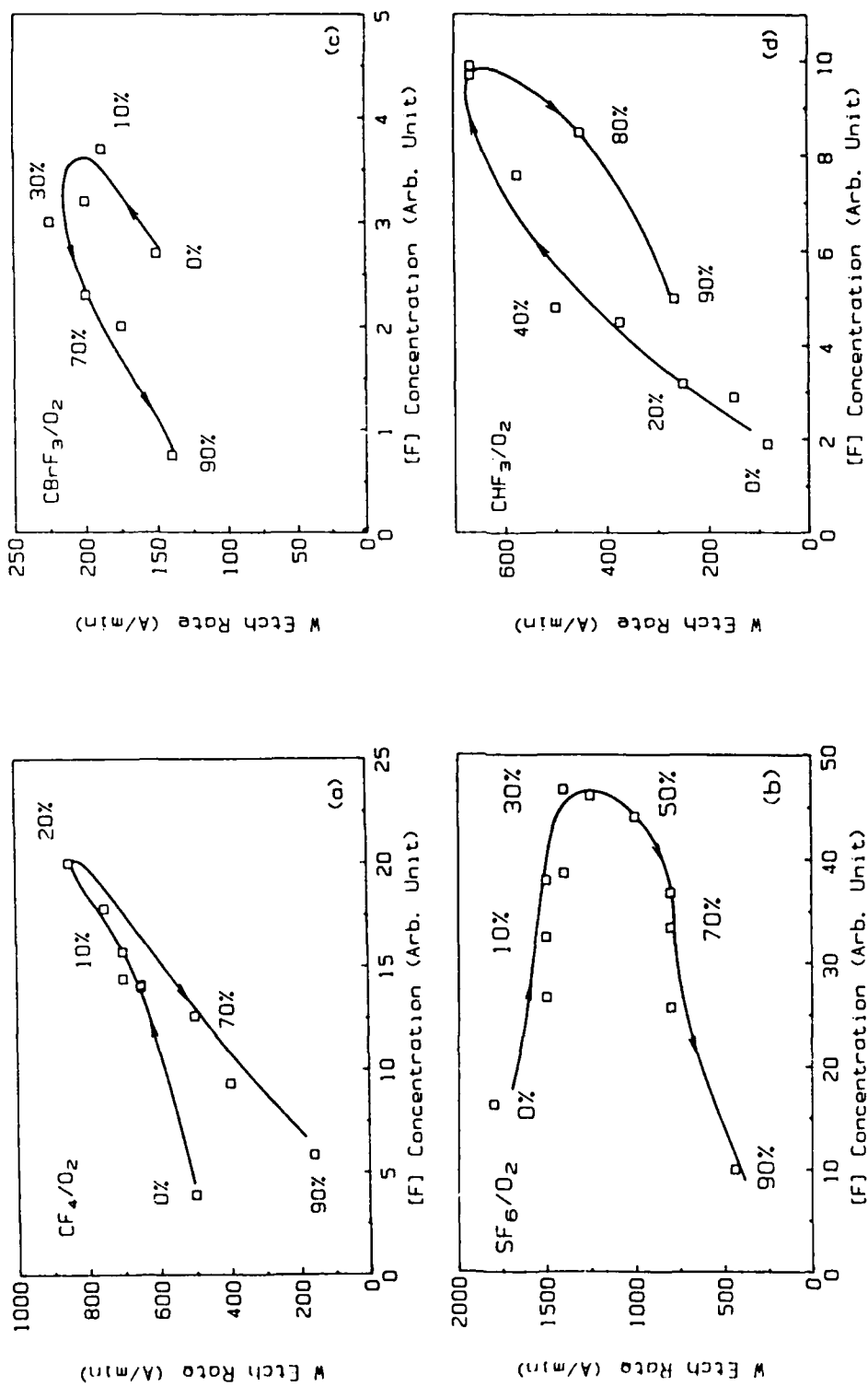
Figure 5.13. Etch rate of W versus [F] density in (a). CF_4, (b). SF_6, (c). $CBrF_3$, (d). CHF_3 with O_2 plasma under RIE mode.
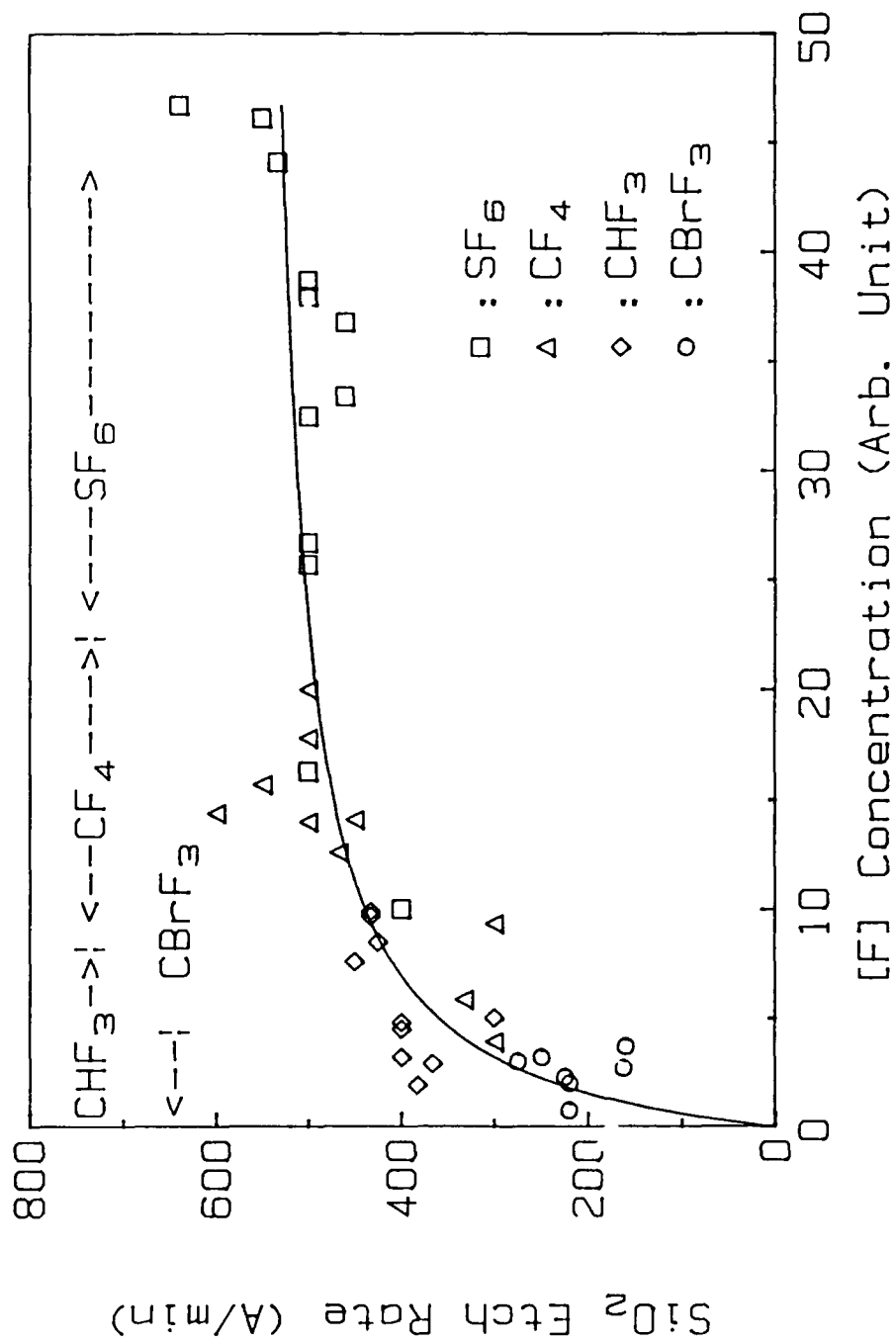
Figure 5.14. Etch rate of SiO_2 versus [F] density in CF_4, SF_6, $CBrF_3$, CHF_3 with O_2 plasma under RIE mode.

The [O] intensity level at each point is taken with respect to the base line level found in the "pure" gas plasma. The arrows along each curve indicate the direction of increasing $O_2\%$ in each gases. The vertical arrows indicate the [F]/[O] ratio value for the maximum [F] concentration. A number of comments can be made about the information contained in Figure 5.15. First, the hysteresis effect in the etch rate is removed by taking both [F] and [O] into account. Second, the etch rate trends for Si and W are the same in each gas plasma. Third, the pattern is substantively different for RIE in CF_4/O_2, SF_6/O_2 and $CBrF_3$ from RIE in CHF_3/O_2. For the former, the etch rate increases with [F]/[O] ratio until it gradually reaches saturation followed, in same cases, by a minor decline. However, in the CHF_3/O_2 case, the pattern is clearly nonmonotonic with a pronounced peak in etch rate present at a [F]/[O] ratio of 1.2 for Si and approximately 0.85 for W. The decrease in etch rate after the peak takes place in mixtures with increasing levels of hydrogen. This clearly points out the inhibiting role of hydrogen on the W and Si etch rate.

5.8 Etching Mechanisms

The basic mechanisms of plasma dissociation of fluorinated gases have been discussed in Chapter 4 except for CF_4, which has a similar mechanism to CHF_3. The etching mechanism of W proposed by Picard et al. [2.107] is shown below :
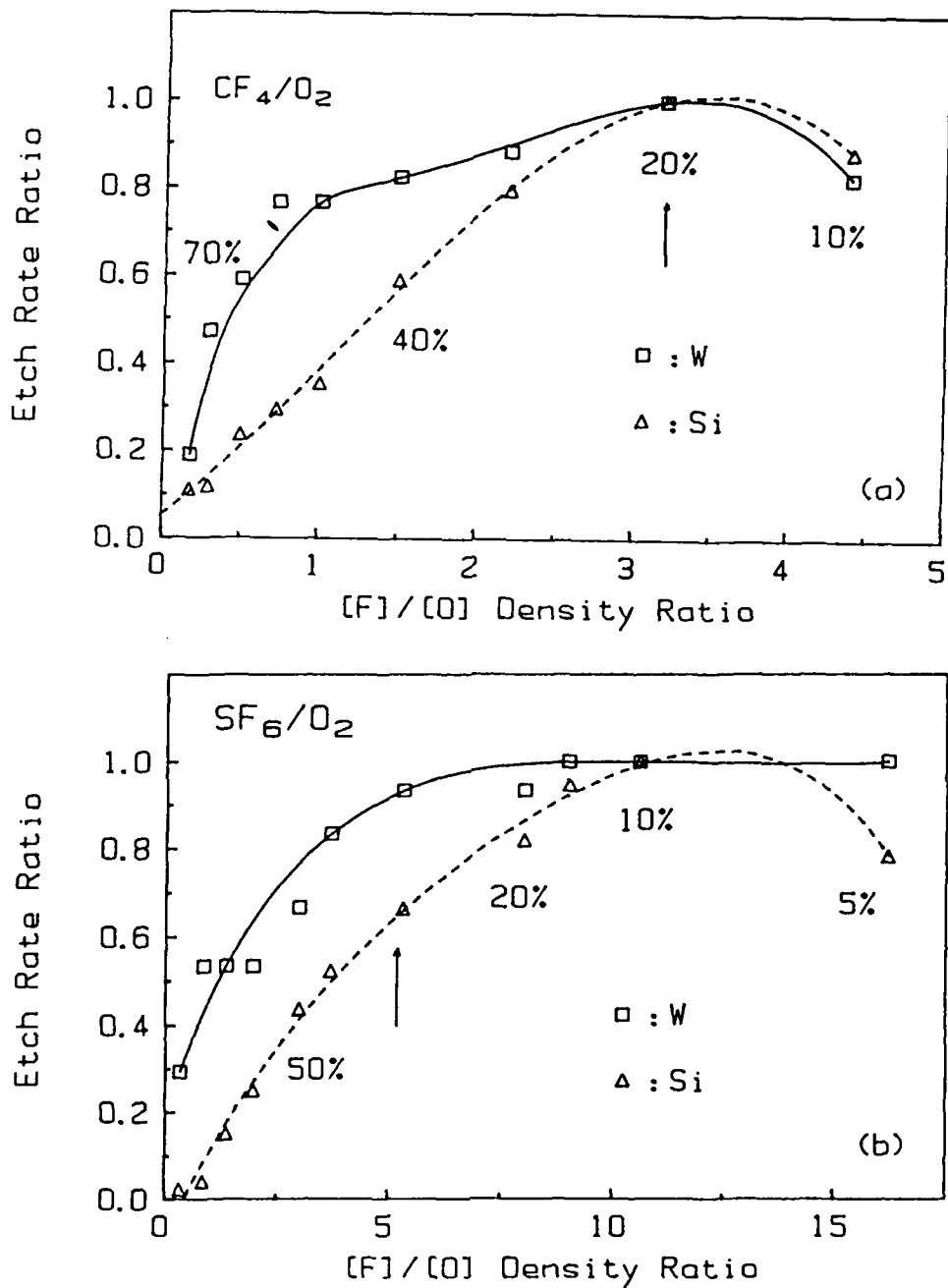
Figure 5.15.   The normalized etch rate ration of W and Si versus [F]/[O] density ratio in (a). CF_4/O_2, (b). SF_6/O_2 plasma.
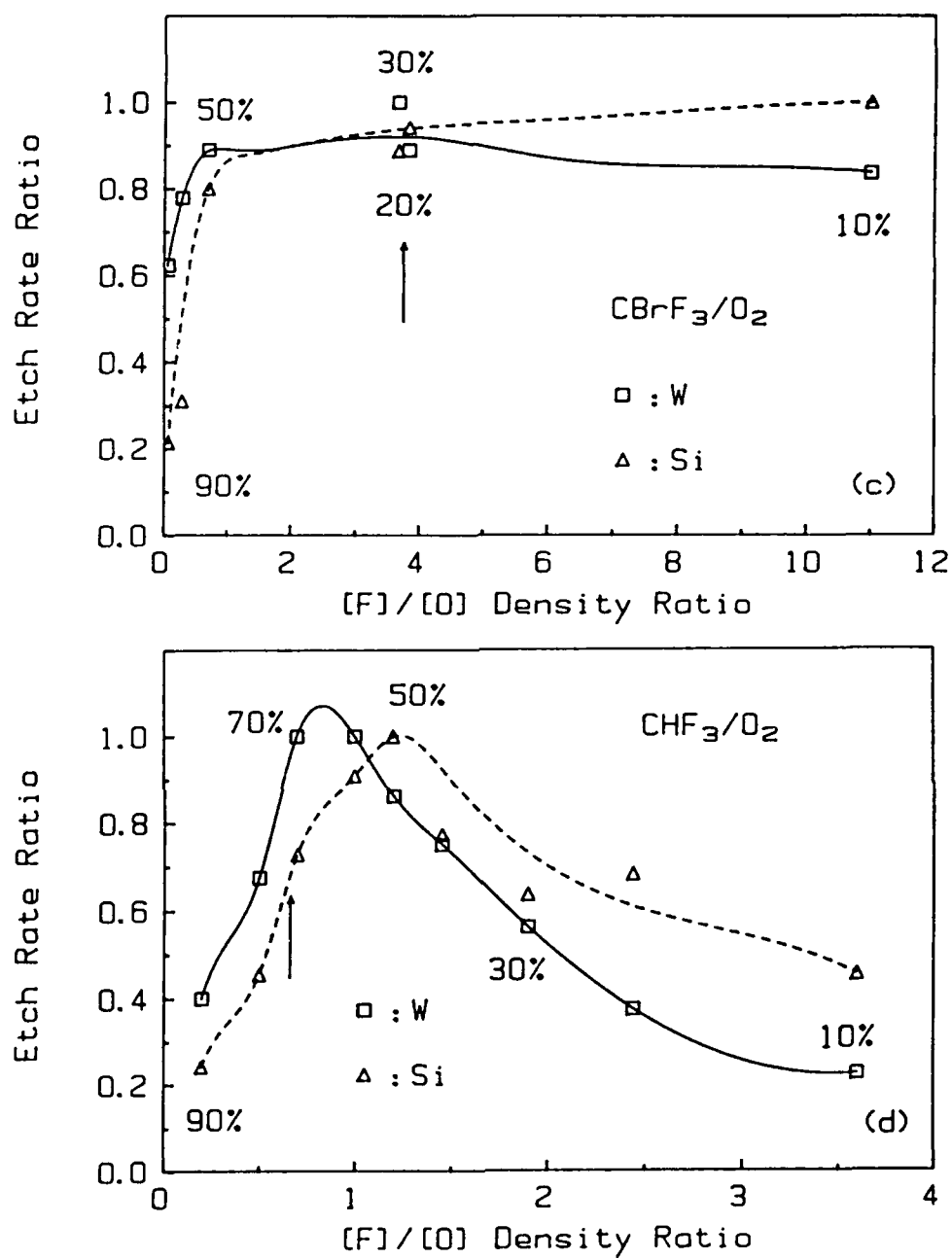
Figure 5.15.   The normalized etch rate ration of W and Si versus [F]/[O] density ratio in (c). $CBrF_3/O_2$, (d). CHF_3/O_2 plasma.

$$(5.1) \ W \ + \ xF \ \text{---}> \ WF_x \ (x = 1 \ \text{to} \ 6)$$

$$(5.2) \ WF_y \ + \ O \ \text{---}> \ WOF_y \ (y = 1 \ \text{to} \ 3)$$
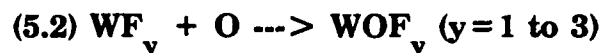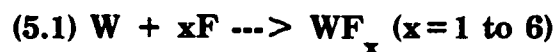
Similarly to SiC etching the fluorine and oxygen atoms are the main reactants in W etching, except, of course, different products are formed. The fluorine is the most active etchant to react with W. This has been shown in previous selective and anisotropic etching experiments and the loading experiment, shown in Figure 5.16. In the later experiment, one 3" W wafer was etched by $CHF_3/70\%O_2$ at 200W, 20mTorr, 20sccm and the fluorine, oxygen and hydrogen density was monitored. The strong decrease of fluorine density after exposing the etching sample has shown its role in etching W in reaction (5.1). The small change of oxygen density illustrates that the reaction (5.2) has an effect in W etching, but clearly not as strong as reaction (5.1) in this case.

Substrate temperature has been varied to improve the W film etch rate, with mir·· results similar to the SiC temperature experiments of section 4.7.3. Because the melting point of tungsten oxyfluoride is higher than 100°C and the chemisorption of oxygen on Si surface is reduced when the temperature is higher than 60°C. Therefore, no improvement in selective ratio has been obtained by using a different substrate temperature.
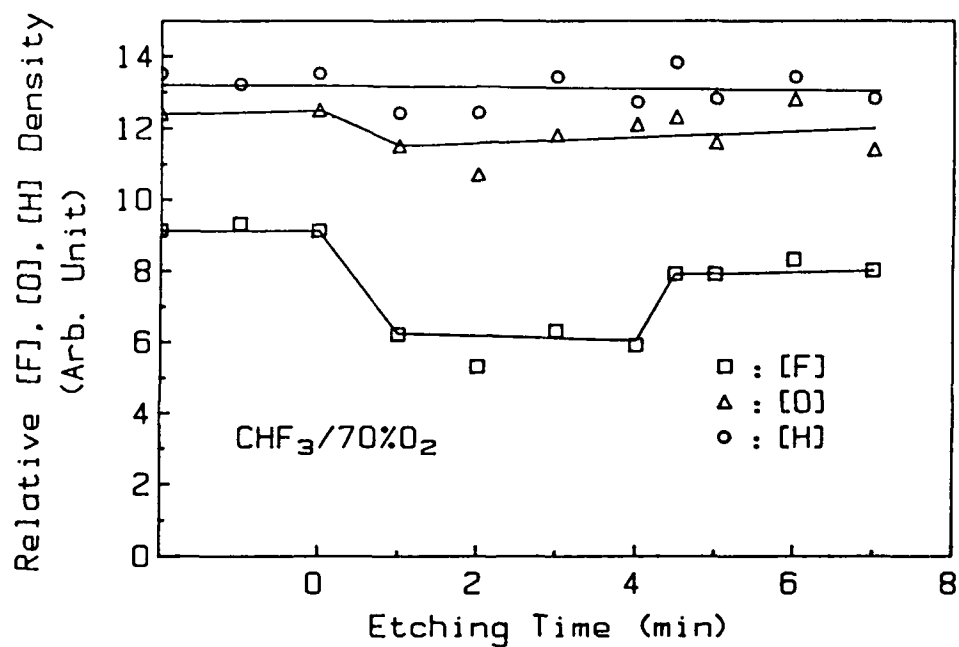
Figure 5.16.　Species density versus etching time in loading experiment by etching one 3" W wafer at $CHF_3/70\%O_2$, 200W, 20mTorr, 20sccm plasma.

CHAPTER 6

SUMMARY AND CONCLUSIONS

The basic thin film properties of SiC and W were investigated by using the rapid thermal processing technique. The potential of RTP was evaluated and the advantages of such processes has been summarized.

For SiC plasma etching, the higher etch rate ratio to Si, 2:1, was found by using $CBrF_3/75\%O_2$ and $CHF_3/90\%O_2$ plasma for the first time in the reactive ion etching mode. The dominant factors of etch rate of SiC were indicated and discussed. The SiC etch rate appears to be controlled by a combination of physical (DC bias) and chemical (fluorine and oxygen density) mechanisms. The chemical reaction model and carbon-blocking model have been established and agree qualitatively with experimental results. The dependence of SiC etch rate and physical reaction is concluded from experiment results by a typical DC bias, -300V. No evidence was obtained that fluorine will react with carbon and help to etch SiC films in these experiments. Good anisotropic profiles were obtained by RIE processes in $CHF_3/90\%O_2$ and $SF_6/35\%O_2$ plasma.

Therefore, to obtain selective SiC to Si etching, one needs to increase the oxygen concentration in order to enhance the SiC etch rate and to depress the fluorine concentration to reduce the Si etch rate. These conditions can be satisfied by choosing low-fluorinated gases (such as CHF_3, $CBrF_3$) and operating at a high oxygen percentage. A certain ion energy (DC bias) is considered to be important particularly for SiC etching. The use of an etching model could be helpful for more advanced experiments for SiC plasma etching in the future.

The reactive ion etching of W films, along with Si, SiO_2 and SiC, was investigated in CF_4/O_2, SF_6/O_2, $CBrF_3/O_2$ and CHF_3/O_2 plasmas. A W:Si etch rate ratio greater than unity was for the first time obtained, in oxygen-rich CHF_3 mixtures. The variation of pressure and power was explored to optimize the etching selectivity and to improve sidewall etching profile. The competing roles of fluorine and oxygen in the etching process was investigated.

The etching techniques for SiC and W have been studied and the results are promising to use for incorporating both materials into Si technology, which is most important role for future device processes in either VLSI or ULSI region.

REFERENCES

[1.1]   A. Lely, Ber. Dtsch. Keram. Ges. 32, 229(1955)

[1.2]   W. V. Muench and I. Pfaffeneder, "Breakdown Field in Vapor-Grown Silicon Carbide p-n Junctions," J. Appl. Phys. Vol. 48(11) , 4831(1977)

[1.3]   D. K. Ferry, "High-Field Transport in Wide-Band-Gap Semiconductor," Physical Rev. B, Vol. 12(6), 2361(1975)

[1.4]   W. V. Muench and E. Pettenpaul, "Saturated Electron Drift Velocity in 6H Silicon Carbide," J. Appl. Phys., Vol. 48(11), 4823(1977)

[2.1]   J. D. Parsons, R. F. Bunshah and O. M. Stafsudd, "Unlocking the Potential of Beta Silicon Carbide," Solid state Technl. 133(Nov. 1985)

[2.2]   E. O. Johnson, "Physical Limitations on Frequency and Power Parameters of Transistor," RCA Review, Vol. 26, 163(June 1965)

[2.3]   R. W. Keys, "Figure of Merit for Semiconductors for High Speed Switches," Proc. IEEE, 60(1), 225(1972)

[2.4]   R. W. Keys, "Power Dissipation in Information Processing," Science, Vol. 168, 796(1970)

[2.5]   R. W. Keys, "Physical Problems and Limits in Computer Logic," IEEE Spectrum, Vol. 6(5), 35(1969)

[2.6]   S. Nishino, H. Suhara and H. Matsunami, "Reproducible Preparation of Cubic-SiC Single Crystals By Chemical Vapor Deposition", Extended Abstracts of the 15th Conference on Solid State Devices and Materials, Tokyo, 317(1983)

[2.7]   A. Suzuki, K. Furukawa, Y. Higashigaki, S. Harada, S. Nakajima and T. Inoguchi, "Epitaxial Growth of β-SiC Single Crystals by Sucessive Two-step CVD," J. of Crystal Growth, 70, 287(1984)

[2.8]   K. Sasaki, E. Sakuma, S. Misawa, S. Yoshida, and S. Gonda, "High-temperature Electrical Properties of 3C-SiC Epitaxial Layers Grown by Chemical Vapor Deposition," Appl. Phys. Lett., 45(1), 72(1984)

[2.9]   P. Liaw and R. F. Davis, "Epitaxial Growth and Characterization of β-SiC Thin Films," J. Electrochem. Soc., Vol. 132(3), 642(1985)

[2.10]   G. L. Harris, K. H. Jackson, G. J. Felton, K. R. Osborne, K. Fekade, and M. G. Spencer, "Low-Pressure Growth of Single Crystal Silicon Carbide," Materials Lett. Vol. 4(2), 77(1986)

[2.11]   Y. Fujiwara, E. Sakuma, S. Misawa, K. Endo, and S. Yoshida, "Epitaxial Growth of 3C-SiC on Si by Low-Pressure Chemical Vapor Deposition," Appl. Phys. Lett., 49(7), 388(1986)

[2.12]   Myoung Gi So and John S. Chun, "Growth and Structure of Chemical Vapor Deposited Silicon Carbide from Methyltrichlorosiline and Hydrogen in the Temperature Range of 1100 to 1400°C," J. Vac. Sci. Technol., A6(1), 5(1988)

[2.13]   Y. Furumura, M. Doki, F. Mieno, T. Eshita, T. Suzuki, and M. Maeda, "Hetroepitaxial β-SiC on Si," J. Electrochem. Soc., Vol. 135(5), 1256(1988)

[2.14]   T. Miyazawa, S. Yoshida, S. Misawa, and S. Gonda, "Molecular and Ion Beam Epitaxy of 3C-SiC," Appl. Phys. Lett., 45(4), 380(1984)

[2.15]   K. L. Seaward, T. W. Barbee, Jr., and W. A. Tiller, "The Synthesis of SiCx Films by Dual-Source Sputter Deposition," J. Vac. Sci. Technol., A4(1), 31(1986)

[2.16]   M. M. Rahman and S. Furukawa, "Preparation and Electrical Properties of An Amorphous SiC/Crystalline Si p+ n Hetrojunction," Jap. J. Appl. Phys., 23(5), 515(1984)

[2.17]   C. Y. Chang, Y. K. Fang, C. F. Huang, and B. S. Wu, "Novel Passivation Dielectrics -- The Boron- or Phosphorus- Doped Hydrogenated Amorphous Silicon Carbide Films," J. Electrochem. Soc., 132(2), 418(1985)

[2.18]   J. D. Parsons, R. F. Bunshah, and O. M. Stafsudd, "Unlocking the Potential of Beta Silicon Carbide," Solid State Technol., 11 133(1985)

[2.19]   W. J. Lu, A. J. Steckl, and T. P. Chow, "Completely Consumed Carbide (C³)- A New Process for Dielectric Isolation," Proc. of the 3rd International Symposium on VLSI Science and Technology, Toronto, Canada, May 1985

[2.20]   H. Matsunami, M. Ikeda, A. Suzuki, and T. Tanaka, "SiC Blue LED'S by Liquid-Phase Epitaxy," IEEE Trans. Elec. Dev., Vol. ED-24(7) , 958(1977)

[2.21]   W. V. Munch, "Silicon Carbide Technology for Blue-Emitter Diodes," J. Electronic Matls., Vol. 6(4), 449(1977)

[2.22]   H. Munekata and H. Kukimoto, "Electroluminescence in Hydrogenated Amorphous Silicon-Carbon Alloy," Appl. Phys. Lett., Vol. 42, 432(1983)

[2.23]   H-K. Tsai, S-C. Lee, and W-L. Lin, "An Amorphous SiC/Si Two-Color Dector," IEEE Electron Device Letters, Vol. EDL8(8) , 365(1987)

[2.24]   Y. Tawada, J. Takada, N. Fukada, M. Yamaguchi, H. Yamagishi, K. Nishimura, M. Kondo, Y. Hosokawa, K. Tsuge, T. Nakayama and I. Hatano, "Stability of an Amorphous SiC/Si Tanden Solar Cell with Blocking Barriers," Appl. Phys. Lett. Vol.48(9), 584(1986)

[2.25]   Y. Kuwano and S. Tsuda, "Amorphous Silicon Solar Cells Using a-SiC Materials," Abstracts of 1st International Conference on Amorphous Crystalline Silicon Carbide and Related Materials, D.C. Washington, 16(1987)

[2.26]   W. V. Munch and P. Hoeck, "Silicon Carbide Bipolar Transistor," Solid State Electron., Vol. 21, 479(1978)

[2.27]   A. O. Konstantinov, D. P. Litvin, and V. I. Sankin, "Sharp Silicon Carbide p-n Junction of High Structural Quality," Sov. tech. Phys. Lett. 7(11), 572(1981)

[2.28]   K. Shibahara, S. Nishino and H. Matsunami, "Metal-Oxide-Semiconductor Characteristics of Chemical Vapor Deposited Cubic-SiC," Japan. J. Appl. Phys., Vol. 23, L862(1984)

[2.29]   Y. Kondo, T. Takahashi, K. Ishii, Y. Hayashi, E. Sakuma, S. Misawa, H. Daimon, M. Yamanak, and S. Yoshida, "Experimental 3C-SiC MOSFET," IEEE Electron Device Letters, Vol. EDL-7(7), 404(1986)

[2.30]   K. Shibahara, T. Saito, S. Nishino, and H. Matsunami, "Fabrication of Inversion-Type n-Channel MOSFET's Using Cubic-SiC on Si(100)," IEEE Electron Device Letters, Vol. EDL-7(12) , 692(1986)

[2.31]   J. W. Palmour, H. S. Kong, and R. F. Davis, "High-Temperature Depletion-Mode Metal-Oxide-Semiconductor Field-Effect Transistors in Beta-SiC Thin Films," Appl. Phys. Lett., 51(24), 2028(1987)

[2.32]   G. Kelner, S. Binari, K. Sleger, and H. Kong, " β-SiC/Si MESFET's and Buried-Gate JFET's", IEEE Electron Device Letters., Vol. EDL-8(9), 428(1987)

[2.33]   M. M. Rahman and S. Furukawa, "Preparation and Electrical Properties of An Amorphous SiC/Crystalline Si p+ n Hetrojunction," Jap. J. Appl. Phys., 23(5), 515(1984)

[2.34]   S. C. Jwo and C-Y. Chang, "Amorphous Silicon/Silicon Carbide Hetrojunction Bulk Unipolar Diodes (HEBUD)," IEEE Electro. Dev. Lett. Vol. EDL-7, No.12, 689(1986)

[2.35]   T. Sugii, T. Ito, Y. Furumura, M. Doki, F. Mieno, and M. Maeda, "Epitaxial SiC Emitter for High Speed Bipolar VLSIs,", in Tech. Dig. 1986 Symp. VLSI Tech., 45(1986)

[2.36]   T. Sugii, T. Ito, Y. Furumura, M. Doki, F. Mieno, and M. Maeda, "β-SiC/Si Hetrojunction Bipolar Transistors with High Current Gain," IEEE Electron Device Letters, Vol. 9(2) , 87(1988)

[2.37]   W-j. Lu, A. J. Steckl, T. P. Chow and W. Katz, "Electrical Characteristics of Si Devices Fabricated with Completely Consumed Carbide (C^3) Dielectric Isolation Process," J. Electrochem. Soc., 133(6), 1180(1986)

[2.38]   T. P. Chow and A. J. Steckl, "A Critique of Refractory Gate Applications for MOS VLSI," Ch.2 in VLSI Electronics, Vol. 9 , N. Einspruch, ed., Academic Press, NY (1985)

[2.39]   N. E. Miller and I. Beinglass, "CVD Tungsten Interconnect and Contact Barrier Technology for VLSI," Solid State Technol., 25, 85(Dec. 1982)

[2.40]   P. A. Gargini, Ind. Res. Dev., 25, 141(1983)

[2.41]   D. M. Brown, W. E. Engeler, M. Garfinkel, and P. V. Gray, "Self-Registered Molybdenum-Gate MOSFET," J. Electrochem. Soc., <u>115</u> 874(1968)

[2.42]   D. M. Brown, W. R. Cady, J. W. Sprague, and P. Salvagni, IEEE Trans. Electron Devices, <u>ED-18</u> 931(1971)

[2.43]   J. M. Shaw and J. A. Amick, "Vapor-Deposited Tungsten as a Metallization and interconnection Material for Silicon Devices," RCA Rew., <u>31</u>, 306(1970)

[2.44]   C. M. Miller-Smith, A. C. Adams, R. H. Kaiser, and R. A. Kushner, "Chemically Vapor Deposited Tungsten for Semiconductor Metallizations," J. Electtrochem. Soc., <u>121</u>, 298(1974)

[2.45]   T. O. Sedgwick, "Short Time Annealing", in C. J. Dell'Oca and W. M. Bullis, Eds., VLSI Science and Technology, <u>Vol.</u> <u>82-7</u>, 130 The Electrochemical Soc., Pennington, NJ 1982

[2.46]   A. Gat, "Heat-Pulse Annealing of Arsenic-Implanted Silicon with a CW Arc Lamp", IEEE Electron Device Lett., EDL-2, 85(1981)

[2.47]   J. Narayan, W. L. Brown and R. A. Lemons, Eds., "Laser-Solid Interactions and Transient Thermal Processing of Materials," Materials Research Society Symposia Proceedings (North-Holland, New York, 1984), Vol. 13.

[2.48]   J. C. C. Fan and N. M. Johnson, Eds., "Energy Beam-Solid Interactions and Transient Thermal Proceeding," Materials Research Society Symposa Proceeding (North-Holland, New York, 1984), Vol. 23.

[2.49]   J. F. Gibbons, Ed., "Semiconductor and Semimetals : CW beam Processing of Silicon and Other Semiconductors" (Academic, New York, 1984, Vol. 17.

[2.50]   R. K. Surridge, B. J. Sealy, A. D. E. C'Cruz, and K. G. Stephens, Proceedings of the International Symposium on GaAs and Related Compounds, Inst. Phys. Conf. Ser. <u>33a</u>, 161(1977)

[2.51]   K. Nishiyama, M. Arai, and N. Watanabe, "Radiation Annealing of Boron-Implanted Silicon with a Halogen Lamp," Jap. J. Appl. Phys. <u>19</u>, L563(1980)

[2.52]　　J. Narayan and O. W. Holland, "Rapid Thermal Annealing of Ion-Implanted Semiconductor," J. Appl. Phys., 56, 2913(1984)

[2.53]　　T. Sedgewick, Mat. Res. Soc. Symp. Proce., MRS Spring Metting Vol. 71, 403(1986)

[2.54]　　J. F. Gibbons, C. M. Gronet, and K. E. Williams, "Limited Reaction Processing : Silicon Epitaxy," Appl. Phys. Lett. 47(7), 721(1985)

[2.55]　　C. M. Gronet, J. C. Sturm, K. E. Williams, and J. F. Gibbons, "Thin, Highly Doped Layers of Epitaxial Silicon Deposited by Limited Reaction Processing," Appl. Phys. Lett., 48(15), 1012(1986)

[2.56]　　R. K. Shukla, P. W. Davies, and B. M. Tracy, "The formation of Titanium Silicide by Arsenic Ion Beam Mixing and Rapid Thermal Annealing," J. Vac. Sci., Technol., B4, 1344(1986)

[2.57]　　T. Seidel, R. Knoell, G. Poli, B. Schwartz, F. A. Stevie, and P. Chu, "Temperature Transients in Heavily Doped and Undoped Silicon Using Rapid Thermal Annealing," J. Appl. Phys. 57, 1317(1985)

[2.58]　　C. Russo, Microelectron. Manufact. Test. 9, 18(1986)

[2.59]　　L. Pfeiffer, J. M. Phillips, T. P. Smith, III, W. M. Augustyniak, and K. W. West, "Use of a Rapid Anneal to improve CaF$_2$:Si(100) Epitaxy," Appl. Phys. Lett. 46, 947(1985)

[2.60]　　R. Singh, Proceedings of the Symposium on Silicon Nitride and Silicon Dioxide thin insulating Films, Electrochemical Society Fall meeting San Diego, CA, Oct. 9-24, 1986, edited by V. K. Kapoor (Electrochemical Society, New York, 1987), Vol. 87-10, 448

[2.61]　　T. O. Sedgwick, F. M. d'Heurle, and S. A. Cohen, Electrochem. Soc. Spring Meet, Ext. Abstr. 83-1, 604(1983)

[2.62]　　D. L. Kwong, R. Kwor, C. Araujo, R. E. Jones, and D. C. Meyers, Electrochem. Soc. Fall Meet. Ext Abstr. 83-2, 448(1983)

[2.63]　　G. S. Oehrlein, C. M. Ransom, S. N. Chakravarti, and Y. H. Lee, "Silicon Near-Surface Disorder and Etch Residues Caused by CClF$_3$/H$_2$ Reactive Ion Etching," Appl. Phys. Lett., 46, 686(1985)

[2.64]   A. Rohatgi, P. Rai-Choudhry, S. J. Fonash, P. Lester, R. Singh, P. J. Caplan, and E. H. Poindexter, "Characterization and Control of Silicon Surface Modification Produced by CCl_4 Reactive Ion Etching," J. Electrochem. Soc. 133, 408(1986)

[2.65]   J. Nulman, J. P. Krusivs, and A. Gat, IEEE Electron Device Lett., EDL-6, 205(1985)

[2.66]   M. M. Moslehi, S. C. Shatas, and K. C. Saraswat, Appl. Phys. Lett., 47, 1353(1985)

[2.67]   V. Murali and S. P. Murarka, J. Appl. Phys., 60, 4327(1986)

[2.68]   J. Nulman, J. P. Krusius, and L. Rathbum, Technical Digest, International Electron Devices Meeting, 169(1984)

[2.69]   J. Nulman and J. P. Krusius, Appl. Phys. Lett. 47, 148(1986)

[2.70]   C. C. Chang, A. Kamgar, and D. Kahng, "High-Temperature Rapid Thermal Nitridation of Silicon Dioxide for Future VLSI Applications," IEEE Electron Device Lett., EDL-6, 476(1985)

[2.71]   T. O. Sedgwick, "Short Time Annealing," J. Electrochem. Soc. 130, 484(1983)

[2.72]   G. K. Celler and T. E. Seidel, in "Silicon Integrated Circuits, Part C, Applied Solid State Science," edited by D. Kahng (Academic, Orlando, FL, 1(1985).

[2.73]   C. Russo, Proceedings of the 5th International Conference on Ion Implantation Equipment and Techniques, Vermont, July 23-27, 1984, Varian Semiconductor Equipment Group Report No. 69(1984)

[2.74]   Y. A. Vodakov and E. N. Mokhov, in Silicon Carbide 1973, edited by R. C. Marshall, J. W. Faust, Jr. and C. E. Ryan, 508 (U. of South Carolina Press. Columbia, SC, 1973)

[2.75]   F. A. Leith, W. J. King and P. McNally, Air Force Contract AFCRL-67-0123, Ion Physics Co., (1967)

[2.76] H. L. Dunlap and O. J. Marsh, "Diodes in Silicon Carbide by Ion Implantation," Appl. Phys. Lett. 15, 311(1969)

[2.77] O. J. Marsh and H. L. Dunlap, "Ion-Implanted Junction and Conducting Layers in SiC," Rad. Effects 6, 301(1970)

[2.78] J. A. Edmond, H. J. Kim and R. F. Davis, "Rapid Thermal Annealing of Al and P Implanted Single Crystal Beta Silicon Carbide Thin Films," Mat. Res. Soc. Symp. Proc. Vol. 52, 157(1986)

[2.79] Jae Ryu, H. j. Kim and R. F. Davis, "Rapid Thermal Annealing of B or N implanted monocrystalline Beta-SiC Thin Films and its Effect on Electrical Properties and Device Performance," Mat. Res. Soc. Symp. Proc. Vol. 52, 165(1986)

[2.80] S. M. Irving, "A Plasma Oxidation Process for Removing Photoresist Films," Solid State Technol.,14(6), 47(1971)

[2.81] S. M. Irving, K. E. Lemons, and G. E. Bobos, "Gas Plasma Vapor Etching Process," U.S. Patent 3,615,956 (field March 27, 1969; patented Oct. 26, 1971)

[2.82] D. L. Flamm, Plasma Chem., Plasma Process, 1, 37(1981)

[2.83] H. F. Winters, J. W. Coburn, and J. T. Chang, "Surface Processes in Plasma Assisted Etching Environments," J. Vac. Sci. Technol. B1(2), 469(1983)

[2.84] J. W. Faust, Jr., "The Etching of SiC Carbide," p403 in "Silicon Carbide- A High Temperature Semiconductor," edited by J.R.O'Connor and J. Smilten, Pergamon Press, 1960

[2.85] R. C. Marshell, J. W. Faust, Jr. and C. E. Ryan, "Silicon Carbide-1973,"

[2.86] V. J. Jennings, "The Etching of Silicon Carbide," Mat. Res. Bull. 4, S199(1969)

[2.87] V. J. Jennings, A. Sommer and H. C. Chang, "The Epitaxial Growth of Silicon Carbide," J. Electrochem. Soc. 113, 31(1965)

[2.88]   T. Gabor and V. T. Jennings, "The Effect of Stirring on The Etching Characteristics of Silicon Carbide," J. Electrochem. Soc., 3, 31(1965)

[2.89]   R. C. Smith, "Gaseous Etching of Silicon Carbide in Chlorine-Cotaining Ambients," J. Electrochem. Soc. 110, 184C

[2.90]   Y. A. Vodakov, E. N. Mokhov and M. B. Reifman, "Diffusion of Boron and Aluminum in n-SiC," Sov. Phys. Solid State, 8, 1040(1966)

[2.91]   W. F. Knippenberg, "Growth Phenomena in Silicon Carbide," Philips Res. Repts. 19, 161(1963)

[2.92]   R. C. Purdy, "Effect of Temperature Treatment on Abrasive and Abrasive Products," 17, 39(1934)

[2.93]   A. C. Lea, Trans. Bri. Ceram. Soc. 40, 93(1941)

[2.94]   T. L. Chu and R. B. Campbell, "Chemical Etching of Silicon Carbide with Hydrogen," J. Electgrochem. Soc. 12, 955(1965)

[2.95]   W. J. Lu, Ph.D. Thesis, "Silicon Carbide : Thin Film Properties and Applications in VLSI", at Rensselaer Polytechnic Institue, p.78, 80(1985)

[2.96]   J. Sugiura, W-J. Lu, K. C. Cadien and A. J. Steckl, J. Vac. Sci.,Tech., "Reactive Ion Etching of SiC Thin Films Using Fluorinated Gases," Vol. B4, 349 (Jan./Feb. 1986)

[2.97]   S. Krongelb, "Process for Patterning SiC by Reactive Ion Etching," IBM, Technical Disclosure Bulletin, Vol. 23(2), 828(July, 1980)

[2.98]   J.W. Plamour, R.F. Davis , T.M. Wallett and K.B. Bhasin, "Dry Etching of β-SiC in CF_4 and CF_4+ O_2 Mixtures," J. Vac. Sci. Technol. A, Vol. 4(3), 590(May/Jun 1986)

[2.99]   S. Dohmae, K. Shibahara, S. Nishino and H. Matsunami, "Plasma F+ of CVD Grown Cubic SiC Single Crystals," Jap. J. Appl. Phys., Voi. _ ., .), L873(Nov. 1985)

[2.100] J. W. Palmour, R.F. Davis, P. Astell-Burt and P. Blackborow, "Surface Characteristics of Monocrystalline β-SiC Dry Etching in Fluorinated Gases," Mat. Res. Soc. Symp. Proc., Vol.76. 185(1987)

[2.101] G. Kelner, S. C. Binari, and P.H. Klein, "Plasma Etching of β-SiC," J. Electrochem. Soc., Vol.134, No.1, 253(Jan. 1987)

[2.102] W-S. Pan and A.J. Steckl, Mat. Res. Soc. Symp. Proc. "Anisotropic and Selective Reactive Ion Etchinh of SiC in CHF₃ and Oxygen Plasma," Vol.76, 157(1987)

[2.103] S. Adachi and N. Susa, "Reactive Ion Etching of Tungsten films Sputter Deposited on GaAs," J. Electrochem. Soc. Vol. 132(12), 2981(1985)

[2.104] N. Susa, "Comparison of GaAs, Tungsten, and Photoresist Etch Rates and GaAs Surfaces Using RIE with CF_4, CF_4+N_2, and SF_6+N_2 Mixtures," J. Electrochem. Soc., Vol. 132(11), 2763(1985)

[2.105] J.N. Randall and J.C. Wolfe, "High-Resolution Pattern Definition in Tungsten", Appl. Phys. Lett., Vol.39 , 742(1981)

[2.106] C. C. Tang and D. W. Hess, "Tungsten Etching in CF₄ and SF₆ Discharges", J. Electrochem. Soc.,Vol. 131 , 115, Jan(1984)

[2.107] A. Picard and G. Turban, "Plasma Etching of Refractory Metals (W,Mo,Ta) and Silicon in SF₆ and SF₆-O₂. An Analysis of Reaction Products", Plasma Chemistry and Plasma Processing,Vol.5(4) , 333(1985)

[2.108] M. L. Schattenburg, I. Plotnik and Henry I. Smith, "Reactive-ion Etching of 0.2μm Period Grating in Tungsten and Molybdenum Using CBrF₃", J. Vac. Sci. Technol. B., Vol.3(1) , 272, (Jan/Feb 1985)

[2.109] Harold F. Winters, "The Etching of W(111) with XeF₂," J. Vac. Sci. Technol., A3(3), 700(1985)

[2.110] A. Bensaoula, E. Grossman, and A. Ignatiev, "Etching of Tungsten with XeF₂ : An x-ray Photoelectron Spectroscopy Study," J. Appl. Phys. 62(11), 4587(1987)

[2.111] R.C. Weast, CRC Handbook of Chemistry and Physics, 6th Ed., (Chemical Rubber, Cleveland, Ohio, 1975-1976), B-154(1975-1976)

[2.112] R. J. Saia, B. Gorowitz, D. Woodruff, and D. M. Brown, "Plasma Etching Methods for The Formation of Planarized Tungsten Plugs Used in Multilevel VLSI Metallizations," J. Electrochem. Soc. Vol. 135(4), 936(1988)

[3.1] AutoEL R-II Automatic Ellipsometer Instruction Manual, Rudolph Research

[3.2] W. J. Lu, A. J. Steckl, T. P. Chow, and W. Katz, "Thermal Oxidation of Sputtered Silicon Carbide Thin Films," J. Electrochem. Soc., Vol. 131(8) 1907(1984)

[3.3] "Handbook of Chemistry and Physics," R. C. West, Editor, 62nd ed. CRC Press, Cleveland, OH(1981-1982)

[3.4] D. L. Barret, R. B. Campbell, "Electron Mobility Measurements in SiC Polytypes," J. Appl. Phys. 38, 53(1967)

[3.5] S. Kobayai, "Calculation of the Energy Band Structure of the β-SiC Crystal by the Orthogonalized Plane Wave Method," J. Phys. Soc. Jpn., 13, 261(1958)

[3.6] F. Bassani, M. Yoshimine, "Electronic Band Structure of Group IV Elements and of III-V Compounds," Phys. Rev. 130, 20(1963)

[3.7] H. G. Junginger and W. V. Haeringen, "Energy Band Structures of Four Polytypes of Silicon Carbide Calculated with the Empirical Pseudopotential Method," Phys. Stat. Sol. 37, 709(1970)

[3.8] F. Herman, J. P. Van Dyke, and R. L. Kortum, "Electronic Structure and Optical Spectrum of Silicon Carbide," Mat. Res. Bull. 4, S167(1969)

[3.9] F. Herman, Proc. IRE 43, 1703(1955)

[3.10] Fan, Shepherd, and Spitzer, Paper in Photocondutivity Conference, p. 184, John Wiley & Sons, New York (1965)

[3.11] H. Y. Fan, Paper in Repts. on Prog. in Pyhsics 19, 107(1956)

[3.12] G. G. MacFarlane and V. Roberts, "Infrared Absorption of Germanium near the Lattice Edge," Phys. Rev. 97(6), 1714(1955)

[3.13]   G. G. MacFarlane and V. Roberts, "Infrared Absorption of Silicon near the Lattice Edge," Phys. Rev. 98, 1865(1955)

[3.14]   W. J. Choyke and L. Patrick, "Absorption of Light in Alpha SiC near the Band Edge," Phys. Rev. 108, 25(1957)

[3.15]   E. A. Fagen, "Optical Properties of Amorphous Silicon Carbide Films," Silicon Carbide-1973 edited by R. C. Marshall, J. W. Faust, Jr., and C. E. Ryan, 542(1973)

[3.16]   T. T. Sheng, R. B. Marcus, F. Alexander, and W. A. Read, "Structural and Electrical Properties of Sputtered Tungsten Films," Thin Solid Films 14, 289(1972)

[3.17]   P. L. Sha, IEEE Trans. Electron Devices ED-26, 631(1979)

[4.1]   R. W. B. Pearse and A. G. Gaydon, "The Identification of Molecular Spectura," London (1950)

[4.2]   J.W. Coburn and M. Chen, "Optical Emission Spectroscopy of Reactive Plasmas: A Method for Correlating Emission Intensities to Reactive partical Density," J. Appl. Phys., Vol. 51(6), 3134(1980)

[4.3]   d'Agostino, V. Colaprico, and F. Cramarossa, "The Use of 'Actinometer' Gases in Optical Diagnostics of Plasma Etching Mixtures: SF_6-O_2," Plasma Chem. and Plasma Proc., Vol. 1(4), 365(1981)

[4.4]   d'Agostino, F. Cramarossa, S. De Benedictis, and G. Ferraro, "Spectroscopic Diagnostics of CF_4-O_2 Plasmaa During Si and SiO_2 Etching Processes," J. Appl. Phys. Vol. 52(3), 1259(1981)

[4.5]   J.W. Coburn and M. Chen, "Dependence of F atom Density on Pressure and Flow Rate in CF_4 Glow Discharges as Determined by Emission Spectroscopy," J. Vac. Sci. Technol., Vol. 18(2), 353(1981)

[4.6]   A. Picard, G. Turban and B. Grolleau, "Plasma Diagnostics of a SF_6 Radiofrequency Discharge Used for The Etching of Silicon," J. Phys. D:Appl. Phys. 19, 911(1985)

[4.7]   C.J. Mogab, A.C. Adams and D.L. Flamm, "Plasma Etching of Si and SiO$_2$-The Effect of Oxygen Addition to CF$_4$ Plasma", J. Appl. Phys., Vol.49, 3796(1978)

[4.8]   L. M. Ephrath and E. J. Petrillo, "Parameter and Reactor Dependence of Selective Oxide RIE in CF$_4$+H$_2$," J. Electrochem. Soc. 129, 2282(1982)

[4.9]   J. W. Palmour, R. F. Davis, P. Astell-Burt, and P. Blackborow, "Surface Characteristics of Monocrystalline β-SiC Dry Etched in Fluorinated Gases," Mat. Res. Soc. Symp. Proc. Vol. 76, 185(1987)

[4.10]   C.J. Mogab, "The Loading Effect in Plasma Etching," J. Electrochem. Soc., 124, 1262(1977)

[4.11]   C.J. Mogab and H.J. Levinstein, "Anisotropic Plasma Etching of Polysilicon," 17(3), 721(1980)

[4.12]   Y.Y. Tu, T.J. Chuang and H.F. Winters, "Chemical Sputtering of Fluorinated Silicon," Phys. Rev. B., 23(1981)

[4.13]   C. Cardinaud, A. Rhounna, G. Turban, and B. Grolleau, "Contamination of Silicon Surfaces Exposed to CHF$_3$ Plasma," J. Electrochem. Soc. Vol. 135(6), 1472(1988)

[5.1]   T.P. Chow and A.J.Steckl,"Plasma Etching of Refractory Gates for VLSI Applications", J. Electrochem. Soc., Vol. 131, 2325(Oct. 1984)

[5.2]   R. Pinto, K.V. Ramanathan and R.S. Babu, "Reactive Ion Etching in SF$_6$ Gas Mixtures",J. Electrochem. Soc. Vol. 134 , 165(1987).

[5.3]   R.A.H. Heinecke, "Control of Relative Etch Rates of SiO$_2$ and Si Plasma Etching", Sol. State Electron., Vol.18, 1146 (1975).

[5.4]   H.W. Lehmann and R.Widmer, "Profile Control by Reactive Sputter Etching", J. Vac. Sci. Technol., Vol.15 , 319(1978)

[5.5]   R. d'Agostino and D.L. Flamm, "Plasma Etching of Si and SiO$_2$ in SF$_6$-O$_2$ Mixtures", J. Appl. Phys. Vol.52 , 163(1981)

"Investigation of Refractory Materials and Related VLSI Processes"

ONR CONTRACT N00014-81-K-0605   PROJECT NO. NR056-768

Personnel Who Participated in Research

A.J. Steckl	Principal Investigator
T.P. Chow	Ph.D. Student
W.-J. Lu	Ph.D. Student
W.S. Pan	Ph.D. Student
K. Hamzeh	M.S. Student
C.D. Rude	M.S. Student
B.J. Baliga	Scientific Collaborator
R. Jerdonek	Scientific Collaborator
W. Katz	Scientific Collaborator
J. Sugiura	Scientific Collaborator

TECHNICAL REPORT #1

"Refractory $MoSi_2$ and $MoSi_2$/Polysilicon Bulk CMOS Circuits" by Chow, Steckl and Jerdonek/IEEE Electron Device Letters, April 1982

TECHNICAL REPORT #2

"Characterization of $NbSi_2$ Thin Films" by Rude, Chow, Steckl/Journal of Applied Physics, April 1982.

TECHNICAL REPORT #3

"Plasma Etching of Sputtered Mo and $MoSi_2$ Thin Films in NF_3 Gas Mixtures" by Chow and Steckl/Journal of Applied Physics, August, 1982.

TECHNICAL REPORT #4

"The Development of Refractory Metallization for High-Speed VLSI Circuits" by Steckl and Chow/Proceedings of the 4th International Brazil Conference on Microelectronics, February 1983.

TECHNICAL REPORT #5

"Thermal Oxidation of Niobium Silicide Thin Films" by Chow, Hamzeh and Steckl/Journal of Applied Physics, August 1983.

TECHNICAL REPORT #6

"A Review of Plasma Etching of Refractory Metal Silicides" by Chow and Steckl/Proceedings of the 4th Symposium on Plasma Processing, Electrochemical Society, October 1983.

TECHNICAL REPORT #7

"Thin Film Properties of Sputtered Niobium Silicide on SiO_2 and on n^+ Poly-Si" by Chow, Lu, Steckl and Baliga/Proceedings of Electrochemical Society Meeting, October 1983.

TECHNICAL REPORT #8

"Refractory Metal Silicides: Thin-Film Properties and Processing Technology" by Chow and Steckl/IEEE Transactions on Electron Devices, January 1985.

TECHNICAL REPORT #9

"Thermal Oxidation of Sputtered Silicon Carbide Thin Films" by Lu, Steckl, Chow and Katz/Journal of Electrochemical Society, January 1985.

TECHNICAL REPORT #10

"Plasma Etching of Refractory Gates for VLSI Applications" by Chow and Steckl/Journal of the Electrochemical Society, February 1985.

TECHNICAL REPORT #11

"Thin Films Properties of Sputtered Niobium Silicide on SiO_2, Si_3N_4 and on N^+Poly-Si" by Chow, Lu, Steckl and Baliga/Journal of the Electrochemical Society, March 1986.

TECHNICAL REPORT #12

"Completely Consumed Carbide - A New Process for Dielectric Isolation" by Lu, Steckl and Chow/Proceedings of the Electrochemical Society, March 1985.

TECHNICAL REPORT #13

"Electrical Characteristics of Si Devices Fabricated with Completely Consumed Carbide (C_3) Dielectric Isolation Process" by Lu, Steckl and Chow/Journal of the Electrochemical Society, June 1986.

TECHNICAL REPORT #14

"Reactive Ion Etching of SiC Thin Films Using Fluorinated Gases" by Sugiura, Lu, Cadien and Steckl/Journal of the Vacuum Science and Technology, January/February 1986.

TECHNICAL REPORT #15

"Anisotropic and Selective Reactive Ion Etching of SiC in CHF_3 and Oxygen Plasma" by Pan and Steckl/Proceedings of the Materials Research Society, 1986.

TECHNICAL REPORT #16

"Selective Reactive Ion Etching of Tungsten Films in Flourinated Gases" by Pan and Steckl/Journal of Vacuum Science and Technology, July/August, 1988.

TECHNICAL REPORT #17

"Reactive Ion Etching for SiC Device Fabrication" by Pan and Steckl/Springer Proceedings in Physics, 1989.

TECHNICAL REPORT #18

"Mechanisms in Reactive Ion Etching of Silicon Carbide Thin Films" by Pan and Steckl/Prepared for publication in Springer Proceedings in Physics, 1989.

TECHNICAL REPORT #19

"Reactive Ion Etching of SiC Thin Films by Mixtures of Fluorinated Gases and Oxygen" by Pan and Steckl/Prepared for publication in the Journal of the Electrochemical Society, 1989.